TU/e EINDHOVEN UNIVERSITY OF TECHNOLOGY

# Parameter estimation in Hindmarsh-Rose neurons

*Citation for published version (APA):*
Steur, E. (2006). *Parameter estimation in Hindmarsh-Rose neurons*. (DCT rapporten; Vol. 2006.073). Technische Universiteit Eindhoven.

*Document status and date:*
Published: 01/01/2006

*Document Version:*
Publisher's PDF, also known as Version of Record (includes final page, issue and volume numbers)

*Please check the document version of this publication:*

• A submitted manuscript is the version of the article upon submission and before peer-review. There can be important differences between the submitted version and the official published version of record. People interested in the research are advised to contact the author for the final version of the publication, or visit the DOI to the publisher's website.
• The final author version and the galley proof are versions of the publication after peer review.
• The final published version features the final layout of the paper including the volume, issue and page numbers.

Link to publication

*General rights*
Copyright and moral rights for the publications made accessible in the public portal are retained by the authors and/or other copyright owners and it is a condition of accessing publications that users recognise and abide by the legal requirements associated with these rights.

• Users may download and print one copy of any publication from the public portal for the purpose of private study or research.
• You may not further distribute the material or use it for any profit-making activity or commercial gain
• You may freely distribute the URL identifying the publication in the public portal.

If the publication is distributed under the terms of Article 25fa of the Dutch Copyright Act, indicated by the "Taverne" license above, please follow below link for the End User Agreement:

www.tue.nl/taverne

*Take down policy*
If you believe that this document breaches copyright please contact us at:

openaccess@tue.nl

providing details and we will investigate your claim.

Download date: 04. Oct. 2023

# Parameter Estimation in Hindmarsh-Rose Neurons

E. Steur

DCT 2006.073

Traineeship report

Coach(es): I.Y.Tyukin, PhD, DrSc.

Supervisor: prof.dr. H.Nijmeijer

Technische Universiteit Eindhoven
Department Mechanical Engineering
Dynamics and Control Group

Eindhoven, June, 2006

**Abstract**

At the RIKEN Brain Science Institute membrane potential of single neurons is recorded as function of the applied current stimuli. This particular study deals with the identification of the input-output dynamics of these single neurons. The goal is to fit the parameters of a known neuronal model on the measured data. The model to make the fit with was chosen to be the Hindmarsh-Rose 1984 model. Common identification techniques can not be used in combination with the Hindmarsh-Rose model because the model can not be transformed into a required canonical form. Therefore, an identification algorithm is developed making use of contracting and wandering dynamics. The algorithm is successfully validated by simulations with generated signals. A fit with the original Hindmarsh-Rose model to the recorded signals is not obtained. However, there is strong evidence that it is possible to make a fit with a slightly modified model.

# Contents

# Chapter 1

# Introduction

At the RIKEN Brain Science Institute (BSI) in Wako-shi, Japan, different fields of neuroscience are explored. The institutes research activities can be divided in the following groups:

- *Understanding the Brain* - what does it mean to be human?
- *Protecting the Brain* - can humans escape from disease and aging?
- *Creating the Brain* - what can we learn from the human brain?
- *Nurturing the Brain* - how does the human mind develop?

Furthermore there are the *Advanced Technology Development Group*, which focuses on developing new materials and research technology, and the *Research Resources Center*, which provides internal research support. The institute has about $40.000$ square meters of laboratory and common space and there are over $400$ employees.

In a recently established collaboration between two laboratories at Riken BSI, the Laboratory for Perceptual Dynamics, part of the *Computational Neuroscience Research Group* (Creating the Brain), and the Semyanov Research Unit, part of the *Neuronal Circuit Mechanisms Research Group* (Understanding the Brain), a project is set up dealing with identification of the input-output behavior of single neurons. The Semyanov Research Unit is capable of recording membrane potential, membrane conductances and even ionic currents in living single neurons or ensembles of neurons. The main idea of this project is to take a known, mathematical or biophysical, neuronal model and fit the models parameters to measured data. Given that neuronal models are nonlinear and the recordings are corrupted with noise, this is a real challenge. After a successful estimation of the parameters, the model will be augmented such that it can describe substance induced tonic currents. These tonic currents are activated by a neurotransmitter that is received by extra-synaptic receptors. The relatively simple neuronal models can help understanding the complex signalling mechanisms in our brain on a elementary level, i.e. on the level of the single neuron. Realistic artificial neural networks, using these models as engines, can be build and compared with measured signals. Ideally, the identified neurons can be used building artificial brains.

In Chapter 2 a short introduction to neuronal dynamics is given. Some of the measurements of the single neurons that have been made and how these recordings are obtained can be found in this chapter as well. In the next chapter some background information of neuronal models is given. Especially the Hindmarsh-Rose model will be treated extensively. After these necessary preparations a start can be made with the identification process. The machinery of the used identification algorithm

is explained in Chapter 4, followed by some obtained results which are written down in Chapter 5. Chapter 6 completes the report with conclusions and recommendations.

## 1.1 Notations

Throughout this report the following notations will be used. The symbol $\mathbb{R}$ denotes the field of real numbers. The symbol $\mathbb{R}_+$ indicates the positive real numbers. The Euclidian norm in $\mathbf{x} \in \mathbb{R}^n$ is denoted by $\|\mathbf{x}\|$. For a vector field $\mathbf{f}$ on $\mathbb{R}^n$ and a function $\mathbf{g}$ on $\mathbb{R}^m$ we denote by $L_{\mathbf{f}}^k\mathbf{g}$ the $k^{\text{th}}$ directional derivative of $\mathbf{g}$ with respect to $\mathbf{f}$ thus $L_{\mathbf{f}}^0\mathbf{g} = \mathbf{g}$, $L_{\mathbf{f}}^{k+1}\mathbf{g} = L_{\mathbf{f}}\left(L_{\mathbf{f}}^k\mathbf{g}\right)$. By $L_\infty^n[t_0, T]$ we denote the space of all functions $\mathbf{f} : \mathbb{R}_+ \to \mathbb{R}^n$ such that $\|\mathbf{f}\|_{\infty,[t_0,T]} = \sup\{\|\mathbf{f}(t)\|, t \in [t_0, T]\} < \infty$, and $\|\mathbf{f}\|_{\infty,[t_0,T]}$ stands for the $L_\infty^n[t_0, T]$ norm of $\mathbf{f}(t)$. Let $\mathcal{A}$ be a set in $\mathbb{R}^n$, and $\|\cdot\|$ be the usual Euclidean norm in $\mathbb{R}^n$. By $\|\cdot\|_{\mathcal{A}}$ the following induced norm is denoted:

$$\|\mathbf{x}\|_{\mathcal{A}} = \inf_{\mathbf{q}\in\mathcal{A}}\{\|\mathbf{x} - \mathbf{q}\|\}.$$

Finally, the notation $\|\mathbf{x}\|_{\mathcal{A}_\Delta}$ stands for the following:

$$\|\mathbf{x}\|_{\mathcal{A}_\Delta} = \begin{cases} \|\mathbf{x}\|_{\mathcal{A}} - \Delta, & \|\mathbf{x}\|_{\mathcal{A}} > \Delta \\ 0, & \|\mathbf{x}\|_{\mathcal{A}} \leq \Delta \end{cases}$$

for some $\Delta \in \mathbb{R}_+$.

# Chapter 2

# Neuronal Dynamics

The brain computes! Sensory signals are transformed into various biophysical variables, such as membrane potential and firing rates, which are subsequently used in various processes we call computations. An important element in this signaling process is the single neuron. In the beginning neurons were regarded as single functional units, which could only act in active or resting state. In the last 50 years the view on signalling and the role of single neurons has been changed tremendously, realizing now information is encoded in membrane potential and firing rates and signals decay in distance [1].

## 2.1 Signalling

A single neuron can be represented as an electrical circuit, build of different compartments consisting of capacitors, conductances and leak voltages. Each neuron has a resting state with corresponding resting potential $V_{rest}$, which value can vary from as high as -30mV to as low as -90mV depending on circumstances. In this state the neuron is in a dynamical equilibrium. Ionic currents, particulary sodium and potassium current, are flowing across the membrane in such a way that the net current is zero. Applying some stimuli will force the neuron from this equilibrium and make the neuron excitable. If the stimuli is large enough such that a threshold value, the threshold potential $V_{thres}$, is crossed, the neuron will generate action potentials and starts to fire. On the other hand, if the stimuli is such that $V_{thres}$ is not passed, the neuron will return to its resting state.

We distinguish two different kind of stimuli; Depolarizing stimuli and hyperpolarizing stimuli. A depolarizing stimuli, or outward current ($+I_{inj}$), that is a positive charge flowing from the inside of the neuron to the outside, will make the inside of the cell more positive. In neuroscience the neuron

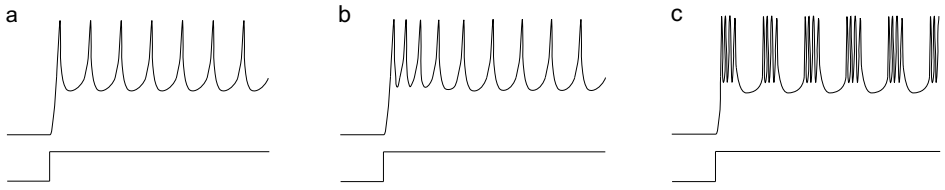


Figure 2.1: Examples of spiking dynamics. a) Regular spiking. b) Spiking with frequency adaptation. c) Bursting.

is said to be depolarized. An inward current ($-I_{inj}$) will make the inside of the cell more negative, the neuron is called hyperpolarized. The signals generated by the neuron as response on stimuli do exist in various modes depending on the type of neuron and stimuli. Figure 2.1 shows some examples of different modes of spiking dynamics or spike trains. Detailed information about biophysical features and different spiking modes can be found in [6].

## 2.2 Tonic Currents

Not too long ago, scientists thought communication between neurons took only place in specific contact areas, synapses. There do exist two types of synapses; Electrical synapses, also referred to as gap-junctions and the more common chemical synapses. Electrical synapses provide a direct, high-conductance pathway between neurons, whereas chemical synapses do not offer such a direct pathway. At chemical synapses there is a presynaptic input at the presynaptic side of the synapse, which is subsequently translated into a chemical signal. Receptors on the postsynaptic side do receive these chemical signals and transform them back into electrical signals. During this process of transitions there is a chance the signal is shunted by the extracellular space. Furthermore there are also chemicals that are waisted in terms of spillover (Figure 2.2). Quite recently scientists discovered that besides synaptic receptors also extra-synaptic receptors do exist, mainly tonic $GABA_A$ receptors. These $GABA_A$ receptors are sensitive for the chemical gamma-aminobutyric acid (GABA), one of the major inhibitory neurotransmitter in the human body, and give rise to GABA mediated tonic currents. These tonic currents are, in their turn, said to be modulating the gain and lowering the firing frequency and have therefore influence on the signalling process [19]. One of the goals of the project is to model the influence of tonic currents in terms of signalling. Since less is known about the dynamics of tonic currents, the implementation of the mechanism making a model capable of describing tonic currents is yet unknown. Assuming a mapping of the influence of tonic currents at the membrane potential can be made, one can build more realistic single neurons, which can be used in artificial networks. Nowadays neurons in neural networks are coupled via direct linear or non-linear interconnections. Building artificial neural networks with this "new" neuron demands a continuous, distributive approach, which is more close to real world situation.

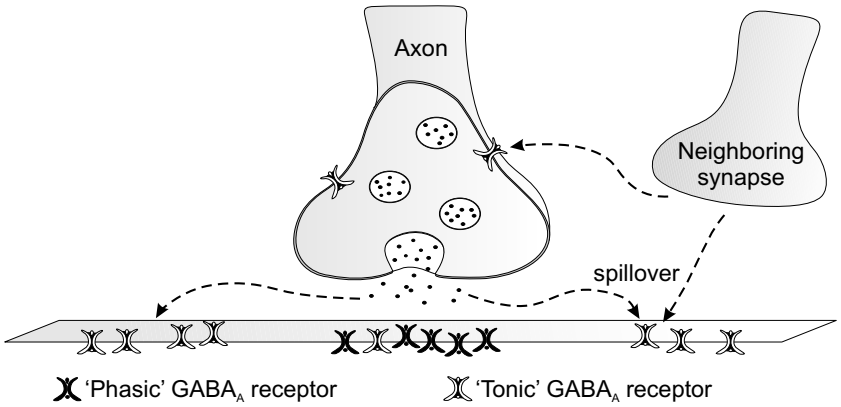


Figure 2.2: Neuron in its natural, chemical environment. Extra-synaptic receptors do receive chemicals, $GABA_A$, due to spillover of released chemicals from the axon and other neighboring synapses.

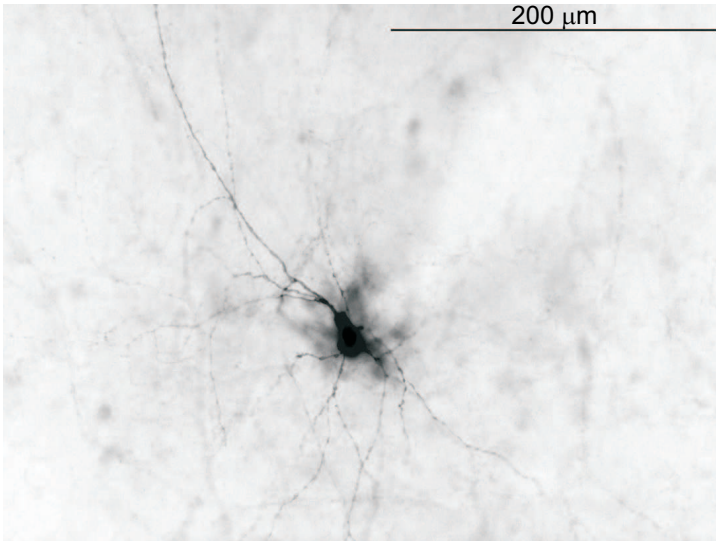


Figure 2.3: Neuron from the hippocampus of mice. One can clearly see its soma, axon and dendrites. Photo is taken by the Semyanov Research Unit

## 2.3 Single Neuron Measurements

An important part of this project is the recording of signals of single neurons. We require for the identification process that at least some input-output behavior of the neuron is known. The Semyanov Research Unit at Riken performs measurements in a current clamped setup of membrane potential of single neurons from the hippocampus of mice. Such a neuron is shown in Figure 2.3. The measurement of signals of neurons is a very delicate process. First the neuron has to be extracted from a slice of the hippocampus, followed by inserting a micropipette in its membrane. In this process the cell can easily be destroyed. The micropipette acts as measurement probe and stimulator. Because this micropipette does not disturb the flow of ionic currents across the membrane, the current clamped setup is close to the natural situation of the neuron. In the current clamped setup a depolarizing or hyperpolarizing current input is applied to the neuron. This injected current is kept at a fixed level (clamped) via some feedback and therefore the membrane potential will change. This membrane potential is recorded and regarded as output of the neuron. The temperature during the measurements is controlled which is necessary since the membrane conductances might be influenced by temperature gradients. In this setup measurements are obtained of a neuron in its natural, chemical environment. A consequence is that the influence of tonic currents is measured as well. In the sequel this type of measurement will be referred to as the *control* situation. To eliminate the tonic currents the antagonist picrotoxin (PTX) is used which blocks the tonic $GABA_A$activated receptors. Measurements of where tonic current are blocked will be denoted as the *PTX* case. These measurements have to be performed after the measurements in the control case since the treatment with $PTX$ is irreversible. The equipment in the laboratory did allow measurements with sampling rates up to 6kHz. A performed measurement of the membrane potential of the neuron in the control situation is depicted in Figure 2.4. Appendix B shows all the recorded signals.

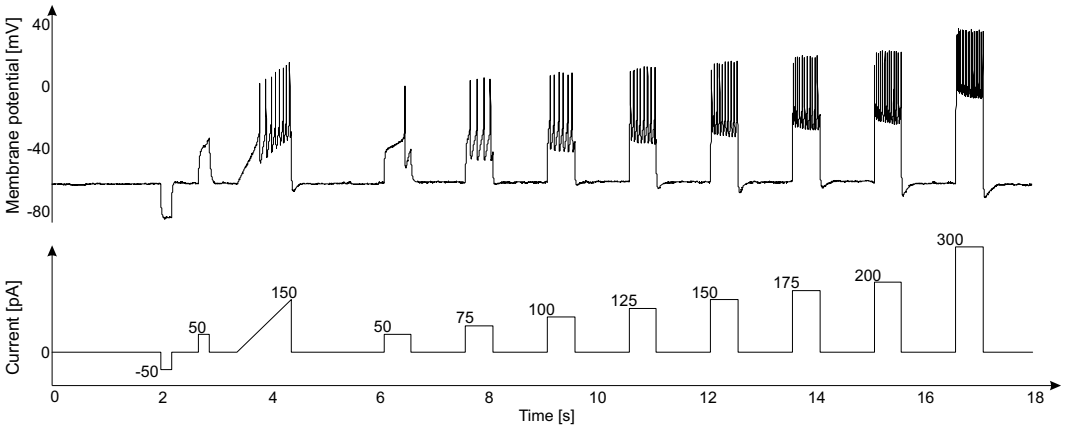


Figure 2.4: Measured membrane potential as response on hyperpolarizing and depolarizing current stimuli.

# Chapter 3

# Hindmarsh-Rose Neuronal Model

Throughout the years, many neuronal models are developed for different purposes. These models vary from true biophysical ones, like the Hodgkin-Huxley model, to simplified models for studying synchronization theories in large ensembles of neurons. Which model to use depends mainly on the biological features that need to be described and the costs of implementation.

## 3.1 Neuronal Models

In this section a brief overview of different neuronal models will be presented. More detailed information can be found in [6].

*a. Biophysical models*
One of the most important model in computational neuroscience is the 1952 Hodgkin-Huxley model [5]. Hodgkin and Huxley gave an explanation of action potential generation in the axon of the giant squid in terms of time- and voltage-dependent sodium and potassium conductances, $G_{Na}$ and $G_K$ respectively. The state of $G_{Na}$ is governed by three activation particles $m$ and one inactivating particle $h$. The sodium conductance is regulated by four activating particles $n$. The dynamics of these particles is given by first-order differential equations consisting of voltage dependent terms, time constants and steady-state activation or inactivation, bringing up the total number of differential equations to four. Morris-Lecar suggested a simple, two-dimensional model to describe oscillations in barnacle giant muscle fiber. Just like the Hodgkin-Huxley model, the Morris-Lecar model consists of a membrane potential equation and two currents. However, this model contains two activation particles $n$ and $m$, from which only particle $n$ is described using a differential equation. Although this model is able to reproduce various types of spiking, it can not exhibit bursting modes without adding an extra equation. These biological models are beloved by biophysicists since they are biophysically plausible and the parameters are in most cases measurable. However, they are very expensive in terms of flops and the number of parameters is large. To obtain a fit of the recorded signals to a biophysical model it is required to measure all individual ionic currents. Since for this study only input-output signals are measured it is not possible to use a biophysical model.

*b. Integrate-and-Fire models*
The most simple neuronal model is the so called Integrate-and-Fire model, which is widely used in computational neuroscience. Perfect Integrate-and-Fire models describe the behavior in a subthreshold domain where the neuron is modeled using only a single capacitance. When the threshold is crossed the neuron is said to be firing. Integrate-and-Fire models come in several flavors. One

popular variant of the Integrate-and-Fire model is the Leaky-Integrate-and-Fire model,

$$\dot{v} = I + a - bv, \quad \text{if } v \geq v_{th}, \text{ then } v \leftarrow c, \tag{3.1}$$

where $v$ equals the membrane potential, $I$ is the input current, $a$, $b$, $c$ are parameters, and $v_{th}$ represents the threshold value. If state $v$ passes $v_{th}$,the state is resetted to $c$. Although these models are efficient, they can only feature very little types of spiking behavior. Other variants such as Integrate-and-Fire-or-Burst or Integrate-and-Fire-with-Adaptation are able to produce more of the biological features. However, none of the Integrate-and-Fire models do give a realistic description of the spiking dynamics of the neuron and therefore they are actually only used to test analytical results or simulate very large ensembles of neurons.

*c. Phase-plane models*
Between the biophysical models on the one hand and the simple Integrate-and-Fire models on the other hand, there is a third category of models which we will refer as phase-plane models, since its dynamics can be relatively easy understood throughout phase-plane analysis. These models can exhibit a large number of biophysical features and are relatively simple and efficient. These proporties make phase-plane models very suitable for the goals of this particular project. The identification will therefore be based on one of the most complete phase-plane models, the Hindmarsh-Rose model.

## 3.2 The 1982 Model

The Hindmarsh-Rose equations are developed to study synchronization of firing of two snail neurons without the need to use the full Hodgkin-Huxley equations. The natural choice that time was to use the FitzHugh-Nagumo model, which is more or less a simplification of the Hodgkin-Huxley equations. FitzHugh and Nagumo observed independently that in the Hodgkin-Huxley equations, the membrane potential $V(t)$ as well as sodium activation $m(t)$ evolve on similar time-scales during an action potential, while sodium inactivation $h(t)$ and potassium activation $n(t)$ change on similar, although slower time scales. As a result, a model simulating spiking behavior can now be represented by the following equations

$$\begin{array}{l} \dot{x} = a(y - f(x) + I(t)), \\ \dot{y} = b(g(x) - y) \end{array}, \tag{3.2}$$

where state $x$ represents membrane potential and $y$ an recovery variable. The function $f(x)$ is cubic, the function $g(x)$ is linear, parameters $a, b$ are time constants and $I(t)$ is the external applied or clamping current as function of time $t$. However, this model does not provide a very realistic description of the rapid firing of the neuron compared to the relatively long interval between firing. In their attempts to achieve a more realistic description of firing, Hindmarsh and Rose did replace the linear function $g(x)$ in the FitzHugh-Nagumo equations with a quadratic function. How this slight modification makes the model capable describing rapid firing with a long interspike interval can be explained looking at the nulcline diagram, shown in Figure 3.1. When the limit-cycle crosses the $x$-nulcline at $C$, it is trapped in the narrow channel between the nulclines and can leave only near point $A$. In this channel, both $\dot{x}$ and $\dot{y}$ are small since the state is close to both nulclines and therefore the state changes slowly, which gives rise to a large, more realistic interspike interval. Furthermore, this model gives an explanation for the approximately linear relationship between firing frequency $f$ and the applied external current $I(t)$. Let the interspike interval $\tau_i$ be the time spent in the narrow channel. From a linear combination of the equations (3.2) we obtain

$$b\dot{x} + a\dot{y} = ab\,(g(x) - f(x)) + abI. \tag{3.3}$$

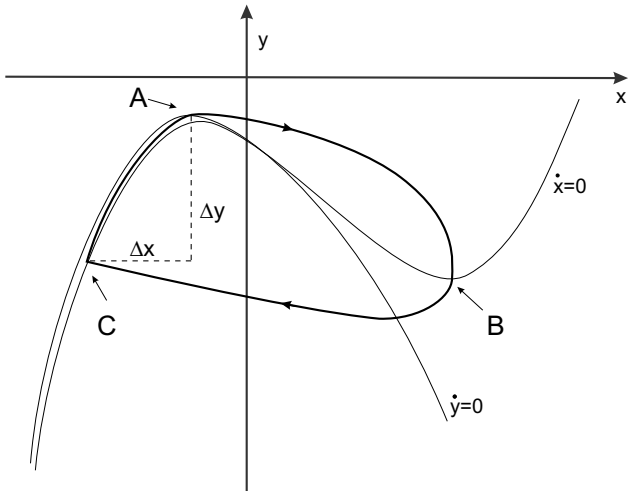


Figure 3.1: Nulclines $\dot{x} = 0$, $\dot{y} = 0$ (thin lines) and firing limit-cycle (thick line) of the 1982 model.

Integration of (3.3) from the time the state enters the channel $t = 0$ till the time the channel is left $t = \tau_i$ and ignoring the term $ab\,(g(x) - f(x))$ since in the channel $f(x) \approx g(x)$, results in the following expression

$$b\Delta x + a\Delta y \approx abI\tau_i, \tag{3.4}$$

where $\Delta x$ and $\Delta y$ are the changes in the $x$ and $y$ when the state is in the narrow channel. Because $\Delta x$ and $\Delta y$ are not much affected by changes in $I$, the firing frequency will scale linearly with the applied current

$$f \propto \frac{1}{\tau_i} \propto I. \tag{3.5}$$

## 3.3 The 1984 Model

Although the 1982 model provided a more realistic description of the rapid firing, the model does not exhibit many biological features of the neuron such as bursting and adaptation. In order to let the model describe triggered firing, Hindmarsh and Rose realized the model required more than the one equilibrium point of the 1982 model. At least one point for the subthreshold stable resting state and one point inside the firing limit cycle. Since the nulclines in the former model are very close in the subthreshold region, only a small deformation of these nulclines is required to make them intersect and thus create the additional equilibrium points. The equations were chosen to be

$$\begin{aligned} \dot{x} &= -x^3 + 3x^2 + y + I, \\ \dot{y} &= 1 - 5x^2 - y, \end{aligned} \tag{3.6}$$

whose nulclines are shown in Figure 3.2. The explanation of the firing mechanism of equations (3.6) is shown in the nulcline diagram. Initially the neuron is in at resting state, corresponding with point $A$ in the diagram, which is a stable node. By applying a large enough depolarizing current pulse, the $x$-nulcline will be lowered such that the saddle point $B$ and point $A$ meet and finally vanish. From this point the state will rise up the narrow channel and enter a stable limit cycle. However, terminating

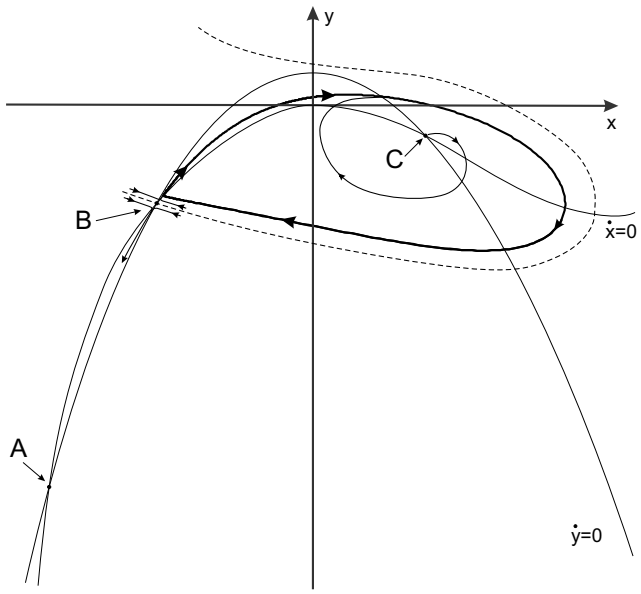


Figure 3.2: Nulclines $\dot{x} = 0$, $\dot{y} = 0$ (thin lines) and limit-cycle (thick line) of the 1984 model. Point $A$ is a stable node, point $B$ is a saddle and point $C$ is an unstable node inside the limit cycle. The dashed line represents the saddle point separatrix.

of the firing is not possible by simply ending the stimulus. The state will only leave the limit cycle after a suitable hyperpolarizing pulse is applied. In order to terminate firing the model is augmented with a third state, the adaptation variable $z$. This extra variable represents a slowly varying current, changing the applied current $I$ to the effective input $I - z$. The value of $z$ needs to raise when the neuron is in its firing state. An equation fulfilling those requirements is the first order differential equation

$$\dot{z} = r\left(s\left(x - x_0\right) - z\right), \tag{3.7}$$

where $x_0$ is the $x$-coordinate of the stable subthreshold equilibrium point in the case no external current is applied, i.e. $I = 0$. The full set of equations of the model are

$$\begin{aligned} \dot{x} &= -x^3 + 3x^2 + y + I - z, \\ \dot{y} &= 1 - 5x^2 - y, \\ \dot{z} &= r\left(s\left(x - x_0\right) - z\right). \end{aligned} \tag{3.8}$$

Because of this third equation the model can describe adaptation of the firing frequency. Furthermore, suitable choices of parameters $s$ and $r$ made the model exhibit also biological phenomena as bursting, chaotic bursting and post-inhibitory rebound. Figure 3.3 shows simulations with the 1984 model for $r = 0.001$ and $s = 1$. These plots show the $x$-state, $y$-state, $z$-state and a three-dimensional phase-plot. Figure 3.4 shows the response of the model for $r = 0.005$ and $s = 4$ with different inputs.

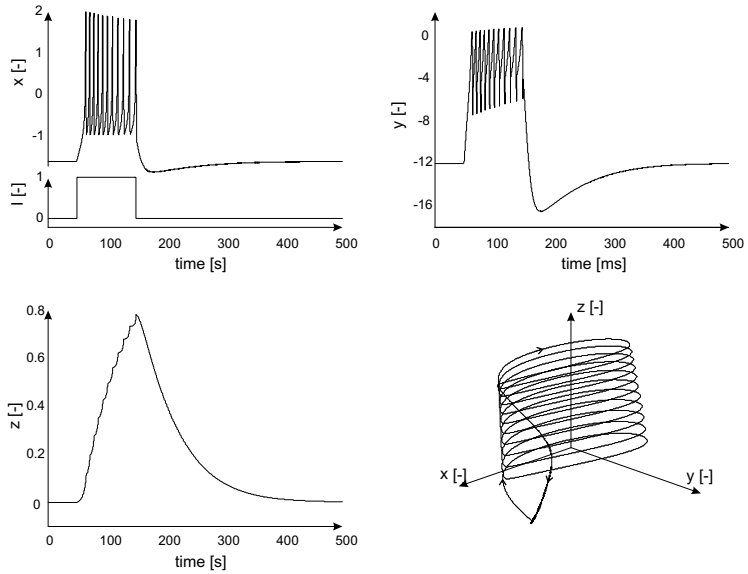


Figure 3.3: Hindmarsh-Rose simulations for $r = 0.001$ and $s = 1$. The plots show the states of the 1984 Hindmarsh-Rose as function of the applied (current) input $I$.

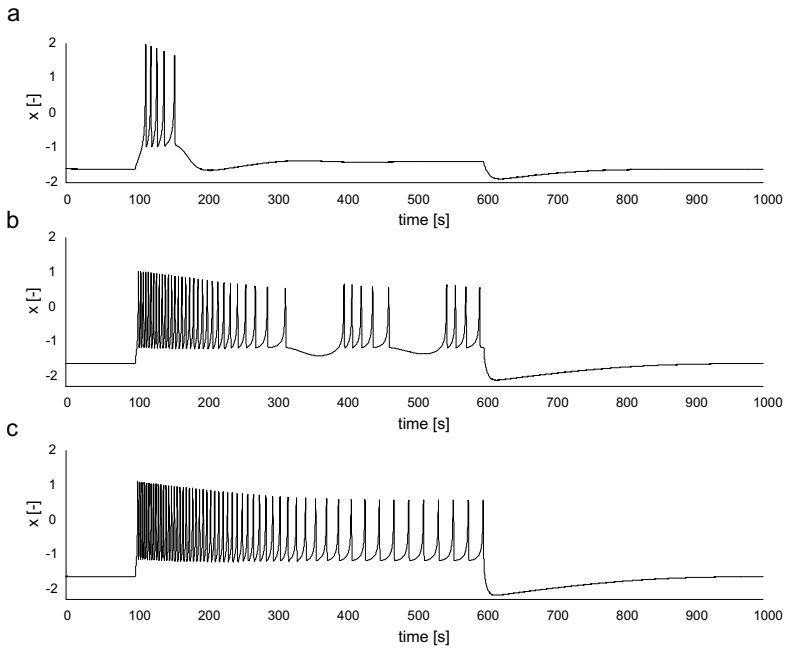


Figure 3.4: Hindmarsh-Rose simulations for $r = 0.005$ and $s = 4$ with a block-shaped input from $t = 100s$ till $t = 600s$ for $(a)$ $I = 1$, $(b)$ $I = 3.25$ and $(c)$ $I = 4$. In the first case we see the cell responds with a single burst. For $I = 3.25$ the bursting is chaotic, while for $I = 4$ the cell is spiking constantly for as long as input $I$ is present.

# Chapter 4

# Identification: Parameter and State Observations

In this chapter the focus will be on the (off-line) technique to estimate the parameters of the Hindmarsh-Rose model from the measured input-output data. It will be assumed the membrane potential can be completely described by the Hindmarsh-Rose equations

$$\mathcal{S} \quad = \quad \begin{cases} \dot{x}_1 = \frac{1}{T_s}\left(-ax_1^3 + bx_1^2 + x_2 - x_3 + a_0 u(t)\right), \\ \dot{x}_2 = \frac{1}{T_s}\left(c - dx_1^2 - \beta x_2\right), \\ \dot{x}_3 = \frac{1}{T_s} r\left(s\left(x_1 - x_0\right) - x_3\right), \end{cases} \tag{4.1}$$

where $\mathbf{x} = [x_1\, x_2\, x_3]^T \in \mathbb{R}^3$, input $u(t) \in \mathbb{R}$ and constants $a, a_0, b, c, d, \beta, r, s, x_0 > 0$. The state $x_1$ represents membrane potential, $x_2$ is an internal fast current and $x_3$ represents a slow varying current. The constant $T_s$ is a time scaling factor that allows the output of the Hindmarsh-Rose model to be in the millisecond time range instead of seconds. However, instead of using this time scaling factor it is also possible to "stretch" the time axis of the measured signals. In this study the time axis of the measured signal will be multiplied with a factor 1000 and therefore $T_s = 1$ will be used. Signals $x_1(t),\ u(t)$ and constant $x_0$ are measurable and therefore assumed to be known. Note this parametrization of system $\mathcal{S}$ is identical to the original 1984 Hindmarsh-Rose equations except for the constants $a_0$ and $a_1$, which are additional weight factors that provide some extra freedom to obtain a proper fit.

## 4.1 Adaptive Observers

The classical way of solving problems where states need to be reconstructed and a number of parameters need to be estimated is using adaptive observers [8],[14],[15]. Adaptive observer can be designed for systems of the form:

$$\begin{aligned} \dot{\mathbf{z}} &= A\mathbf{z} + \psi_0(y,u) + \sum_{i=1}^{p} \psi_i(y,u)\theta_i(t) \\ y &= C\mathbf{z}, \end{aligned} \tag{4.2}$$

where $\mathbf{z} \in \mathbb{R}^n$, $y \in \mathbb{R}$, $(\theta_1, \cdots, \theta_p)$ are unknown, possible time-varying parameters and

$$A = \begin{bmatrix} 0 & 0 & \cdots & 0 & 0 \\ 1 & 0 & \cdots & 0 & 0 \\ \vdots & \vdots & \ddots & \vdots & \vdots \\ 0 & 0 & \cdots & 1 & 0 \end{bmatrix}, \qquad C = \begin{bmatrix} 0 & 0 & \cdots & 0 & 1 \end{bmatrix}.$$

The system (4.2) is said to be in *adaptive observer canonical form*. However, the Hindmarsh-Rose equations are given, like most non-linear systems, in the following form:

$$\begin{aligned} \dot{\mathbf{x}} &= \mathbf{f}(\mathbf{x}) + q_0(\mathbf{x}, u) + \sum_{i=1}^{p} \theta_i q_i(\mathbf{x}, u) \\ &= \mathbf{f}(\mathbf{x}) + q_0(\mathbf{x}, u) + Q(\mathbf{x}, u)\boldsymbol{\theta}, \end{aligned} \tag{4.3}$$

$$y = h(\mathbf{x}),$$

where $\mathbf{x} \in \mathbb{R}^n$, $u \in \mathbb{R}^m$, $\boldsymbol{\theta} \in \mathbb{R}^p$, $y \in \mathbb{R}$ and smooth functions $\mathbf{f} : \mathbb{R}^n \to \mathbb{R}^n$, $h : \mathbb{R}^n \to \mathbb{R}$ and $q_i : \mathbb{R}^n \times \mathbb{R}^m \to \mathbb{R}^n$, $0 \leq i \leq p$. The parameter vector $\boldsymbol{\theta}$ is supposed to be constant, $\mathbf{x}$ is the state and $u(t)$ is the (control) input which is known. System (4.3) has to be transformed into system (4.2) via a coordinate transformation $\mathbf{z} = \Phi(\mathbf{x})$. A necessary condition for the existence of such a coordinate transformation is that $(\mathbf{f}, h)$ is an observable pair, i.e. the following should hold:

$$rank \left\{ d\left( L_{\mathbf{f}}^{j} h(\mathbf{x}) \right) : 0 \leq j \leq n-1 \right\} = n, \quad \forall \mathbf{x} \in \mathbb{R}^n. \tag{4.4}$$

In the case of system $\mathcal{S}$ this condition is not fulfilled. Therefore it is not possible to use adaptive observers for the estimation of the states and parameters for the system.

## 4.2 Attracting and Wandering Dynamics

Since it is not possible to transform system $\mathcal{S}$ into the adaptive observer canonical form, and thus it is not possible to make use of an adaptive observer, a technique using contracting and wandering dynamics will be proposed to estimate the parameters of the Hindmarsh-Rose model. Therefore the system dynamics will be decomposed into two interconnected subsystems. The first subsystem consists of a stable, contracting part while the dynamics of the second subsystem are wandering. Detailed information about contracting and wandering dynamics can be found in [21], from which a preprint version is included in Appendix D.

First some feedback will be designed such the the error equation, that is the equation that describes the error between signal $x_1$ and the estimated signal $\hat{x}_1$, is of the following form:

$$\dot{\tilde{x}}_1 = f_0(\tilde{x}_1, t) + f(\boldsymbol{\xi}(t), \boldsymbol{\theta}_w) - f(\boldsymbol{\xi}(t), \hat{\boldsymbol{\theta}}_w), \tag{4.5}$$

where $\tilde{x}_1 = x_1 - \hat{x}_1$, $\tilde{x}_1 \in \mathbb{R}$, $\boldsymbol{\theta}_w, \hat{\boldsymbol{\theta}}_w \in \Omega_{\theta_w} \subset \mathbb{R}^2$, functions $\boldsymbol{\xi} : \mathbb{R}_+ \to \mathbb{R}$, $f_0 : \mathbb{R} \to \mathbb{R}$, $f : \mathbb{R} \times \mathbb{R}^2 \to \mathbb{R}$. The function $\boldsymbol{\xi}(t)$ is a function of time which includes available measurements of the state. The vectors $\boldsymbol{\theta}_w, \hat{\boldsymbol{\theta}}_w$ contain the unknown and estimated parameters respectively which belong to a bounded set $\Omega_{\theta_w}$. The function $f_0(\cdot)$ represents the contracting dynamics and the part $f(\boldsymbol{\xi}(t), \boldsymbol{\theta}_w) - f(\boldsymbol{\xi}(t), \hat{\boldsymbol{\theta}}_w)$ represents the wandering dynamics.

In order to estimate the Hindmarsh-Rose parameters using contracting and wandering dynamics, the three-dimensional system $\mathcal{S}$ will be rewritten into the one-dimensional system:

$$\dot{x}_1 = -ax_1^3 + bx_1^2 + \nu + f(\beta, d, t) - sx_1^* + a_0 u(t), \tag{4.6}$$

where

$$\nu = \frac{c}{\beta}, \quad f(\beta, d, t) = e^{-\beta(t-t_0)}x_2(t_0) + \int_0^t e^{-\beta(t-\tau)}dx_1^2(\tau)d\tau.$$

The expression $\nu + f(\beta, d, t)$ is the analytical solution of the $x_2$-dynamics of $\mathcal{S}$. In the sequel the exponential decaying part of $f(\beta, d, t)$ will be neglected such that

$$f(\beta, d, t) = \int_0^t e^{-\beta(t-\tau)}dx_1^2(\tau)d\tau.$$

The $x_3$-dynamics of the Hindmarsh-Rose equations can be considered as a low-pass filter. The signal $x_3$ can be written as filter-gain $s$ multiplied by the filtered signal $(x_1 - x_0)$ using filter

$$H(j\omega) = \frac{1}{\frac{1}{r}j\omega + 1}. \tag{4.7}$$

The signal $x_1^*$ in (4.6) denotes this low-pass filtered $(x_1 - x_0)$ such that $sx_1^*$ describes the complete $x_3$-dynamics. The signal $x_1^*$ can be determined a priori. It is given that the $x_3$-dynamics actually only change the applied input $u$ into an effective input $u - x_3$ and the interspike interval $\tau_i$ is inversely proportional to $u$ (see Chapter 3). The development of the (normalized) interspike intervals in time will look like the response of a first-order system on a block-shaped input. Therefore, the parameter $r$ can be estimated by making a fit of the function $1 - e^{-r(t-t_s)}$ through the points that indicate the calculated normalized interspike intervals, where $t_s$ represents the moment of time where the input is applied. Figure 4.1 shows the development of interpike intervals in time.

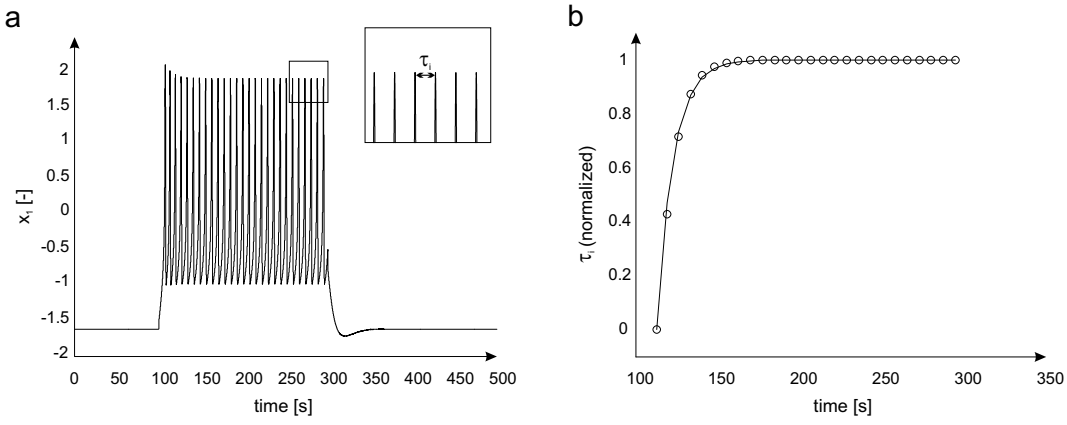


Figure 4.1: a) State $x_1$ with interspike intervals $\tau_i$. b) Calculated interspike intervals (circles) and the fit (solid line) from which parameter $r$ can be obtained.

Now, consider the following candidate observer to estimate the parameters of (4.6):

$$\begin{aligned}\dot{\hat{x}}_1 &= -\hat{a}x_1^3(t) + \hat{b}x_1^2(t) + \hat{\nu} - \hat{s}x_1^*(t) + \hat{a}_0 u(t) + \mu\,(x_1 - \hat{x}_1) + f(\hat{\beta}, \hat{d}, t) \\ &= \boldsymbol{\zeta}(t)^T\hat{\boldsymbol{\theta}} + \mu\,(x_1 - \hat{x}_1) + f(\hat{\beta}, \hat{d}, t),\end{aligned} \tag{4.8}$$

where $\mu > 0$ and

$$\boldsymbol{\theta} = \begin{bmatrix} a \\ b \\ \nu \\ s \\ a_0 \end{bmatrix}, \qquad \boldsymbol{\zeta}(t) = \begin{bmatrix} -x_1^3(t) \\ x_1^2(t) \\ 1 \\ -x_1^*(t) \\ u(t) \end{bmatrix}.$$

Combining (4.6) and (4.8) results in the error equation, which is given by:

$$\underbrace{\dot{\tilde{x}}_1 = -\mu\tilde{x}_1 + \boldsymbol{\zeta}(t)^T\tilde{\boldsymbol{\theta}}} + f(\beta, d, t) - f(\hat{\beta}, \hat{d}, t), \tag{4.9}$$

where $\tilde{\boldsymbol{\theta}} = \boldsymbol{\theta} - \hat{\boldsymbol{\theta}}$. In combination with a suitable parameter update law the parameter error $\tilde{\boldsymbol{\theta}}$ will be forced to zero. Then, the underbraced part of (4.9) will be contracting, that is $\lim_{t\to\infty} \tilde{x}_1(t) = 0$.

In the next two subsections the focus will be on the design of the contracting dynamics and the wandering dynamics, respectively.

### 4.2.1 Contracting Dynamics

In this subsection the precieze design of the contracting dynamics is taken into account. Let us start with (4.9), neglecting the term $f(\beta, d, t) - f(\hat{\beta}, \hat{d}, t)$ for this moment:

$$\dot{\tilde{x}}_1 = -\mu\tilde{x}_1 + \boldsymbol{\zeta}(t)^T\tilde{\boldsymbol{\theta}}. \tag{4.10}$$

The state $\tilde{x}_1$ will go to the origin for increasing time if and only if the parameters stored in $\boldsymbol{\theta}$ are estimated correctly. Therefore, the following parameter update law will be used to force $\hat{\boldsymbol{\theta}} \to \boldsymbol{\theta}$:

$$\dot{\hat{\boldsymbol{\theta}}} = \gamma_a\tilde{x}(t)\boldsymbol{\zeta}(t), \tag{4.11}$$

where $\gamma_a > 0$. Equations (4.10) and (4.11) can be combined into the following $linear\ time\ varying\ (LTV)$ system:

$$\begin{bmatrix} \dot{\tilde{x}}_1 \\ \dot{\tilde{\boldsymbol{\theta}}} \end{bmatrix} = \begin{bmatrix} -\mu & \boldsymbol{\zeta}(t)^T \\ -\gamma_a\boldsymbol{\zeta}(t) & \mathbf{0} \end{bmatrix} \begin{bmatrix} \tilde{x}_1 \\ \tilde{\boldsymbol{\theta}} \end{bmatrix} \quad . \tag{4.12}$$

LTV systems of this form are exponential stable if the following conditions hold [12], [17]:

1. function $\boldsymbol{\zeta}(t)$ is piece-wise continuous and bounded,
2. $\boldsymbol{\zeta}(t)$ fulfills the persistently exciting condition, that is

**Definition 1 (Persistence of Excitation)** *The function $\boldsymbol{\zeta}(t)$ is said to be persistently exciting (PE) if and only if there exists constants $\alpha > 0$ and $L > 0$ such that for all $t \in \mathbb{R}_+$ the following holds:*

$$\int_t^{t+L} \boldsymbol{\zeta}(\tau)\boldsymbol{\zeta}(\tau)^T d\tau \geq \alpha I_d, \tag{4.13}$$

*where $I_d$ is the identity matrix.*

Since all signals in $\boldsymbol{\zeta}(t)$ are known and indeed piecewise continuous and bounded, condition 1 is fulfilled. Condition 2 has to be investigated (numerically) for each individual case. Assuming both conditions do hold, system (4.12) is exponentially stable. The rate of convergence $\rho$ is defined as:

$$\| \mathbf{w}(\tau) \|_{\infty,[t_0,t]} \leq e^{-\rho(t-t_0)} \| \mathbf{w}_0 \|, \tag{4.14}$$

where

$$\mathbf{w} = \begin{bmatrix} \tilde{x}_1 \\ \tilde{\boldsymbol{\theta}} \end{bmatrix}, \quad \mathbf{w}_0 = \mathbf{w}(t = t_0).$$

In the sequel it will be assumed, for simplicity, that the convergence rate of the error $\tilde{x}_1$ is equal to this convergence rate $\rho$. A rate of convergence larger than $\rho$ does not make the identification method not going to work. It only indicates that the gain $\gamma_w$, which will be specified in the next section, can be increased.

### 4.2.2 Wandering Dynamics

In this subsection the focus will be on the design of the wandering dynamics. Reconsider the error equation (4.9) given that the contracting dynamics (4.12) are exponentially stable:

$$\tilde{x}_1 = -\rho \tilde{x}_1 + f(\beta, d, t) - f(\hat{\beta}, \hat{d}, t). \tag{4.15}$$

The wandering dynamics will search for the values of the remaining parameters in some bounded domain $\Omega_\beta \times \Omega_d$, where $\beta, \hat{\beta} \in \Omega_\beta$ and $d, \hat{d} \in \Omega_d$, until $f(\hat{\beta}, \hat{d}, t) \to f(\beta, d, t)$ and thus $\tilde{x}_1 \to 0$. This search is performed with low speed, such that the contracting dynamics have time to reach its steady state.

The first thing that is required is boundedness of the function $f(\cdot)$ in terms of its parameters:

$$\begin{aligned} |f(\beta, d, t) - f(\hat{\beta}, \hat{d}, t)| &\leq |f(\beta, d, t) - f(\hat{\beta}, d, t)| + |f(\hat{\beta}, d, t) - f(\hat{\beta}, \hat{d}, t)| \\ &\leq D_{f,\beta} |\beta - \hat{\beta}| + D_{f,d} |d - \hat{d}|, \end{aligned} \tag{4.16}$$

where

$$D_{f,\beta} = \max_{\beta,\hat{\beta} \in \Omega_\beta, d \in \Omega_d} \left\{ \frac{1}{\beta \hat{\beta}} d \, \| \, x_1^2(\tau) \, \|_{\infty,[t_0,t]} \right\}, \quad D_{f,d} = \max_{\hat{\beta} \in \Omega_\beta} \left\{ \frac{1}{\hat{\beta}} \, \| \, x_1^2(\tau) \, \|_{\infty,[t_0,t]} \right\}. \tag{4.17}$$

The derivation of $D_{f,\beta}$ and $D_{f,d}$ can be found in Appendix A.

Next, the following auxiliary system will be introduced:

$$\dot{\boldsymbol{\lambda}} = \Sigma(\boldsymbol{\lambda}), \tag{4.18}$$

where $\boldsymbol{\lambda} \in \Omega_\lambda \subset \mathbb{R}^\lambda$ is bounded and $\Sigma : \mathbb{R}^\lambda \to \mathbb{R}^\lambda$ is locally Lipschitz. System (4.18) is assumed to be *Poisson stable* in $\Omega_\lambda$, that is:

**Definition 2 (Poisson stability)** *The system (4.18) is called Poisson stable in $\Omega_\lambda$ if*

$$\forall \boldsymbol{\lambda}' \in \Omega_\lambda, t' \in \mathbb{R}_+ \Rightarrow \exists t'' > t' : \| \boldsymbol{\lambda}(t'', \boldsymbol{\lambda}') - \boldsymbol{\lambda}' \| \leq \epsilon, \tag{4.19}$$

*where $\epsilon$ is an arbitrary small positive constant. Moreover, the trajectory $\boldsymbol{\lambda}(t, \boldsymbol{\lambda}_0)$ is dense in $\Omega_\lambda$:*

$$\forall \boldsymbol{\lambda}' \in \Omega_\lambda, \epsilon \in \mathbb{R}_+ \Rightarrow \exists t \in \mathbb{R}_+ : \| \boldsymbol{\lambda}' - \boldsymbol{\lambda}(t, \boldsymbol{\lambda}_0) \| < \epsilon, \tag{4.20}$$

*where $\boldsymbol{\lambda}_0 = \boldsymbol{\lambda}(t_0)$.*

Define the system (4.18) with the following set of equations:

$$\begin{aligned} \dot{\lambda}_1 &= \lambda_2, \\ \dot{\lambda}_2 &= -\omega_1^2 \lambda_1, \\ \dot{\lambda}_3 &= \lambda_4, \\ \dot{\lambda}_4 &= -\omega_2^2 \lambda_3, \quad \boldsymbol{\lambda}_0 = (1,0,1,0)^T, \end{aligned} \tag{4.21}$$

where $\omega_1, \omega_2 \in \mathbb{R}_+$. Furthermore the Poisson stability criterium is satisfied.

In addition, an output function $\boldsymbol{\eta}(\boldsymbol{\lambda}) : \mathbb{R}^4 \to \mathbb{R}^2$ is selected that will translate $\boldsymbol{\lambda}$ into estimations of the parameter $\beta$ and $d$. This output function is required to be locally Lipschitz, that is:

$$\| \eta(\boldsymbol{\lambda}') - \eta(\boldsymbol{\lambda}'') \| \leq D_\eta \| \boldsymbol{\lambda}' - \boldsymbol{\lambda}'' \|, \quad \boldsymbol{\lambda}', \boldsymbol{\lambda}'' \in \Omega_\lambda, \tag{4.22}$$

such that $\boldsymbol{\eta}(\Omega_\lambda)$ is dense in $\Omega_\beta \times \Omega_d$. For $\Omega_\beta = [\beta_{min}, \ldots, \beta_{max}]$ and $\Omega_d = [d_{min}, \ldots, d_{max}]$ function $\boldsymbol{\eta}(\boldsymbol{\lambda}) = (\eta_1(\boldsymbol{\lambda}), \eta_2(\boldsymbol{\lambda}))$ is defined as:

$$\begin{aligned} \hat{\beta} = \eta_1(\boldsymbol{\lambda}) &= \tfrac{\beta_{max} - \beta_{min}}{2} \left( \tfrac{2 \arcsin(\lambda_1)}{\pi} + 1 \right) + \beta_{min}, \\ \hat{d} = \eta_2(\boldsymbol{\lambda}) &= \tfrac{d_{max} - d_{min}}{2} \left( \tfrac{2 \arcsin(\lambda_3)}{\pi} + 1 \right) + d_{min}. \end{aligned} \tag{4.23}$$

The Lipschitz constant $D_\eta$ in (4.22) for the chosen $\boldsymbol{\eta}(\boldsymbol{\lambda})$ is given by:

$$D_\eta = \max \left( \frac{(\beta_{max} - \beta_{min}) \cdot \omega_1}{\pi}, \frac{(d_{max} - d_{min}) \cdot \omega_2}{\pi} \right). \tag{4.24}$$

The constants $\omega_1$ and $\omega_2$ in (4.21) need to be chosen with some care. Only by choosing $\frac{\omega_1}{\omega_2}$ equal to an irrational number, we ensure that every point in the domain $\Omega_\beta \times \Omega_d$ is visited. More details are given in Figure 4.2.

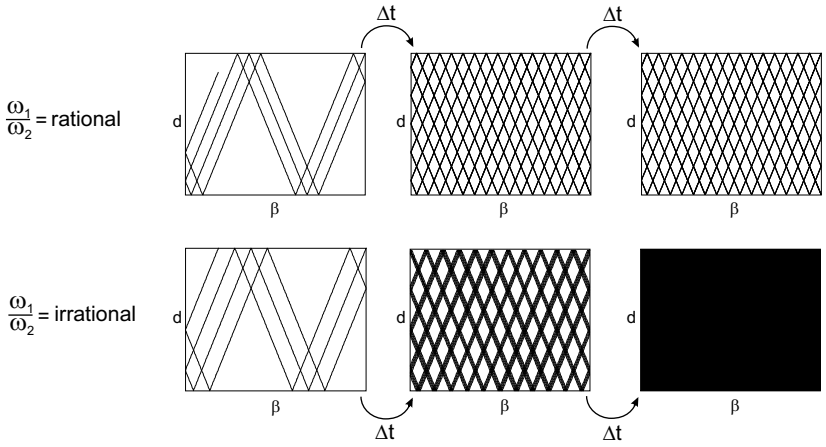


Figure 4.2: The figure on top shows the case that $\frac{\omega_1}{\omega_2}$ is a rational number. As a result, the search will finally end up at the same points, even if time goes to infinity. In the case where $\frac{\omega_1}{\omega_2}$ is an irrational number, every point in the searching domain $\Omega_\beta \times \Omega_d$ is visited after sufficient time.

Finally, an accurate interconnection between the contracting dynamics and the wandering dynamics needs to be determined. This interconnection will be defined as follows:

$$\begin{aligned}
\dot{\lambda}_1 &= \gamma_w \parallel \tilde{x}_1(t) \parallel_{\Delta(\delta)} \cdot \lambda_2, \\
\dot{\lambda}_2 &= -\gamma_w \parallel \tilde{x}_1(t) \parallel_{\Delta(\delta)} \cdot \omega_1^2 \lambda_1, \\
\dot{\lambda}_3 &= \gamma_w \parallel \tilde{x}_1(t) \parallel_{\Delta(\delta)} \cdot \lambda_4, \\
\dot{\lambda}_4 &= -\gamma_w \parallel \tilde{x}_1(t) \parallel_{\Delta(\delta)} \cdot \omega_2^2 \lambda_3, \quad \boldsymbol{\lambda}_0 = (1,0,1,0)^T,
\end{aligned} \tag{4.25}$$

where $\delta > 0$ is a pre-defined error tolerance. Furthermore the gain $\gamma_w$ satisfies the inequality:

$$0 < \gamma_w \leq -\rho \left( ln \frac{d_s}{\kappa D_\beta} \right)^{-1} \frac{\kappa - 1}{\kappa} \frac{1}{D_\lambda \left( D_\beta \left( 1 + \frac{\kappa}{1 - d_s} \right) + 1 \right)}, \tag{4.26}$$

with $D_\beta = 1$, $D_\lambda = \max(D_{f,\beta}, D_{f,d}) \cdot D_\eta \cdot \max\limits_{\boldsymbol{\lambda} \in \Omega_\lambda} \parallel \Sigma(\boldsymbol{\lambda}) \parallel$, $d_s \in (0,1)$ and $\kappa \in (1, \infty)$.

By choosing the gain $\gamma_w$ according to (4.26), we ensure the contracting part has enough time to reach its steady-state. More detail about the derivation of (4.26) can be found in the section D.5 of the Appendix. Now, for some $\boldsymbol{\theta}'$ in a neighborhood of $\boldsymbol{\theta}$, $\beta'$ in a neighborhood of $\beta$ and $d'$ in a neighborhood of $d$, in combination with the observer (4.8), wandering dynamics (4.23) and interconnection (4.25), the following does hold:

$$\lim_{t \to \infty} \parallel \tilde{x}_1 \parallel = 0, \quad \lim_{t \to \infty} \hat{\boldsymbol{\theta}} = \boldsymbol{\theta}', \quad \lim_{t \to \infty} \hat{\beta}(t) = \beta', \quad \lim_{t \to \infty} \hat{d}(t) = d',$$

which should result in a successful fit of the measurements to the model.

The identification algorithm is implemented in $Matlab$, which code can be found in Appendix C. This implementation in $Matlab$ is rather slow, probably due to the large number of function calls in the *ode*-solver. A solution to this problem is found in implementing the algorithm in the low-level programming langue $C$++, which turns out to be more then hundred times faster then the $Matlab$ algorithm with similar accuracy. This implementation can be found in Appendix C as well. Note that this $C$++ algorithm is not at its final stage. For instance, it is not possible with the presented algorithm to keep track of the error, something that is strongly recommended in problems like this.

## 4.3 Searching Domain $\Omega_\beta \times \Omega_d$

For the wandering dynamics it is required that the searching domain $\Omega_\beta \times \Omega_d$ is known. Of course it is always possible to choose some arbitrary domain. However, there is a chance that an arbitrary chosen searching domain will not include the "real" parameter values. On the other hand, the domain can be chosen too large such that it will take a long time to find the right parameter values. Therefore the searching domain will be estimated using a feasibility study based on stability proporties of the Hindmarsh-Rose model.

It is known that the 1984 model has three equilibrium points, which will be denoted by $x_0, x_{th}, x_{sp}$ representing the stable resting potential, the threshold value and the equilibrium point inside the limit cycle, respectively. These equilibrium points are given by the roots of the equation:

$$x_1^3 + p x_1^2 = q, \tag{4.27}$$

where

$$p = \frac{1}{a} \left( \frac{d}{\beta} - b \right), \quad q = \frac{1}{a} \left( a_0 u(t) + \frac{c}{\beta} \right)$$

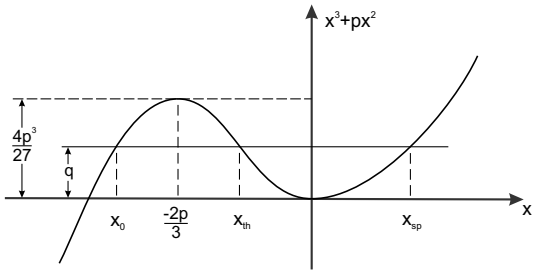


Figure 4.3: Equilibrium points of the Hindmarsh-Rose model.

In the case that $u(t) = 0$ and the state is thus at its stable equilibrium, we require all three equilibrium points do exist. The condition for the existence of three equilibrium points is that $27q < 4p^3$, or that

$$27\frac{c\,a^2}{\beta} < 4\left(\frac{d}{\beta} - b\right)^3. \tag{4.28}$$

Figure 4.3 gives a graphical representation of this condition. Because $a, b, c, d, \beta > 0$ it follows immediately that

$$\frac{d}{\beta} > b. \tag{4.29}$$

When the state reaches the threshold value $x_{th}$, only two equilibrium points will remain since $x_0$ and $x_{th}$ meet and become a single point. Furthermore, when the neuron is spiking and thus the state is in the limit cycle, there will only be one equilibrium point left, that is the one within the limit-cycle. Let us, in addition, analyse stability proporties of the equilibrium points. In this analysis, the $x_3$-dynamics will be neglected since the influence of these dynamics are generally small. Only in the part of the signal where there is firing frequency adaptation the $x_3$-dynamics are involved.

Consider the linear approximation of (4.1)

$$\dot{\bar{\mathbf{x}}} = A(x_{eq})\bar{\mathbf{x}}, \tag{4.30}$$

where

$$A(x_{eq}) = \begin{bmatrix} -3a{x_{eq}}^2 + 2bx_{eq} & 1 \\ -2dx_{eq} & -\beta \end{bmatrix}.$$

The type of equilibrium point $x_{eq}$ is determined by the signs of the determinant and the trace of $A(x_{eq})$. The determinant and trace are given by:

$$\begin{aligned} det(A) &= 3a\beta x_{eq}^2 + 2(d - b\beta)x_{eq}, \\ tr(A) &= -3ax_{eq}^2 + 2bx_{eq} - \beta. \end{aligned} \tag{4.31}$$

The determinant of $A(x_{eq})$ is positive for all values of $x_{eq}$ except for those between $\frac{-2\left(\frac{d}{\beta}-b\right)}{3a}$ and $0$ whereas the trace of $A(x_{eq})$ is negative for all values of $x_{eq}$ besides the ones in the interval $[(b - \sqrt{b^2 - 3a\beta})/3a, \ldots, (b + \sqrt{b^2 - 3a\beta})/3a]$. From this last interval it follows directly that

$$b^2 > 3a\beta. \tag{4.32}$$

Table 4.1: Stability regions

| region | values of $x_{eq}$ | $sgn(det(A))$ | $sgn(tr(A))$ | type of equilibrium point |
|---|---|---|---|---|
| **I** | $x < \frac{-2\left(\frac{d}{\beta}-b\right)}{3a}$ | - | + | stable focus |
| **II** | $\frac{-2\left(\frac{d}{\beta}-b\right)}{3a} < x < 0$ | - | - | saddle node |
| **III** | $0 < x < \frac{b-\sqrt{b^2-3a\beta}}{3a}$ | - | + | stable focus |
| **IV** | $\frac{b-\sqrt{b^2-3a\beta}}{3a} < x < \frac{b+\sqrt{b^2-3a\beta}}{3a}$ | + | + | unstable focus |
| **V** | $x > \frac{b+\sqrt{b^2-3a\beta}}{3a}$ | - | + | stable focus |

Table 4.1 shows the different stability regions and the corresponding type of equilibrium point of the Hindmarsh-Rose model. As we can see from Figure 3.2, the resting potential $x_0$ is represented by a stable node and will therefore belong to region **I**. The threshold value $x_{th}$ is in region **II** while it can be described as a saddle-node. The equilibrium point inside the limit-cycle $x_{sp}$ will belong to region **IV**. Thus the following set of inequalities should hold:

$$\begin{array}{c} x_0 < \frac{-2\left(\frac{d}{\beta}-b\right)}{3a} < x_{th}, \\ \frac{b-\sqrt{b^2-3a\beta}}{3a} < x_{sp} < \frac{b+\sqrt{b^2-3a\beta}}{3a}. \end{array} \tag{4.33}$$

Moreover, the maximal amplitude of the membrane potential during spiking $x_{sp,max}$ and the minimal amplitude during spiking $x_{sp,min}$ should satisfy:

$$\begin{array}{l} x_{sp,min} < \frac{b-\sqrt{b^2-3a\beta}}{3a}, \\ x_{sp,max} > \frac{b+\sqrt{b^2-3a\beta}}{3a}. \end{array} \tag{4.34}$$

The main idea is to use inequalities (4.28), (4.29), (4.33) and (4.34) to find the suitable ranges for both the parameters $\beta$ and $d$. However, simulations have shown that satisfying these inequalities is not sufficient to bound the range of the parameter $d$, and therefore the searching domain $\Omega_\beta \times \Omega_d$ cannot be determined. To put some extra restrictions on the domain, it is possible to include equation (4.27) for all equilibrium points. Implementing this equation for $x_0$ will not give any problems, but in the case of $x_{th}$ and $x_{sp}$ some value has to be assigned to $a_0$. Note that the threshold input $a_{0,th}$ at $x_{th}$ can be determined from the ramp-input in the measurements. It is possible to estimate $a_0$ roughly by taking the derivative of signal $x_1$. At the time the block-shaped unit pulse is initiated, a peak will arise in the derivation of the signal $x_1(t)$. The amplitude of this peak is a measure for $a_0$ (Figure 4.4). Given this estimation of $a_0$, equation (4.27) can be evaluated for some points in the neighborhood of $a_0$. However, including these extra equations still do not result in complete boundedness of the searching domain. An extra restriction is necessary. Therefore, consider the solution of the $x_2$-dynamics:

$$x_2(t) = e^{-\beta(t-t_0)}x_2(t_0) + \int_{t_0}^{t} e^{-\beta(t-\tau)}\left(c - dx_1^2(\tau)\right)d\tau. \tag{4.35}$$

Neglecting the exponentially decaying term, (4.35) can be upperbounded by $\frac{c}{\beta}$. Its lower bound is given by $\frac{1}{\beta}(c - dx_{max}^2)$, where $x_{max}$ is the maximal value of $x_1(t)$. Furthermore, it is known that at the points $x_{sp,min}$ and $x_{sp,max}$, which denote the minimal and maximal value of $x_1$ during spiking

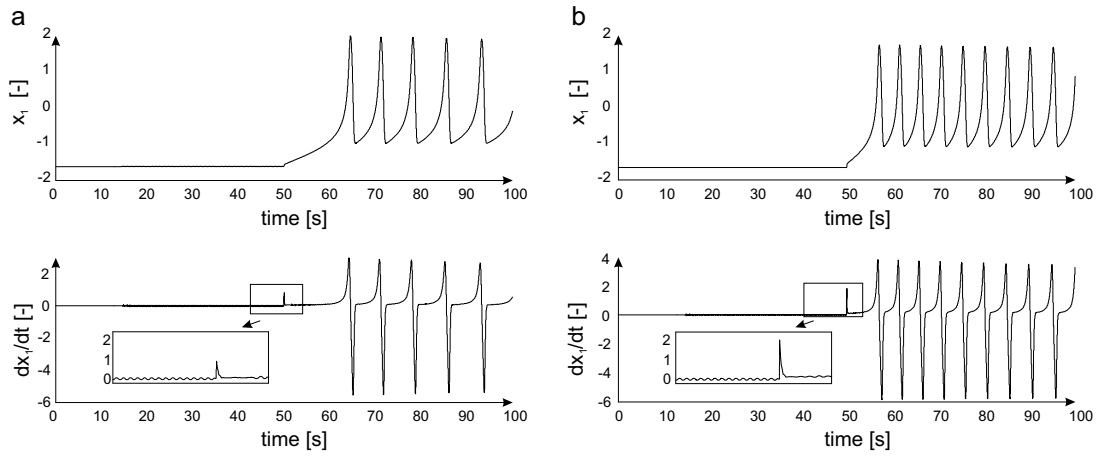


Figure 4.4: Response of the Hindmarsh-Rose model on block-shaped current stimuli. On top the state $x_1$ is plotted. The derivative of the signals is plotted below. a) Stimuli with $a_0 = 1$. b) Stimuli with $a_0 = 2$. In both cases we see the peak at the derivative is a rough estimation of $a_0$ given the input has an amplitude of 1.

respectively, the derivative $\dot{x}_1$ is equal to zero since the function $x_1(t)$ is changing sign at these points. This will give another restriction on the feasible domain, that is:

$$\begin{aligned} \tfrac{1}{\beta}(c - dx_{max}^2) &< ax_{sp,min}^3 - bx_{sp,min}^2 - a_0 < \tfrac{c}{\beta}, \\ \tfrac{1}{\beta}(c - dx_{max}^2) &< ax_{sp,max}^3 - bx_{sp,max}^2 - a_0 < \tfrac{c}{\beta}. \end{aligned} \tag{4.36}$$

Inequalities (4.28), (4.29), (4.33), (4.34), (4.36) together with the equilibrium equation (4.27) evaluated at all equilibrium points will bound the space of all parameters. Therefore searching domain $\Omega_\beta \times \Omega_d$ can be determined from this feasibility analysis based on the stability proporties of the Hindmarsh-Rose model.

# Chapter 5

# Main Results

In the previous chapter the technique to make a fit of measured signals to the Hindmarsh-Rose model is presented. To properly validate this technique, a signal is generated using the Hindmarsh-Rose equations (4.1). Testing with a generated signal will exclude the possibility that the signal could not be described by the model. Furthermore all parameter values are surely constant and known a priori.

## 5.1 Simulations

The signal to test the presented identification technique with will be generated from system (4.1) with the following set of parameters:

$$a = 1,\ b = 4,\ a_0 = 1,\ c = 1,\ d = 6,\ \beta = 1,\ r = 0.01,\ s = 1.$$

As input signal $u(t)$ two $500s$ long block-shaped current stimuli with amplitudes $0.75$ $[-]$ and $1$ $[-]$ are applied. The signal has a period of $2000s$ and is repeated constantly during the parameter estimation process. Figure 5.1 shows the input and generated signal.

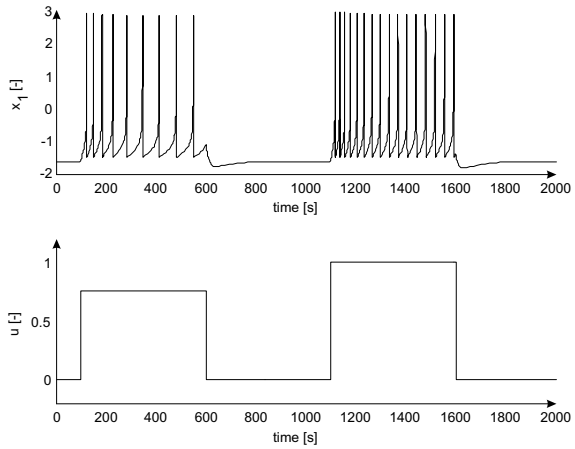


Figure 5.1: Simulation generated signal. The figure on the top shows the output $x_1(t)$ of the system. At the bottom the applied stimuli $u(t)$ is plotted.

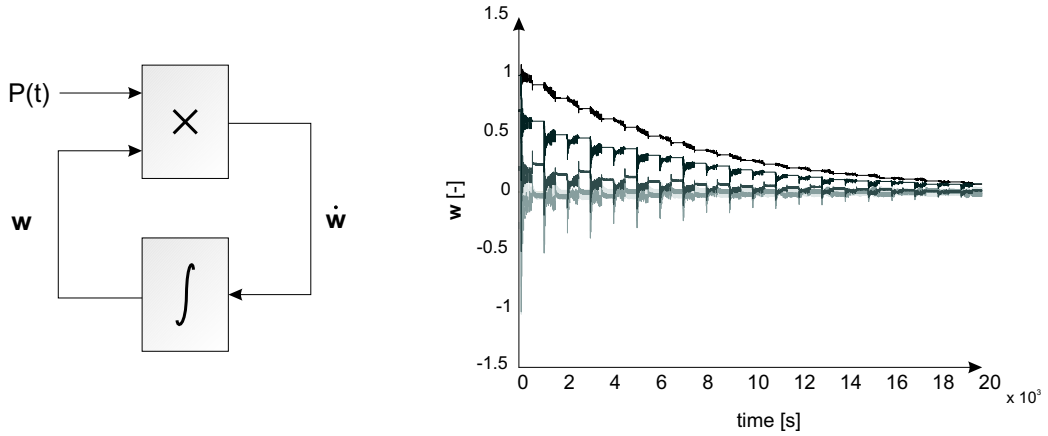


Figure 5.2: Convergence of the $LTV$ system. On the left the block-scheme is drawn. The plot on the right shows the convergence of the system in time with initial condition $\mathbf{w}_0 = [1\,1\,1\,1\,1\,1]^T$.

Let us focus on the part describing the contracting dynamics. First it has to be investigated if the signals are "rich" enough such that estimated parameters values will converge to the desired values. In other words, it has to be investigated if the persistently exciting condition does hold. Numerical simulations show that this condition is satisfied for the period $L = 2000s$ with $\alpha = 0.022$. As a result the $LTV$ system (4.12) is exponentially stable. The next thing to do is to choose constants $\mu, \gamma_a$ and to determine the convergence rate $\rho$. Figure 5.2 shows the $LTV$ system in block-scheme and the convergence of signal $\mathbf{w}$. In this block-scheme the following shorthand notation is used:

$$P(t) = \begin{bmatrix} -\mu & \boldsymbol{\zeta}(t)^T \\ -\gamma_a \boldsymbol{\zeta}(t) & \mathbf{0} \end{bmatrix} \tag{5.1}$$

For $\mu = 0.1$ and $\gamma_a = 100$ the minimal convergence rate $\rho = 0.11$ is found.

Now the contracting dynamics are described and $\rho$ is known, the wandering dynamics can be designed. Therefore, assume $\Omega_\beta = [0.5, \ldots, 2]$ and $\Omega_d = [5, \ldots, 7]$. By choosing constants $\omega_1 = \pi$ and $\omega_2 = 1$ we ensure every point in the bounded searching domain $\Omega_\beta \times \Omega_d$ is visited. Gains $D_\eta$ and $D_f$ are determined using (4.24) and (4.17) where $D_f = \max(D_{f,\beta}, D_{f,d})$. With the given values for $\omega_1$ and $\omega_2$ these gains are determined to be $D_\eta = 1.50$ and $D_f = 17.00$. Furthermore, $\max \parallel \Sigma(\boldsymbol{\lambda}) \parallel = 1$. The maximal $\gamma_w$ is found from (4.26) after optimization of $d_s$ and $\kappa$. With $d_s = 0.58$, $\kappa = 1.61$ we obtain $\gamma_w = 2.74 \cdot 10^{-4}$. Simulations are initiated with several initial conditions with the tolerated error $\delta = 0.25$. The results of the simulation are shown in Figure 5.3. The simulation shows to be successful. All parameter are estimated correctly and the maximal error stays within the pre-defined error tolerance $\delta$.

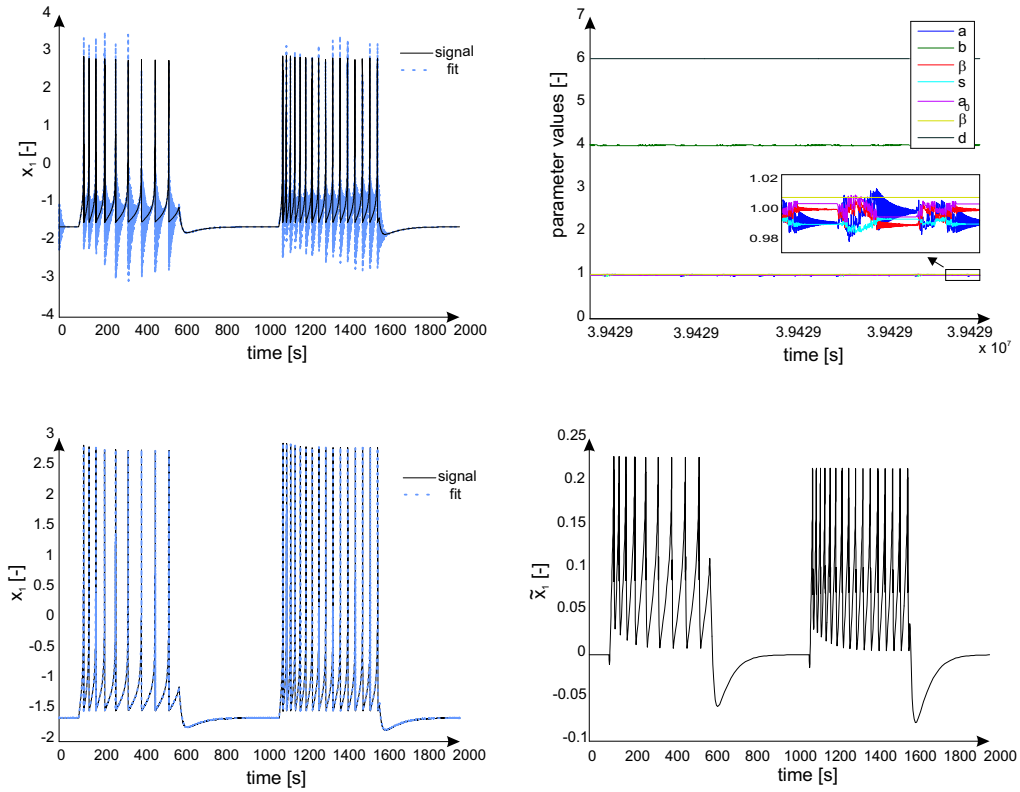


Figure 5.3: Simulation results for the test case. On the top-left the fit with initial conditions is shown. The plot in the top-right shows the parameters after convergence. In the bottom-left we see the successful fit after parameter convergence and the figure in the bottom-right shows the error between the signal and the fit.

## 5.2 Measurements

Now the identification algorithm is successfully validated, the identification using the measured signals can be started. Therefore a single spike train will be selected from the sequence of measurements. Only a single spike train is selected to minimize the influence of possible time-varying membrane conductances. The criteria for this selection is that the interspike intervals show first order behavior. Figure 5.4 shows a selected spike spike train with corresponding interspike intervals. This spike train belongs to the first series of measurements in the PTX case, which can be found in Appendix B.

The selected signal will be discarded from noise by filtering it with a Bessel filter, that is a linear low-pass filter that uses Bessel polynomials. Furthermore the signal will be (spline) interpolated to obtain more measurement points such that smaller time steps can be used in the solver, which in turn should improve accuracy. The measured signal needs to be scaled such that $x_1(t)$ is within the range $[-3, 3]$ which is a typical output range of the Hindmarsh-Rose model. The signal $x_1(t)$ can be obtained by dividing the measured membrane potential $V_m(t)$ by an arbitrary constant. The

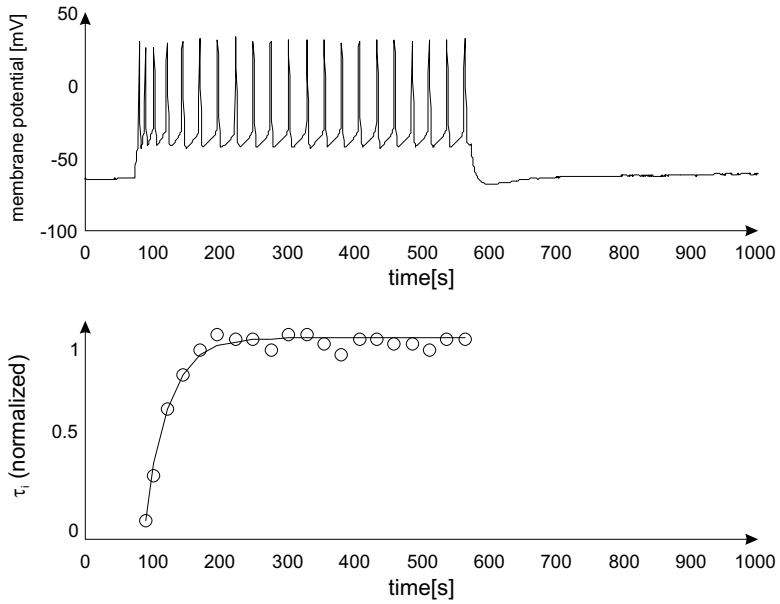


Figure 5.4: The selected single spike train. The figure on top shows the membrane potential as response on a depolarizing current stimuli of $200pA$. Below the interspike intervals $\tau_i$ (circles) and the fit(solid line) are depicted. From these interspike intervals we estimate $r = 0.029$.

parametrization of system (4.1) fully supports this type of scaling. The following scaling is used:

$$x_1(t) = \frac{1}{35} V_m(t)$$

Furthermore, the input function $u(t)$ will be scaled such that $\max(u(t)) = 1$ and the signal $x_1^*(t)$ is obtained by low-pass filtering. Hence, the persistence of excitation of $\boldsymbol{\zeta}(t)$ will be evaluated. Calculations show the persistently exciting condition is fulfilled for $L = 1000s$ and $\alpha = 0.0057$. The contracting dynamics (4.12) are exponentially stable with $\rho = 0.024$ for constants $\mu = 0.2$ and $\gamma_a = 50$.

To design the wandering dynamics properly the searching domains $\Omega_\beta$ and $\Omega_d$ have to be determined. In order to perform the feasibility study described in Section 4.3, information about the threshold values has to be obtained and an estimation of $a_0$ has to be made. As described in Section 4.3 an estimation of $a_0$ can be made by calculating the derivative of signal $x_1(t)$ at the moment of time that the input is applied. We estimate $a_0 \approx 0.4$ by calculating that derivative. From the ramp-input the threshold potential $x_{th}$ and threshold input $a_{0,th}$ are determined. More detail is shown in Figure 5.5. The feasibility study shows $\Omega_\beta = [0.1, \ldots, 1.8]$ and $\Omega_d = [1.5, \ldots, 9]$. With $\omega_1 = \pi, \omega_2 = 1$ and $D_\lambda = 91.07$, we obtain $\gamma_w = 1.68 \cdot 10^{-5}$ with values $d_s = 0.58$ and $\kappa = 1.62$. Simulations are started for several initial conditions, but none of these simulations showed satisfying results, i.e. none of these simulations showed a proper fit. Moreover, the algorithm applied on other selected spike-trains did not produce a fit as well. Unfortunately the $C$++ implementation of the algorithm did not allow to keep track of the error such that it is not possible to determine what is exactly going wrong.

Next, a relaxed problem is investigated with the goal to make a fit on a single spike. A single spike is isolated from a spike train and used to generate repetitive spiking. This signal is shown in Figure 5.6. During this spiking there is no firing frequency adaptation and thus is the influence of the

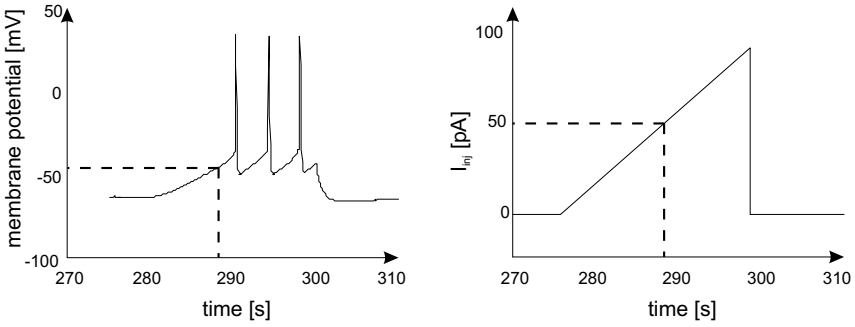


Figure 5.5: On the left the membrane potential as response on a increasing current (ramp) is shown. This input is depicted in the figure on the right. From these figures we determine the threshold potential $V_{th}$ to be $-45mV$ or $x_{th} = -1.28$, and the threshold input $a_{0,th} \approx 0.1$.

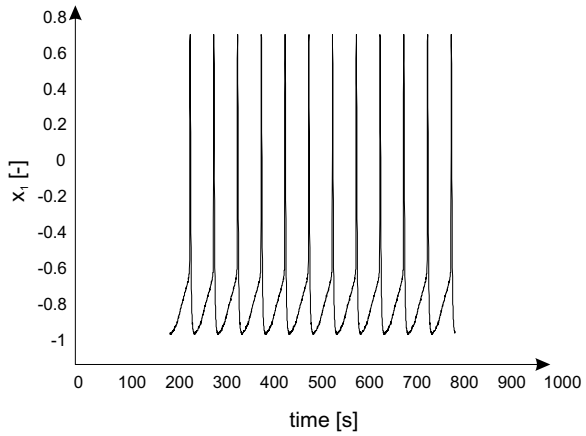


Figure 5.6: Repeated sequence of a single spike.

$x_3$-dynamics minimal. Therefore, the complete $x_3$ dynamics are neglected. Furthermore the input involved is constant. Again, the contracting dynamics and the wandering dynamics are designed properly. However, still there is no fit obtained.

The question arises why it is not possible to obtain a proper fit. There is a possibility that the Hindmarsh-Rose model is not suitable to describe the measured signals. Parameters might for instance be time-varying while they are assumed to be constant. It is also possible that the parametrization of system (4.1) is still too restrictive. Consider instead of simple scaling (5.2) the following affine transformation:

$$x_1(t) = c_s V_m(t) + c_t, \tag{5.2}$$

where $c_s$ is a positive constant responsible for the scaling and $c_t$ is a constant which realizes the translation. Figure 5.7 shows the possibilities when affine transformation (5.2) is used. A generated signal is manually tuned, scaled and translated to obtaine the fit. This Figure actually shows that it might be very important to include an arbitrary translation. The Hindmarsh-Rose model in its original form is not capable to deal with this affine transformation. Therefore the following parametrization of the

Hindmarsh-Rose equations is proposed:

$$\begin{aligned} \dot{x}_1 &= -ax_1^3 + bx_1^2 + \psi_1 x_1 + x_2 - x_3 + a_0 u, \\ \dot{x}_2 &= c - dx_1^2 + \psi_2 x_1 - \beta x_2, \\ \dot{x}_3 &= r\left(s\left(x_1 - x_0\right) - x_3\right). \end{aligned} \tag{5.3}$$

The constants $\psi_1, \psi_2$, which have undetermined sign, extend the Hindmarsh-Rose model in such a way that translation is included. To apply the proposed identification technique with system (5.3) the contracting dynamics needs to be be extended with an extra dimension and the dimensions of searching dynamics will increase to three. System (4.18) has to be redefined and new equations have to be derived to bound the searching domains. Due to time limitation the identification based on (5.3) is not worked out.

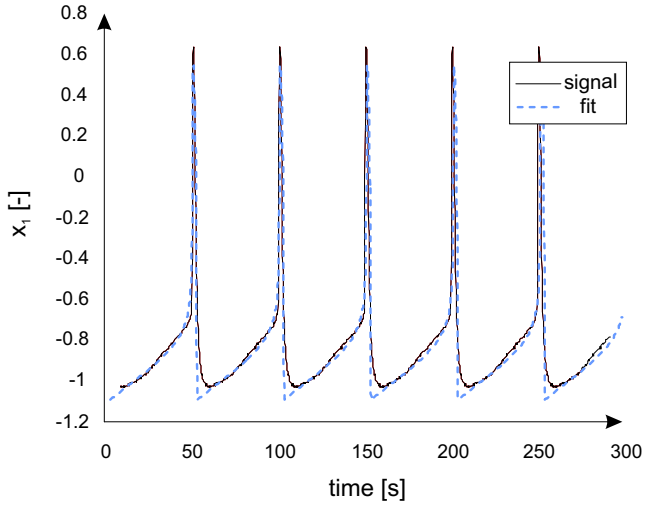


Figure 5.7: Fit on sequence of single spikes using the affine transformation

# Chapter 6

# Conclusions and Recommendations

## 6.1 Conclusions

In this study a method is described to estimate parameters of a neuronal model. The membrane potential is measured from neurons from the hippocampus of mice in a common current clamped setup and in a current clamped setup where tonic $GABA_A$receptors have been blocked by treating the neuron with the chemical Picrotoxin. The model to make the fit with was chosen to be the Hindmarsh-Rose model. This phase-plane model describes a large number of biophysical features with a minimal number of state variables and parameters. The model with the used parametrization did not satisfy the condition of observability and therefore conventional methods like adaptive observers could not be used. Without the ability to use conventional identification techniques, a new technique making use of contracting and wandering dynamics is presented. The contracting dynamics contain parameters that appear linearly in known and measurable signals of the one-dimensional equivalent of the Hindmarsh-Rose model. With a suitable update law and given that the persistently exciting condition does hold, these parameters are estimated correctly and the dynamics of the contracting part are exponentially stable. The wandering dynamics perform a search in a bounded domain for parameter values which can not be estimated by the contracting dynamics. The speed of the search is mainly determined by the time the contracting dynamics need to reach its steady-state. Furthermore, inequalities are presented which are used to determine the feasible searching domain. Next, the algorithm is implemented in $Matlab$ and $C$++, from which the $C$++ implementation turned out to be about hundred times faster then the $Matlab$ solution.

The algorithm is first successfully tested in simulations with a generated signal from the Hindmarsh-Rose equations. In the case where measured signals are used no fit is obtained. Maybe it is not possible to fit a Hindmarsh-Rose model on measured membrane potentials since the model does not deal with time-varying parameter. However, it is more likely that a wrong type of scaling is used. Preliminary results using an affine transformation instead of scaling are promising.

## 6.2 Recommendations

Since there are strong indications that a fit with the use of an affine transformation is possible, it is recommended to work out the presented technique with the contracting and wandering dynamics using the extended Hindmarsh-Rose model which includes the affine transformation. Therefore new equations need to be derived to obtain a feasible searching domain and the wandering dynamics need to be redesigned. Furthermore it might be a better to use a variable step solver, or even a more

advanced solver, in the $C$++ algorithm to increase accuracy. Furthermore it is recommended to extend the $C$++ implementation such that it is possible to keep track of the error.

# Bibliography


[1] Bullock T.H, Bennett M.V.L, Johnston D, Josephson R, Marder E, Fields R.D. *The Neuron Docterine, REDUX*. SCIENCE, vol 310, november 2005.

[2] Chadderton P, Margrie T.W, Hausser M. *Integration of quanta in cerebellar granule cells during sensory processing*. Nature, 2004.

[3] Hindmarsh J.L, Rose R.M. *A model of neuronal bursting using three coupled first order differntial equations*. Proc. R. Soc. Lond. B **221**, 87-102, 1984.

[4] Hindmarsh J.L, Cornelius P. *The Development of the Hindmarsh-Rose model for bursting*. BURSTING: The Genesis of Rhythm in the Nervous System, CH 1, 2005.

[5] Hodgkin A.L, Huxley A.F. *A quantitative description of membrane current and its application to conductionand excitation in nerve*. J.Physol 117, 500-544, 1952.

[6] Izhikevich E.M. *Which Model to Use for Cortical Spiking Neurons?* IEEE trans. on neural networks, september 2004.

[7] Khalil H.K. *Nonlinear Systems*. Prentice Hall, 2002.

[8] Kreisselmeier G. *Adaptive Observers with Exponential Rate of Convergence*. IEEE trans. on Automatic Control, vol. ac-22, no.1, february 1977.

[9] Koch C. *Biophysics of computation*. Oxford University Press, 1999.

[10] Lamsa K, Heeroma J.H, Kullmann D.M. *Hebbian LTP in feed-forward inhibitory interneurons and the temporal fidelity of input discrimination*. Nat Neurosci, 2005.

[11] London M, Hausser M. *Dendritic computation*. Annu Rev Neurosci, 2005.

[12] Loría A. *Explicit convergenve rates for MRAC-type systems*. Automatica, september 2003.

[13] Loría A, Panteley E. *Uniform exponential stability of linear time-varying systems: revisited*. Systems & Control Letters 47, 13-24, 2002.

[14] Marino R. *Adaptive Observers for Single Output Nonlinear Systems*. IEEE trans. on Automatic Control, vol. 35, no.9, september 1990.

[15] Marino R, Tomei P. *Global Adaptive Observers for Nonlinear Systems via Filtered Transformations*. IEEE trans. on Automatic Control, vol. 37, no.8, august 1992.

[16] Mitchell S.J, Silver R.A. *Shunting inhibition modulates neuronal gain during synaptic excitation*. Neuron, 2003.

[17] Morgan A.P, Narendra K.S. *On the stability of nonautonomous differential equations* $\dot{x} = [A + B(t)]x$ *with skew symmetric matrix* $B(t)^*$. SIAM J. Control and Optimization, Vol. 15, No.1, January 1977.

[18] Pouille F, Scanziani M. *Enforcement of temporal fidelity in pyramidal cells by somatic feed-forward inhibition*. Science, 2001.

[19] Semyanov A, Walker M.C, Kullmann D.M, Silver R.A. *Tonically active GABA A receptors: modulating gain and maintaining the tone*. Trends Neurosci, 2004.

[20] Tyukin I.Y, Prokorov D.V., van Leeuwen C. *Adaptation and Parameter Estimation in Systems with Unstable Target Dynamics and Nonlinear Parametrization*. http://arxiv.org/abs/math.OC/0506419, 2005.

[21] Tyukin I.Y, Steur E, Nijmeijer H, van Leeuwen C. *Non-uniform Attractivity, Meta-stability and Small-gain Theorems*. preprint (2006).

# Appendix A

# Gains $D_{f,\beta}$ and $D_{f,d}$

In this appendix, analytical expressions for the gain $D_{f,\beta}$ and $D_{f,d}$ in (4.16) are presented. The error in $\tilde{x}_1(t)$ caused by errors in the parameters $\beta$ and $d$ is given by:

$$\begin{aligned} f(\beta,d,t)-f(\hat{\beta},\hat{d},t) &= \Big(f(\beta,d,t)-f(\hat{\beta},d,t)\Big) \\ &+ \Big(f(\hat{\beta},d,t)-f(\hat{\beta},\hat{d},t)\Big), \end{aligned} \tag{A.1}$$

where

$$x_2(t)=e^{-\beta t}x_2(t=0)+\int_0^t e^{-\beta(t-\tau)}dx_1^2(\tau)d\tau. \tag{A.2}$$

The first part of the righthand side of (A.2) is monotonic decreasing with respect to the time, and its value is assumed to be small. Therefore, this part will be neglected in further analysis. Given $x(t)$ is bounded, $f(\beta,d,t)-f(\hat{\beta},d,t)$ will be bounded by the following expression:

$$d \parallel x_1^2(\tau) \parallel_{\infty,[t_0,t]} \int_0^t \left(e^{-\beta(t-\tau)}-e^{-\hat{\theta}_1(t-\tau)}\right)d\tau. \tag{A.3}$$

With the use of Hadamard's lemma, (A.3) can be explicitly written as some function $D_{f,\beta}(\cdot)$ multiplied by $(\beta-\hat{\beta})$. Therefore, introduce $\beta^\star \in [\beta,\hat{\beta}]$ and a dimensionless number $\varsigma \in [0,1]$ such that

$$\beta^\star=\varsigma\beta+(1-\varsigma)\hat{\beta} \tag{A.4}$$

Equations (A.2) and (A.4) can be combined to the following expression:

$$\begin{aligned} & d \parallel x_1^2(\tau) \parallel_{\infty,[t_0,t]} \left(\int_0^1 \tfrac{\partial}{\partial\beta^\star}\left(\int_0^t e^{-\beta^\star(t-\tau)}\partial\tau\right)\partial\nu\right)(\beta-\hat{\beta}) \\ &= d \parallel x_1^2(\tau) \parallel_{\infty,[t_0,t]} \left(\int_0^1 \tfrac{\partial}{\partial\beta^\star}\left(\tfrac{1}{\beta^\star}\left(1-e^{-\beta^\star t}\right)\right)\partial\nu\right)(\beta-\hat{\beta}) \\ &= d \parallel x_1^2(\tau) \parallel_{\infty,[t_0,t]} \left(\tfrac{-1}{\beta\hat{\beta}}+\tfrac{\beta e^{\beta t}-\hat{\beta}e^{\hat{\beta}t}}{\beta\hat{\beta}(\beta-\hat{\beta})e^{(\beta+\hat{\beta})t}}\right)(\beta-\hat{\beta}) \\ &= D_{f,\beta}(\beta,\hat{\beta},d,t)(\beta-\hat{\beta}). \end{aligned}$$

Denoting the monotonically decreasing part of $D_{f,\beta}$ by $\epsilon_\beta(t)$, it is easy to see $|f(\beta,d,t) - f(\hat{\beta},d,t)|$ will be upperbounded by

$$D_{f,\beta}|\beta - \hat{\beta}| + \epsilon_\beta(t), \tag{A.5}$$

where

$$D_{f,\beta} \quad = \quad \left(\frac{d}{\beta\hat{\beta}}\right) \parallel x_1^2(\tau) \parallel_{\infty,[t_0,t]} .$$

Using the same approach, the bounds of $f(\hat{\beta},d,t) - f(\hat{\beta},\hat{d},t)$ will be derived. Let us again neglect the monotonically decreasing terms, such that the following expression holds:

$$\begin{aligned} &\int_0^t \left(e^{-\hat{\beta}(t-\tau)}\right)(d-\hat{d})x_1^2(\tau)d\tau \\ \leq &\int_0^t \left(e^{-\hat{\beta}(t-\tau)}\right) d\tau(d-\hat{d}) \parallel x_1^2(\tau) \parallel_{\infty,[t_0,t]} . \end{aligned}$$

It is straightforward that (A.6) can be bounded from above by

$$D_{f,d}|d - \hat{d}| + \epsilon_d(t), \tag{A.6}$$

where

$$D_{f,d} \quad = \quad \frac{1}{\hat{\beta}} \parallel x_1^2(\tau) \parallel_{\infty,[t_0,t]}$$

and $\epsilon_d(t)$ is a monotonically decreasing function in time.

# Appendix B

# Recorded Signals

In this project the membrane potential of single neurons from the hippocampus of mice is measured. In total two series of measurements have been acquired.

## B.1 Recordings Series 1

This first series of measurements have been taken at 20 september 2005. Membrane potential is measured from neurons from the hippocampus of mice with a sampling rate 2kHz. The stimuli are shown in Figure B.1.

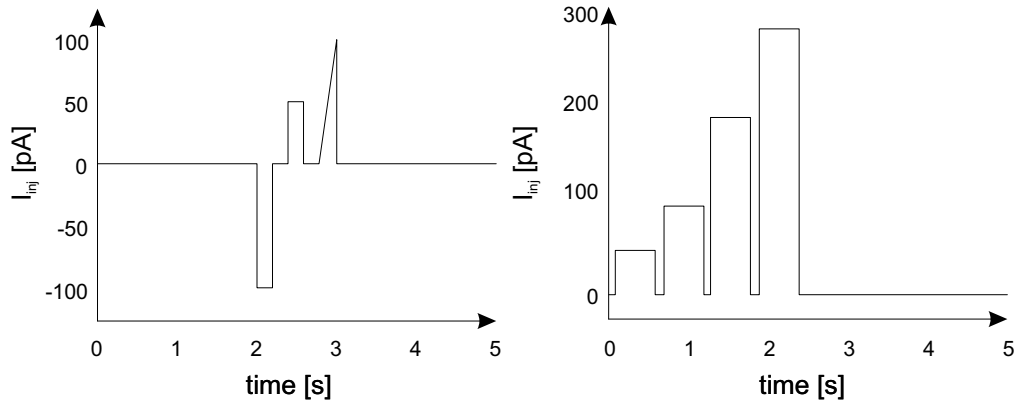


Figure B.1: Applied current stimuli. The sequence of inputs plotted in the figure on the left will be denoted by *input* 1. The figure on the right shows *input* 2.

Figures B.2 and B.4 show the membrane potential as function of input 1 in the control case and the PTX case, respectively. The membrane potential as function of input 2 are shown in Figure B.3 and B.5.

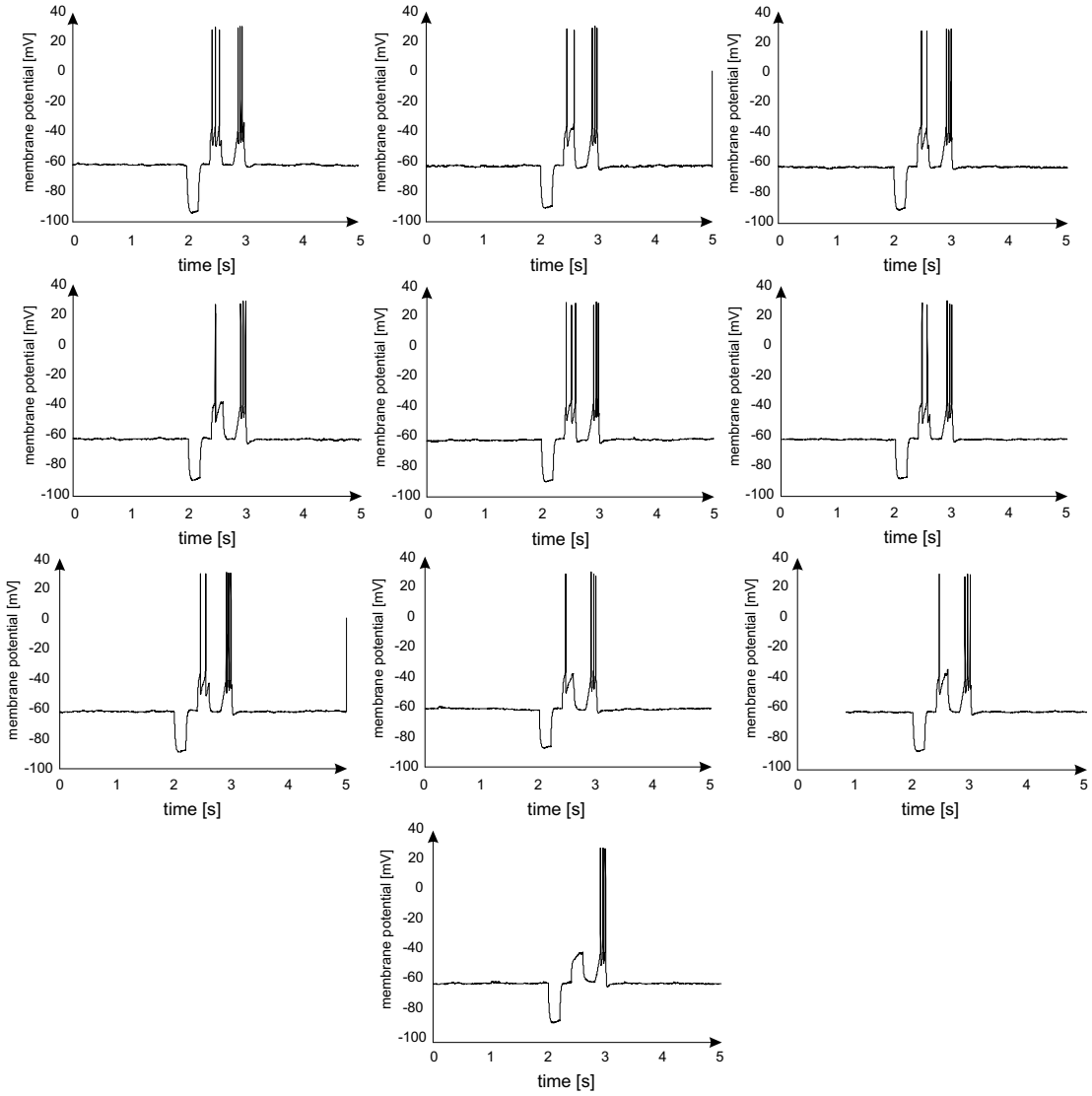


Figure B.2: Control, input 1.

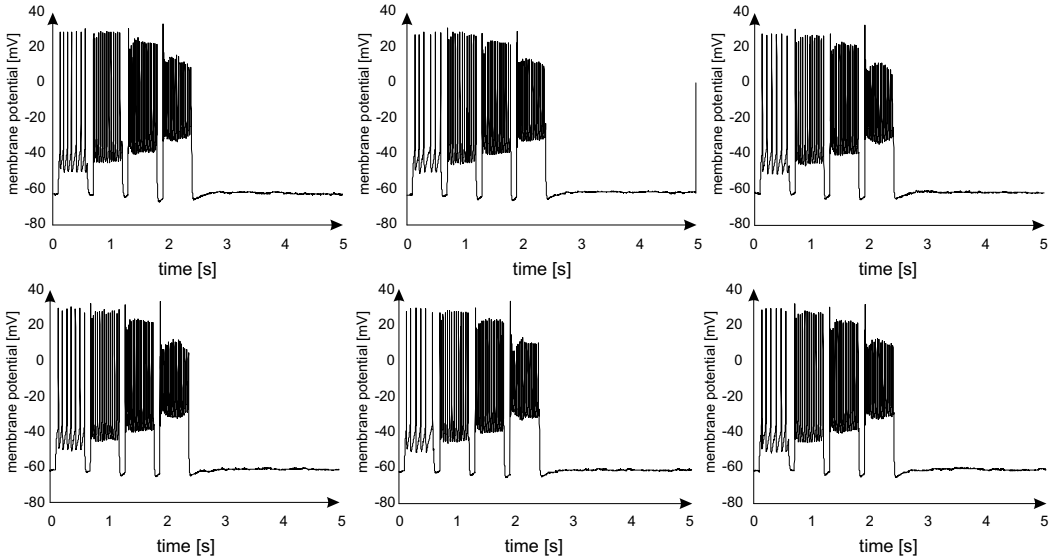


Figure B.3: Control, input 2.

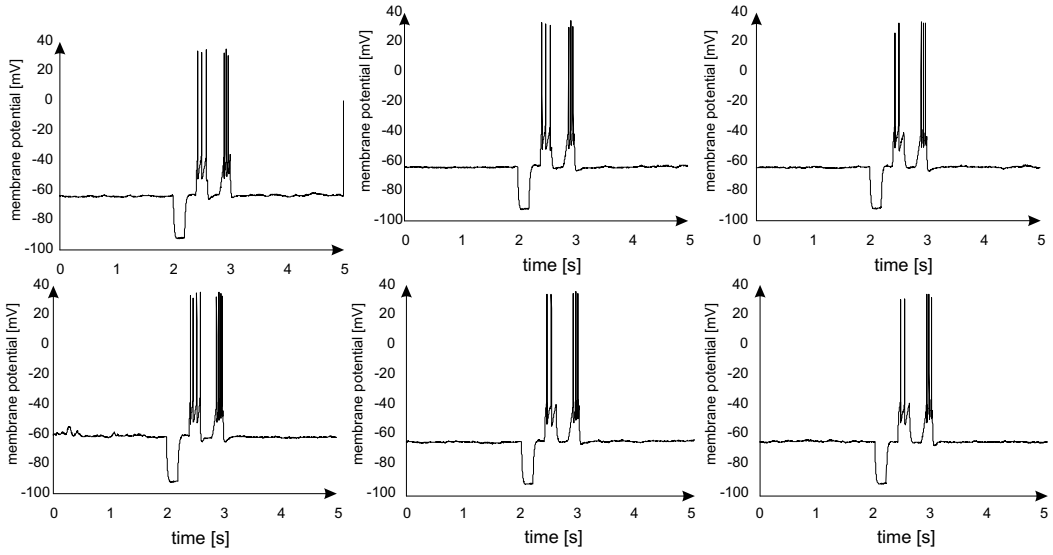


Figure B.4: PTX, input 1.

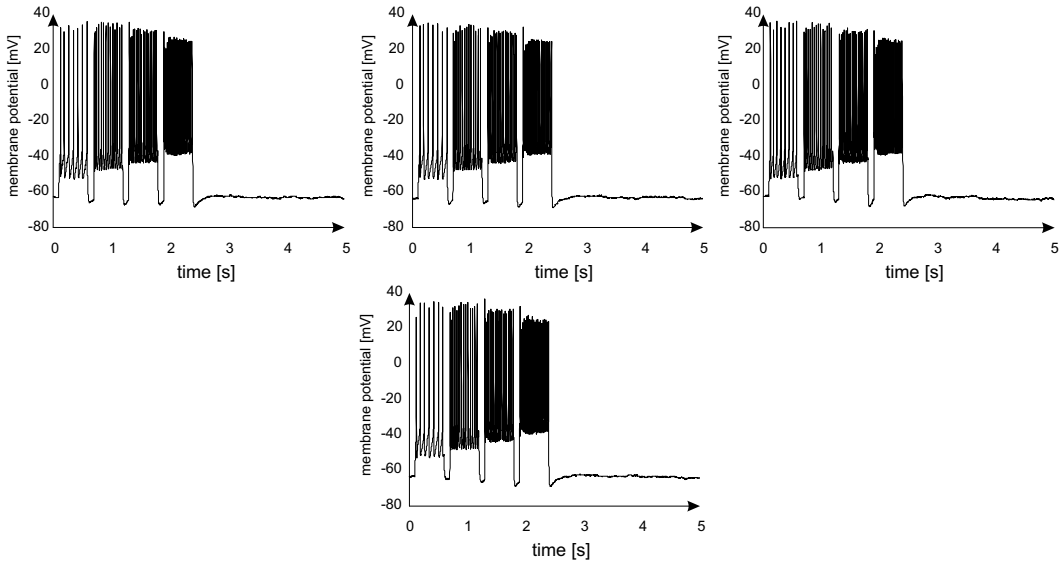


Figure B.5: PTX, input 2.

## B.2 Recordings Series 2

This series of measurements have been taken on 21 september 2005. Again the used neurons are from the hippocampus of mice.Measurements are taken in the control case and the PTX case with sampling rates of 2kHz and 6kHz. Figure B.6 shows the applied current stimuli.

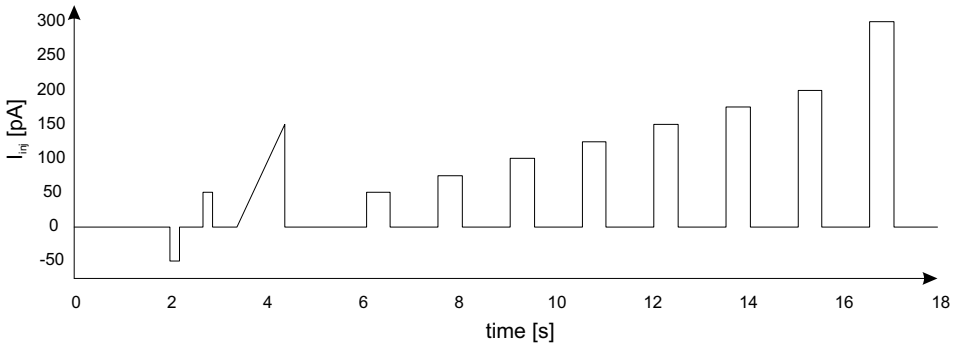


Figure B.6: Applied current stimuli used for measurements of 21 september 2005.

Figures B.7, B.9 and B.10 show the membrane potential measured with a sampling rate of 2kHz in the control case and the PTX case. The measurements performed at 6kHz are given in Figures B.8 and B.11.

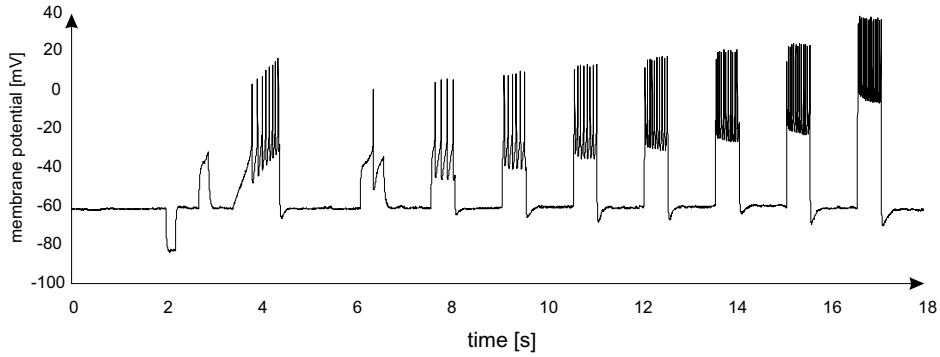


Figure B.7: Control, 2kHz.

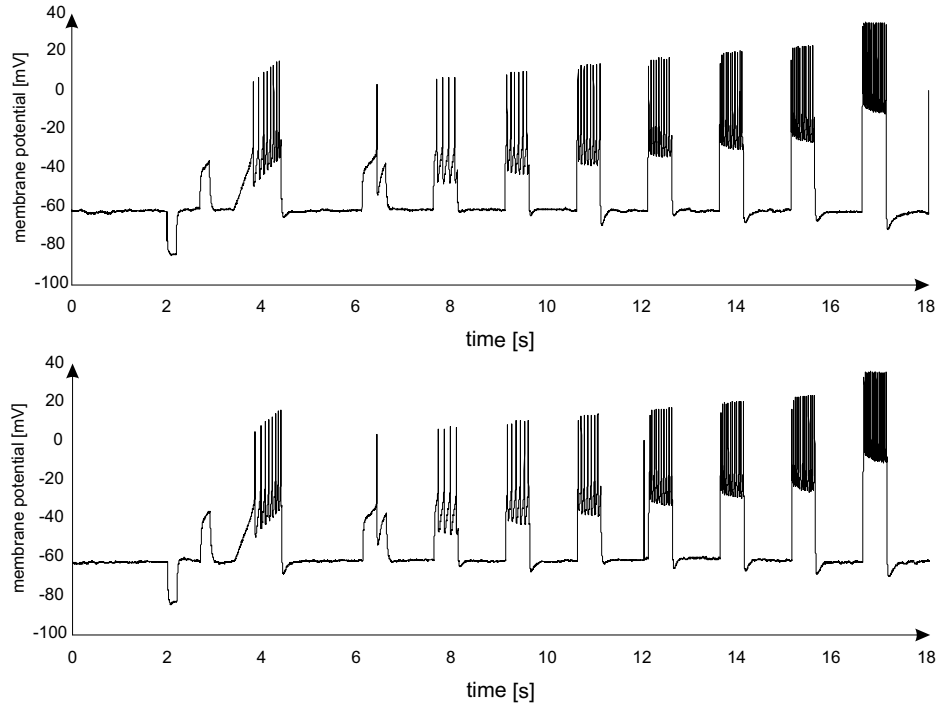


Figure B.8: Control, 6kHz.

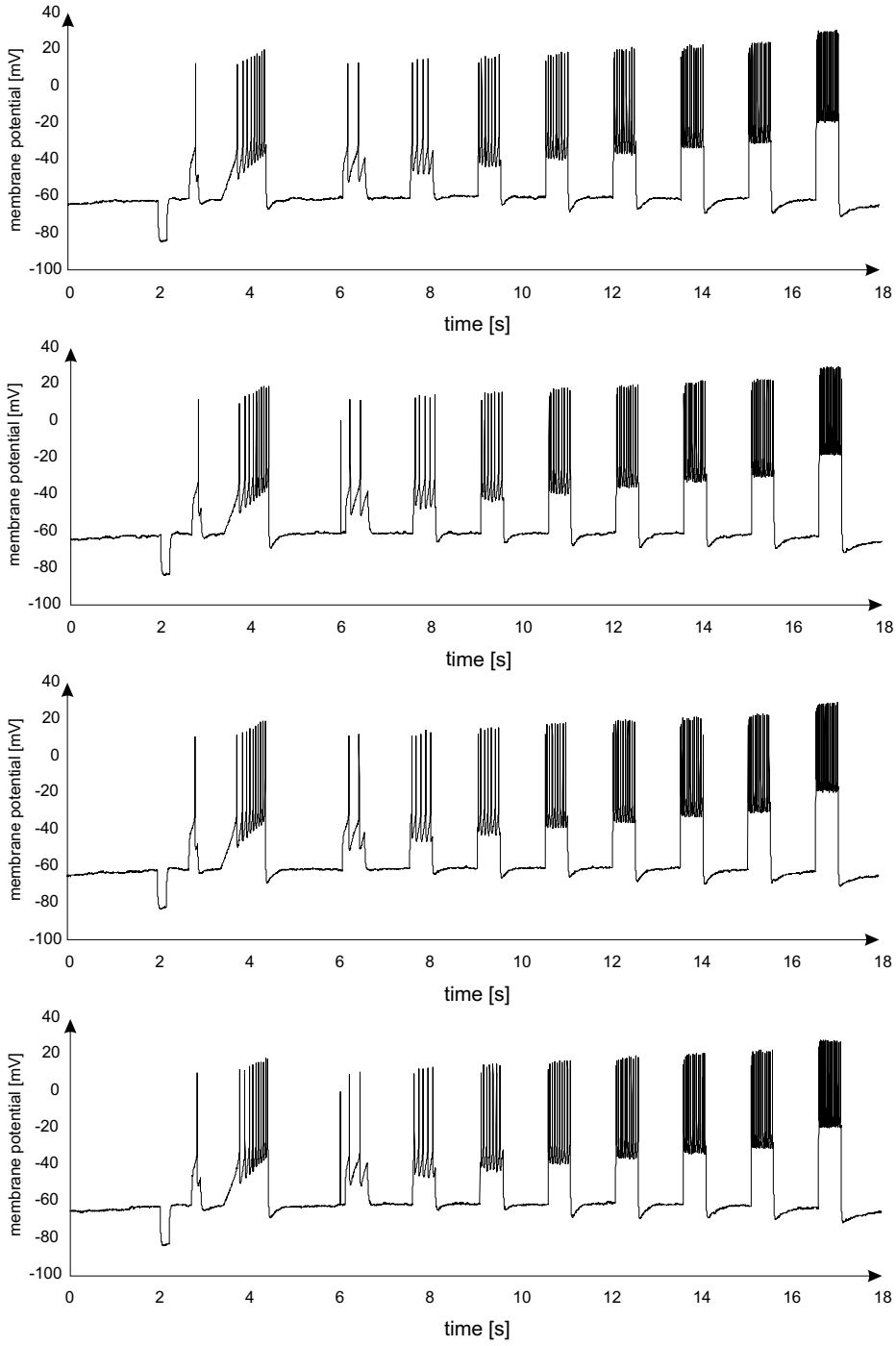


Figure B.9: PTX, 2kHz.

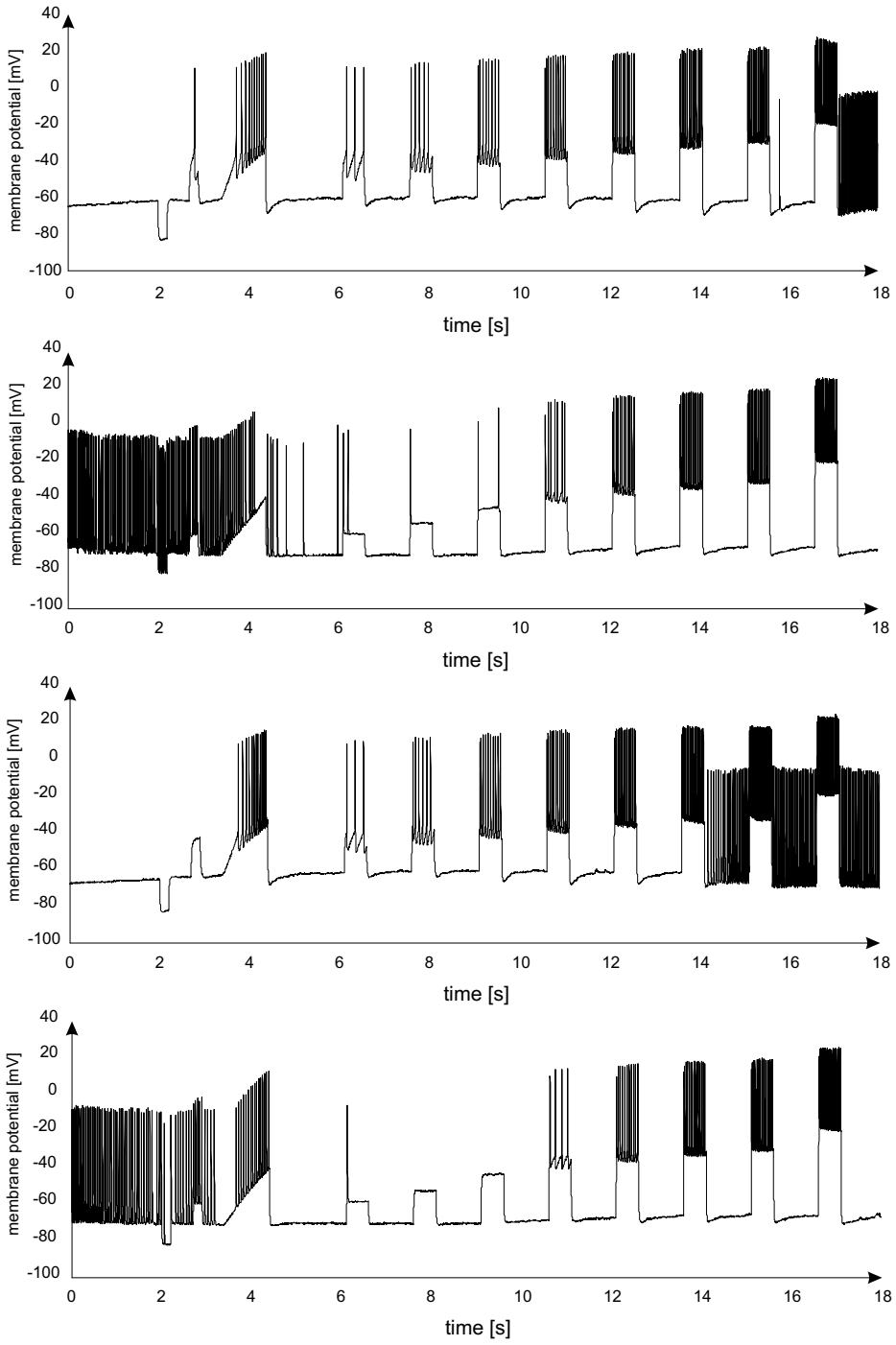


Figure B.10: PTX, 2kHz.

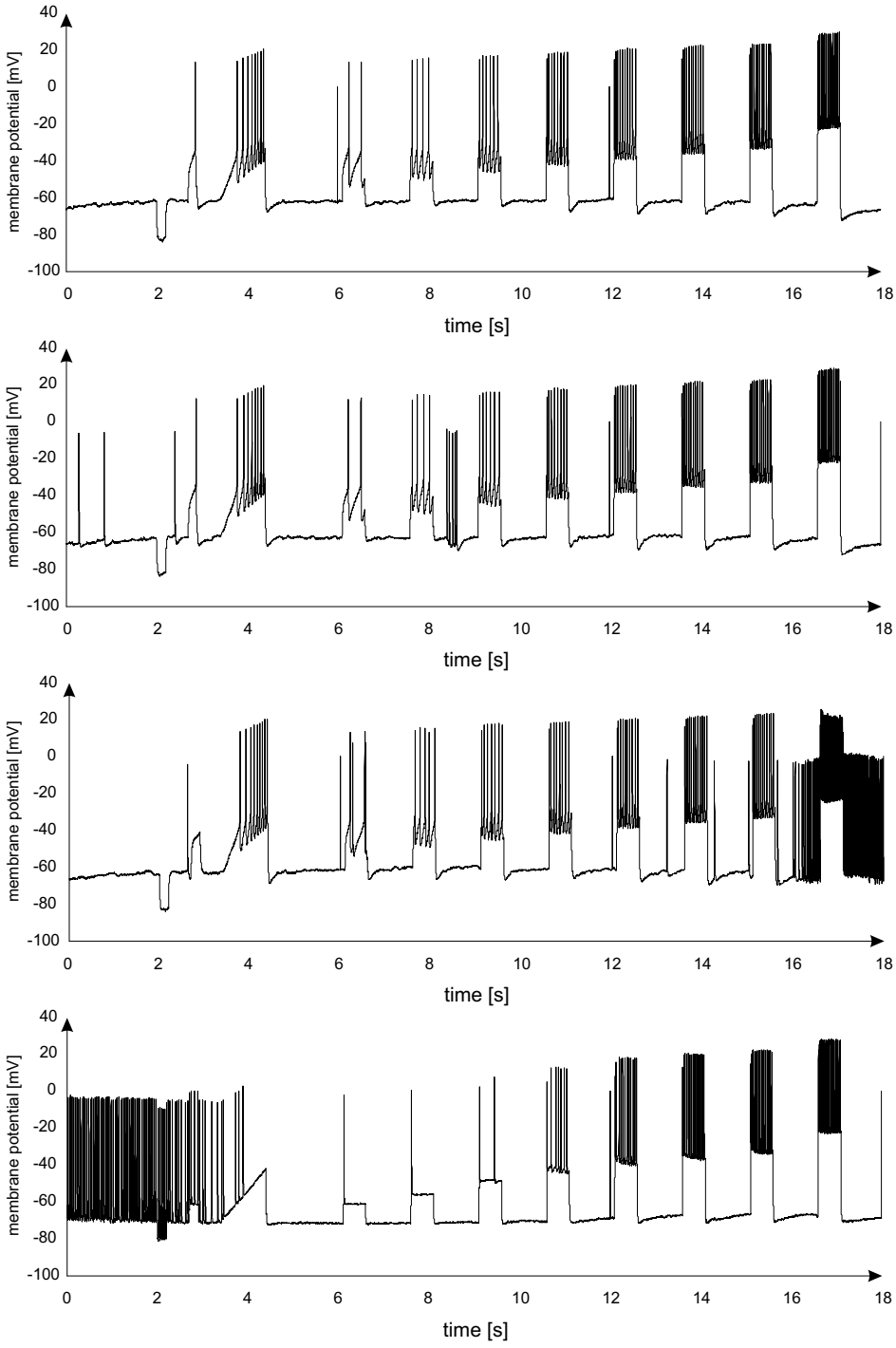


Figure B.11: PTX, 6kHz.

# Appendix C

# Numerical Algorithm

In this appendix the implementation of the identification algorithm in both $Matlab$ and $C$++ is given.

## C.1 Matlab

```
function identification_algorithm

% created by: Erik Steur
% date: 26-okt-2005
%
% %%%%%%%%%%%%%%%%%%%%%%%%%%%%%%%%%%%%%%%%%%%%%%%%%%%%%%%%%%%%%%%%%%%%%%% %
% inputs
% %%%%%%%%%%%%%%%%%%%%%%%%%%%%%%%%%%%%%%%%%%%%%%%%%%%%%%%%%%%%%%%%%%%%%%% %
%
% v(t)        =       membrane potential (scaled)
% v_star(t)   =       low-pass filtered v(t) (cut-off freq. r)
% u(t)        =       injected current (scaled)
%
% %%%%%%%%%%%%%%%%%%%%%%%%%%%%%%%%%%%%%%%%%%%%%%%%%%%%%%%%%%%%%%%%%%%%%%% %
% constants:
% %%%%%%%%%%%%%%%%%%%%%%%%%%%%%%%%%%%%%%%%%%%%%%%%%%%%%%%%%%%%%%%%%%%%%%% %
%
% mu          =       coupling signal/observer
% gamma_a     =       update gain contracting dynamics
% gamma_w     =       update gain wandering dynamics
% omega1      =       omega1
% omega2      =       omega2
% ub_beta     =       upper bound parameter space of beta
% lb_beta     =       lower bound parameter space of beta
% ub_d        =       upper bound parameter space of d
% lb_d        =       lower bound parameter space of d
% delta       =       delta
% Ts          =       time interval measurement
% dTs         =       sample rate measurement
%
```

```
% %%%%%%%%%%%%%%%%%%%%%%%%%%%%%%%%%%%%%%%%%%%%%%%%%%%%%%%%%%%%%%%%%%%%%%%% %

% general
clear all;close all;clc

global mu gamma_a gamma_w omega_1 omega_2 ub_beta lb_beta ub_d lb_d ...
       delta Ts dTs

% read data
load data

% assign parameter values
mu          =
gamma_a     =
gamma_w     =
omega_1     =
omega_2     =
ub_beta     =
lb_beta     =
ub_d        =
lb_d        =
delta       =
Ts          =
dTs         =

% initial conditions
a0          =
b0          =
nu0         =
s0          =
a00         =
x0          =
y0          =

X0 = [x0; y0; a0; b0; nu0; s0; a00];

% generate solution
Tspan = [];

[Tout Xout] = ode23(@id_alg,Tspan,[X0;[1;0;1;0]]);

save Iddata Tout Xout

% %%%%%%%%%%%%%%%%%%%%%%%%%%%%%%%%%%%%%%%%%%%%%%%%%%%%%%%%%%%%%%%%%%%%%%%% %
function dx = id_alg(t,x)

global mu gamma_a gamma_w omega_1 omega_2 ub_beta lb_beta ub_d lb_d ...
       delta Ts dTs

dx = zeros(11,1);
```

```
% Signal value at time t and make a repetitive sequence
V           =       v((mod(t,Ts)/dTs)+1);
V_star      =       v_star((mod(t,Ts)/dTs)+1);
U           =       u((mod(t,Ts)/dTs)+1);

% %%%%%%%%%%%%%%%%%%%%%%%%%%%%%%%%%%%%%%%%%%%%%%%%%%%%%%%%%%%%%%%%%%%%%%% %
% regressor part
% %%%%%%%%%%%%%%%%%%%%%%%%%%%%%%%%%%%%%%%%%%%%%%%%%%%%%%%%%%%%%%%%%%%%%%% %

a     = x(3);
b     = x(4);
nu    = x(5);
s     = x(6);
a0    = x(7);

dx(1) = -a*V^3 + b*V^2 + nu + s*V_star + a0*U + mu*(V-x(1)) - x(2);

% update law

dx(3) = -gamma_a*(-V^3)*(V-x(1));
dx(4) = -gamma_a*(V^2)*(V-x(1));
dx(5) = -gamma_a*(V-x(1));
dx(6) = -gamma_a*(-V_star)*(V-x(1));
dx(7) = -gamma_a*(U)*(V-x(1));

% %%%%%%%%%%%%%%%%%%%%%%%%%%%%%%%%%%%%%%%%%%%%%%%%%%%%%%%%%%%%%%%%%%%%%%% %
% wandering part
% %%%%%%%%%%%%%%%%%%%%%%%%%%%%%%%%%%%%%%%%%%%%%%%%%%%%%%%%%%%%%%%%%%%%%%% %

% auxiliary system with interconnection
dx(8)  = gamma_w*function_delta(V,x(1))*x(9);
dx(9)  = -gamma_w*function_delta(V,x(1))*omega_1^2*x(8);
dx(10) = gamma_w*function_delta(V,x(1))*x(11);
dx(11) = -gamma_w*function_delta(V,x(1))*omega_2^2*x(10);

beta   = (ub_beta-lb_beta)/2 * ( 2*asin(x(8))/pi + 1 ) + lb_beta;
d      = (ub_d-lb_d)/2 * ( 2*asin(x(10))/pi + 1 ) + lb_d;

dx(2) = -d*V^2 - beta*x(2);

% %%%%%%%%%%%%%%%%%%%%%%%%%%%%%%%%%%%%%%%%%%%%%%%%%%%%%%%%%%%%%%%%%%%%%%% %
function y = function_delta(x,xhat)

if abs(x-xhat)<delta,
    y = 0;
else
    y = abs(x-xhat);
end
```

## C.2 *C++*

The algorithm is implemented in *C++* with *GNU* scientific library (*GSL*). Specific information about the *GNU* project and *GSL* can be found at *http://www.gnu.org*. In the *C++* implementation wandering dynamics (4.23), (D.7) are approximated with the equations

$$\begin{array}{l} \beta(t+\Delta t) = \beta(t) + \frac{\omega_1}{\pi} \parallel \tilde{x}_1((t+\Delta t)) \parallel_{\Delta(\delta)} \cdot \phi(\beta, \beta_{min}, \beta_{max}) \cdot \Delta t, \\ d(t+\Delta t) = d(t) + \frac{\omega_1}{\pi} \parallel \tilde{x}_1((t+\Delta t)) \parallel_{\Delta(\delta)} \cdot \phi(d, d_{min}, d_{max}) \cdot \Delta t, \end{array} \tag{C.1}$$

where

$$\phi(\sigma, \sigma_{min}, \sigma_{max}) = \begin{cases} \gamma_w & \text{if } \sigma_{min} \leq \sigma \leq \sigma_{max} \\ -\gamma_w & \text{else} \end{cases} . \tag{C.2}$$

This approximation is used to avoid the special function $\arcsin(\cdot)$.

```
// created by: Peter Jurica, Erik Steur
// date: 8-nov-2005

#include <stdio.h>
#include <memory.h>
#include <math.h>
#include <time.h>
#include <gsl/gsl_integration.h>
#include <gsl/gsl_errno.h>
#include <gsl/gsl_matrix.h>
#include <gsl/gsl_math.h>
#include <gsl/gsl_odeiv.h>


const double PI = 3.14159265358979323846264 3;

const double mu          =   ;
const double gamma_a     =   ;
double gamma_w           =   ;
double gamma_beta        =   gamma_w;
double gamma_d           =   gamma_w;
const double ub_beta     =   ;
const double lb_beta     =   ;
const double ub_d        =   ;
const double lb_d        =   ;
const double delta       =   ;
const double Ts          =   ;
const double dTs         =   ;

// initial conditions
const double x10         =   ;
const double x20         =   ;
const double a0          =   ;
const double b0          =   ;
const double nu0         =   ;
const double s0          =   ;
```

```
const double a00         =   ;
const double beta        =   ;
const double d0          =   ;

static const unsigned int NUMEL = 100001;
double u[NUMEL], v[NUMEL];

// load data
void load_data()
{
    FILE *f = fopen("data.dat","rb");
    fread(u,sizeof(double),NUMEL,f);
    fread(v,sizeof(double),NUMEL,f);
    fread(vstar,sizeof(double),NUMEL,f);
    fclose(f);
}

// function mod
inline double mod(double x, double y)
{
    return x < 0 ? y-fmod(-x,y) : fmod(x,y);
}

//function mod
inline unsigned int fround(double x)
{
    return (unsigned int)( floor(x + 0.5) );
}

// deadzone
inline double phi(double x, double xhat)
{
    return fabs(x - xhat) <= delta ? 0.0 : 1.0;
}

// switch sign of gamma_w
inline void update_gammas(const double x[])
{
    if (x[6] > ub_beta || x[6] < lb_beta)
        gamma_beta = -gamma_beta;
    if (x[7] > ub_d || x[7] < lb_d)
        gamma_d = -gamma_d;
}
// algorithm
inline int func (double t, const double x[], double f[], void *params)
{
    // linear interpolation
    const double di = mod(t,Ts)/dTs;
    const unsigned int ifl = floor(di);
    const unsigned int ice = ceil(di);
```

```
    const double V          =       v[ifl] + (v[ice] - v[ifl])*(di-ifl);
    const double U          =       u[ifl] + (u[ice] - u[ifl])*(di-ifl);
    const double Vstar      =       vstar[ifl] + (vstar[ice] - vstar[ifl])*(di-ifl);


    const double a          =       x[1];
    const double b          =       x[2];
    const double nu         =       x[3];
    const double s          =       x[4];
    const double a0         =       x[5];

    const double aVx0 = fabs((V-x[0]));
    const double pVx0 = phi(V,x[0]);
    const double V2 = V*V;
    const double V3 = V*V2;


    f[0]       =       -a*V3 + b*V2 + x[8] - s*Vstar + nu + a0*U + mu*(V-x[0]);


    f[1]       =       gamma_a*(-V3)*(V-x[0]);
    f[2]       =       gamma_a*V2*(V-x[0]);
    f[3]       =       gamma_a*(V-x[0]);
    f[4]       =       gamma_a*(-Vstar)*(V-x[0]);
    f[5]       =       gamma_a*U*(V-x[0]);

    update_gammas(x);
    f[6]       =       -gamma_beta*aVx0*pVx0;
    f[7]       =       -gamma_d*aVx0*pVx0;

    f[8]       =       -x[7]*V2 - x[6]*x[8];

    return GSL_SUCCESS;
}
// solver
int main_fixed(double* X0)
{
    const gsl_odeiv_step_type * T = gsl_odeiv_step_rk2;
    gsl_odeiv_step * s = gsl_odeiv_step_alloc (T, 10);
    gsl_odeiv_system sys = {func, NULL, 10, NULL};

    double t = 0, t1 = 100;//1000;
    double h = 1e-3;
    double y[10], y_err[10];
    memcpy(y, X0, 10*sizeof(double));
    double dydt_in[10], dydt_out[10];

    GSL_ODEIV_FN_EVAL(&sys, t, y, dydt_in);
```

```
FILE* fout = NULL;
fclose(fopen("simlog.dat","wb"));
double trec_start, elapsed;
time_t start, finish;
time(&start);
int count = 0;
while (true) ///(t < t1)
{

    int status = gsl_odeiv_step_apply (s, t, h,
                                       y, y_err,
                                       dydt_in,
                                       dydt_out,
                                       &sys);

    if (status != GSL_SUCCESS)
      break;

    memcpy(dydt_in, dydt_out, 10*sizeof(double));

    t += h;
    count++;
    if (count%10 == 0)
    {
        if (fout != NULL)
        {
            fwrite(&t,sizeof(double),1,fout);
            fwrite(y,sizeof(double),10,fout);

            if (t >= trec_start + 10.0)
            {
                fclose(fout);
                fout = NULL;
            }
        }

        if (count == (int)(10.0*1.0/h))
        {
            char flag = 0;
            FILE * f = fopen("plotme.txt","rt");
            fread(&flag,sizeof(char),1,f);
            fclose(f);
            if (flag == '1')
            {
                f = fopen("plotme.txt","wt");
                fprintf(f,"0");
                fclose(f);

                fout = fopen("res.dat","wb");
                trec_start = t;
```

```
                }

                count = 0;

                time(&finish);
                elapsed = difftime(finish,start);
                if (elapsed > 600.0)
                {
                    f = fopen("simlog.dat","ab");
                    fwrite(&t,sizeof(double),1,f);
                    fwrite(y,sizeof(double),10,f);
                    fwrite(&gamma_beta,sizeof(double),1,f);
                    fwrite(&gamma_w,sizeof(double),1,f);
                    fclose(f);

                    time(&start);
                }
            }
        }
    }
    fclose(fout);

    gsl_odeiv_step_free (s);
    return 0;
}

int main(void)
{
    load_data();

    double X0[] = { x10,
                    a0,
                    b0,
                    nu0,
                    s0,
                    a00,
                    beta0,
                    d0,
                    x20 };    // 9 states

    int ret = main_fixed(X0);

    return ret;
}
```

# Appendix D

# Non-uniform Attractivity, Meta-stability and Small-gain Theorems

Ivan Tyukin[1] Erik Steur[2], Henk Nijmeijer [3], Cees van Leeuwen[4]

November 24, 2005 (preprint version)

**abstract**

This paper addresses a problem of asymptotic, yet non-uniform in initial conditions, convergence of state of dynamical systems into a given domain of their state space. The necessity to consider non-uniform convergence arises when either the system itself is inherently globally unstable (intermittent, itinerant, or meta-stable) or the problem statements make stable solution impossible (general optimization problems, nonlinear parameter identification and adaptation). Conventional techniques for analysis of convergence to Lyapunov-unstable equilibria, usually rely on detailed knowledge of the properties of the vector-fields of systems or a-priori assume boundeness of the state. In contrast to these we propose a method that does not require boundedness a-priori and relies only on qualitative information about the system dynamics. This information are mere estimates of the input-output maps, steady-state characteristics and decomposability into the interconnection of stable, contracting compartment and unstable, exploratory part. The method can be applied to problems of analysis asymptotic behavior of locally instable systems and systems in the vicinity of attractor ruins, parameter identification and non-dominating adaptation in the presence of nonlinear parametrization. Applications in the design and analysis of models for visual detection and recognition are discussed.

**Keywords:** non-uniform convergence, small-gain, input-output stability

[1]**Corresponding author**. Laboratory for Perceptual Dynamics, RIKEN (Institute for Physical and Chemical Research) Brain Science Institute, 2-1, Hirosawa, Wako-shi, Saitama, 351-0198, Japan, e-mail: {tyukinivan}@brain.riken.jp

[2]Dept. of Mechanical Engineering, Technical University of Eindhoven, The Netherlands

[3]Dept. of Mechanical Engineering, Technical University of Eindhoven, The Netherlands

[4]Laboratory for Perceptual Dynamics, RIKEN (Institute for Physical and Chemical Research) Brain Science Institute, 2-1, Hirosawa, Wako-shi, Saitama, 351-0198, Japan, e-mail: {ceesvl}@brain.riken.jp

## D.1 Notation

Throughout the paper we use the following notational conventions. Symbol $\mathbb{R}$ denotes the filed of real numbers, $\|\mathbf{x}\|$ denotes the Euclidian norm in $\mathbf{x} \in \mathbb{R}^n$, $\mathcal{C}^k$ denotes the space of functions that are at least $k$ times differentiable. Symbol $\mathcal{K}$ denotes the class of all strictly increasing functions $\kappa : \mathbb{R}_+ \to \mathbb{R}_+$ such that $\kappa(0) = 0$. If, in addition, $\lim_{s\to\infty} \kappa(s) = \infty$ we say that $\kappa \in \mathcal{K}_\infty$. Further, $\mathcal{K}_e$ (or $\mathcal{K}_{e,\infty}$) denotes the class of functions whose restriction on $[0, \infty)$ is from $\mathcal{K}$ (or $\mathcal{K}_\infty$). Symbol $\mathcal{KL}$ denotes the class of functions $\beta : \mathbb{R}_+ \times \mathbb{R}_+ \to \mathbb{R}_+$ such that $\beta(\cdot, 0) \in \mathcal{K}$ and $\beta(0, \cdot)$ is monotonically decreasing.

Let it be the case that $\mathbf{x} \in \mathbb{R}^n$ and $\mathbf{x}$ can be partitioned into two vectors $\mathbf{x}_1 \in \mathbb{R}^q$, $\mathbf{x}_1 = (x_{11}, \ldots, x_{1q})^T$, $\mathbf{x}_2 \in \mathbb{R}^p$, $\mathbf{x}_2 = (x_{21}, \ldots, x_{2p})^T$, $q + p = n$, then $\oplus$ denotes the concatenation of two vectors: $\mathbf{x} = \mathbf{x}_1 \oplus \mathbf{x}_2$.

By $L^n_\infty[t_0, T]$ we denote the space of all functions $\mathbf{f} : \mathbb{R}_+ \to \mathbb{R}^n$ such that $\|\mathbf{f}\|_{\infty,[t_0,T]} = \sup\{\|\mathbf{f}(t)\|, t \in [t_0, T]\} < \infty$, and $\|\mathbf{f}\|_{\infty,[t_0,T]}$ stands for the $L^n_\infty[t_0, T]$ norm of $\mathbf{f}(t)$. Let $\mathcal{A}$ be a set in $\mathbb{R}^n$, and $\|\cdot\|$ be the usual Euclidean norm in $\mathbb{R}^n$. By symbol $\|\cdot\|_{\mathcal{A}}$ we denote the following induced norm:

$$\|\mathbf{x}\|_{\mathcal{A}} = \inf_{\mathbf{q}\in\mathcal{A}} \{\|\mathbf{x} - \mathbf{q}\|\}$$

Let $\Delta \in \mathbb{R}_+$ then notation $\|\mathbf{x}\|_{\mathcal{A}_\Delta}$ stands for the following:

$$\|\mathbf{x}\|_{\mathcal{A}_\Delta} = \begin{cases} \|\mathbf{x}\|_{\mathcal{A}} - \Delta, & \|\mathbf{x}\|_{\mathcal{A}} > 0 \\ 0, & \|\mathbf{x}\|_{\mathcal{A}} \le \Delta \end{cases}$$

Symbol $\|\cdot\|_{\mathcal{A}_\infty,[t_0,t]}$ will stand for the following notation:

$$\|\mathbf{x}(\tau)\|_{\mathcal{A}_\infty,[t_0,t]} = \sup_{\tau\in[t_0,t]} \|\mathbf{x}(\tau)\|_{\mathcal{A}}$$

## D.2 Introduction

From systems and control theory to physics, chemistry, or biology, science attributes fundamental importance to analyzing the asymptotic behavior of dynamical systems. Most of these analyses are based around the concept of Lyapunov stability [15], [29], [28], i.e. continuity of the flow $\mathbf{x}(t, \mathbf{x}_0) : \mathbb{R}_+ \times \mathbb{R}^n \to L^n_\infty[t_0, \infty]$ with respect to $\mathbf{x}_0$ [18], in combination with the standard notion of *attracting set* [8]:

**Definition 3** *Set $\mathcal{A}$ is the attracting set iff it is*

*1) closed, invariant, and*

*2) for some neighborhood $\mathcal{V}$ of $\mathcal{A}$ and for all $\mathbf{x}_0 \in \mathcal{V}$ the following holds:*

$$\mathbf{x}(t, \mathbf{x}_0) \in \mathcal{V} \; \forall \; t \ge 0; \tag{D.1}$$

$$\lim_{t\to\infty} \|\mathbf{x}(t, \mathbf{x}_0)\|_{\mathcal{A}} = 0 \tag{D.2}$$

Property (D.1) in Definition 3 stipulates existence of the trapping region $\mathcal{V}$ (neighborhood of $\mathcal{A}$), while property (D.2) ensures attractivity, or convergence, which, due to (D.1), is uniform in $\mathbf{x}_0$ in a neighborhood of $\mathcal{A}$. This uniformity apparently is necessary for continuity in $L^n_\infty[t_0, \infty]$ and, consequently, Lyapunov stability.

Although conventional concepts of the attracting set and Lyapunov stability are a powerful tandem in a various applications, some problems cannot be solved in this framework. Condition (D.1), for example, could be violated in systems with intermittent, itinerant or meta-stable dynamics. And in

general it does not hold when the dynamics, loosely speaking, is exploring rather than contracting. Such systems appear in the analysis of: synchronization [4], [19] [5]; in global optimization [10]; in problems of identification and adaptation in the presence of general nonlinear parameterization [25]; in manoeuvring, path searching [23] and decision making in intelligent systems [26], [27]. Even when it is appropriate to consider a system as stable, the necessity to find a proper Lyapunov function may be an obstacle when the system's dynamics is only partially known. Trading stability requirements for the sake of convergence might be a possible remedy in these cases. Known results in this direction can be found in [11], [21][6].

Despite property (D.1) might not hold or be intentionally abandoned in all these cases, convergence of $\mathbf{x}(t, \mathbf{x}_0)$ to the set $\mathcal{A}$, property (D.2), should still be maintained. This motivates us to study conditions of convergence without requiring that it is uniform in a neighborhood of $\mathcal{A}$. Suitable concept which captures this requirement is the concept of weak or Milnor attraction [17]:

**Definition 4** *Set $\mathcal{A}$ is weakly attracting, or Milnor attracting set if*

*1) it is closed, invariant and*

*2) for some set $\mathcal{V}$ (not necessarily neighborhood of $\mathcal{A}$) with strictly positive measure and for all $\mathbf{x}_0 \in \mathcal{V}$ limiting relation (D.2) holds*

Conventional methods such as La Salle's invariance principle [14] or central manifold theory [6], can, in principle, address the issues of local non-uniform convergence at the expenses of detailed knowledge of vector-fields of the dynamical systems. When such information is not available and the system can be though as mere interconnection of input-output maps, small-gain theorems [30],[12] are usually efficient. These results, however, apply under assumption of stability of each component in interconnection.

In our present study we aim to compromise between generality of input-output approaches [30], [12] and specificity of fundamental notions of limit sets and invariance (notions that play central role in [14], [6]). The object of our study is a class of systems that can be decomposed into an attracting, or stable compartment $\mathcal{S}_a$ and an exploratory, generally unstable part $\mathcal{S}_w$. We show that under specific conditions, which involve only estimates of the input-output maps of $\mathcal{S}_a$ and $\mathcal{S}_w$, there is a set $\mathcal{V}$ in the system state space such that trajectories starting in $\mathcal{V}$ remain bounded. The result is formally stated in Theorem 1. In case an additional measure of invariance is defined for $\mathcal{S}_a$ (steady-state characteristic in our case), weak, Milnor attracting set emerges. Its location is completely defined by the zeros of steady-state response of system $\mathcal{S}_a$. We demonstrate with examples how this basic result can be used in the problems of design and analysis of control systems, identification/adaptation algorithms and systems for processing of visual information.

The paper is organized as follows. In Section 3 we formally state the problem and provide specific assumptions on class of the systems under consideration. Section 4 contains the main results of our present study. In Section 5 we provide several corollaries of the main result to specific problems. Section 6 contains examples, and Section 7 concludes the paper.

[5] See also [20] where the striking difference between stable and "almost stable" synchronization in terms of the coupling strengthes for a pair of the Lorenz oscillators is demonstrated analytically

[6] In our own Examples section, we demonstrate how explorative dynamics can solve the problem of simultaneous state and parameter observation for a system which cannot be transformed into the canonical adaptive observer form [2]

## D.3 Problem Formulation

The paper is concerned with the study of the asymptotic behavior of a system that can be decomposed into two interconnected subsystems $\mathcal{S}_a$ and $\mathcal{S}_w$:

$$\begin{aligned} \mathcal{S}_a &: (u_a, \mathbf{x}_0) \mapsto \mathbf{x}(t) \\ \mathcal{S}_w &: (u_w, \mathbf{z}_0) \mapsto \mathbf{z}(t) \end{aligned} \tag{D.3}$$

where $u_a \in \mathcal{U}_a \subseteq L_\infty[t_0, \infty]$, $u_w \in \mathcal{U}_w \subseteq L_\infty[t_0, \infty]$ are the spaces of inputs to $\mathcal{S}_a$ and $\mathcal{S}_w$ respectively, $\mathbf{x}_0 \in \mathbb{R}^n$, $\mathbf{z}_0 \in \mathbb{R}^m$ stand for the initial conditions, and $\mathbf{x}(t) \in \mathcal{X} \subseteq L^n_\infty[t_0, \infty]$, $\mathbf{z}(t) \in \mathcal{Z} \subseteq L^m_\infty[t_0, \infty]$ are the states.

System $\mathcal{S}_a$ represents the contracting dynamics. More precisely, we require that $\mathcal{S}_a$ is input-to-state stable[7] [22] with respect to a compact set $\mathcal{A}$:

**Assumption 1 (***Contracting dynamics)*

$$\mathcal{S}_a: \quad \|\mathbf{x}(t)\|_{\mathcal{A}} \leq \beta(\|\mathbf{x}(t_0)\|_{\mathcal{A}}, t - t_0) + c\|u_a(t)\|_{\infty,[t_0,t]},\ \forall t_0 \in \mathbb{R}_+,\ t \geq t_0 \tag{D.4}$$

*where function $\beta(\cdot,\cdot) \in \mathcal{KL}$, and $c > 0$ is some positive constant.*

In what follows we will assume that function $\beta(\cdot,\cdot)$ and constant $c$ are known or can be estimated a-priori. Contracting property of unperturbed dynamics of $\mathcal{S}_a$ is specified in terms of function $\beta(\cdot,\cdot)$ in (D.4). Propagation of the input to output is characterized in terms of the continuous mappings which, in our case is chosen for simplicity to be linear. Notice that this mapping should not necessarily be contracting.

System $\mathcal{S}_w$ stands for the searching or wandering dynamics. We will consider $\mathcal{S}_w$ subject to the following conditions:

**Assumption 2 (***Wandering dynamics) System $\mathcal{S}_w$ is forward-complete:*

$$u_w(t) \in \mathcal{U}_w \Rightarrow \mathbf{z}(t) \in \mathcal{Z},\ \forall\, t \geq t_0,\ t_0 \in \mathbb{R}_+$$

*and there exists an "output" function $h : \mathbb{R}^m \to \mathbb{R}$, and two "bounding" functions $\gamma_0 \in \mathcal{K}_{\infty,e}$, $\gamma \in \mathcal{K}_{\infty,e}$ such that the following integral equality holds:*

$$\mathcal{S}_w: \int_{t_0}^{t} \gamma_1(u_w(\tau))d\tau \leq h(\mathbf{z}(t_0)) - h(\mathbf{z}(t)) \leq \int_{t_0}^{t} \gamma_0(u_w(\tau))d\tau,\ \forall\, t \geq t_0,\ t_0 \in \mathbb{R}_+ \tag{D.5}$$

Inequality (D.5) implies *monotonicity* of function $h(\mathbf{z}(t))$ in $t$. For convenience, we assume in addition that there exist functions $\gamma_{0,1} : \mathbb{R}_+ \to \mathbb{R}_+$ and $\gamma_{0,2} : \mathbb{R}_+ \to \mathbb{R}_+$ such that

$$\gamma_0(a \cdot b) \leq \gamma_{0,1}(a) \cdot \gamma_{0,2}(b), \tag{D.6}$$

for all bounded $a, b \in \mathbb{R}_+$. Notice that these functions can always be derived for locally Lipschitz $\gamma_0(\cdot)$. No further assumptions will be imposed a-priori on $\mathcal{S}_a$, $\mathcal{S}_w$.

Let us now consider the following interconnection of (D.4), (D.5) with coupling $u_a(t) = h(\mathbf{z}(t))$, and $u_s(t) = \|\mathbf{x}(t)\|_{\mathcal{A}}$. Hence, equations of the combined system can be written as

$$\begin{aligned} \|\mathbf{x}(t)\|_{\mathcal{A}} \leq& \beta(\|\mathbf{x}(t_0)\|_{\mathcal{A}}, t - t_0) + c\|h(\mathbf{z}(t))\|_{\infty,[t_0,t]} \\ \int_{t_0}^{t} \gamma_1(\|\mathbf{x}(\tau)\|_{\mathcal{A}})d\tau \leq& h(\mathbf{z}(t_0)) - h(\mathbf{z}(t)) \leq \int_{t_0}^{t} \gamma_0(\|\mathbf{x}(\tau)\|_{\mathcal{A}})d\tau, \end{aligned} \tag{D.7}$$

[7] In general, as will be demonstrated later with the examples, our analysis can be carried out for (integral) input-to-output/state stable systems as well.

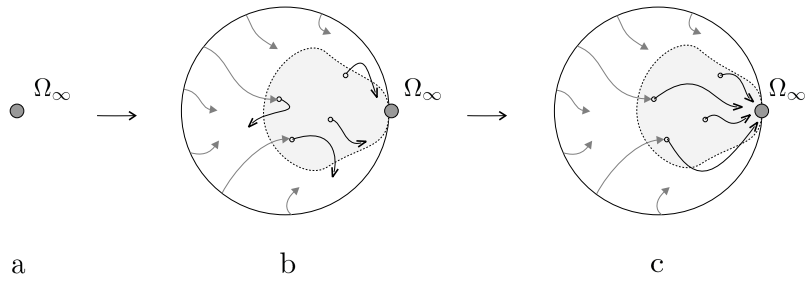


Figure D.1: Emergence of a weak (Milnor) attracting set $\Omega_\infty$

In the present paper we going to address the following set of questions regarding asymptotic behavior of interconnection (D.7): is there a set (weak trapping set in the system state space) such that trajectories of interconnection which start in this set are bounded? It is natural to expect that, existence of such set depends on specific functions $\gamma_0(\cdot)$, $\gamma_1(\cdot)$ in (D.7) and also on properties of $\beta(\cdot,\cdot)$ and values of $c$. In case such set exists and defined, the next question is therefore: where the trajectories will converge and what are the characterizations of these domains?

## D.4 Main Results

In this section we provide formal statements of main results of our present study. In Section D.4.1, we formulate conditions ensuring that there exists a point $\mathbf{x}_0 \oplus \mathbf{z}_0$ such that the $\omega$-limit set of $\mathbf{x}_0 \oplus \mathbf{z}_0$ is bounded in the following sense

$$\|\omega_{\mathbf{x}}(\mathbf{x}_0 \oplus \mathbf{z}_0)\|_{\mathcal{A}} < \infty, \;\; |h(\omega_{\mathbf{z}}(\mathbf{x}_0 \oplus \mathbf{z}_0))| < \infty \tag{D.8}$$

Then we show that the set $\Omega'$ of all points $\mathbf{x}' \oplus \mathbf{z}'$ for which the $\omega$-limit set satisfies condition (D.8) has non-zero volume in $\mathbb{R}^n \times \mathbb{R}^m$.

In order to verify whether an attracting set exists in $\omega(\Omega')$, that is strictly smaller than $\omega(\Omega')$, we use an additional characterization of the contracting system $\mathcal{S}_a$. This characterization is the intuitively clear notion of the input-to state *steady-state characteristics*[8] of a system. It is possible to show that in case system $\mathcal{S}_a$ has a steady-state characteristic, then there exists an attracting set in $\Omega'$ and this set is uniquely defined by the zeros of the steady-state characteristics of $\mathcal{S}_a$. The diagram, illustrating the steps of our analysis as well as the sequence of conditions leading to the emergence of the attracting set in (D.7) is provided in Fig. 1

### D.4.1 Emergence of the trapping region. Small-gain conditions

Before we formulate the main results of this subsection let us first comment briefly on the machinery of our analysis. First of all we introduce three sequences

$$\mathcal{S} = \{\sigma_i\}_{i=0}^{\infty}, \quad \Xi = \{\xi_i\}_{i=0}^{\infty}, \;\; \mathcal{T} = \{\tau_i\}_{i=0}^{\infty}$$

The first sequence, $\mathcal{S}$ (see Fig.2), partitions the interval $[0, h(\mathbf{z}_0)]$, $h(\mathbf{z}_0) > 0$ into the union of shrinking subintervals $H_i$:

$$[0, h(\mathbf{z}_0)] = \cup_{i=0}^{\infty} H_i, \;\; H_i = [\sigma_i h(\mathbf{z}_0), \sigma_{i+1} h(\mathbf{z}_0)] \tag{D.9}$$

For the sake of transparency, let us define this property formally in the form of Condition 1

[8] A more precise definition of the steady-state characteristics is given in Section D.4.2

**Condition 1 (Partition of $\mathbf{z}_0$)** *Sequence $\mathcal{S}$ is strictly monotone and converging*

$$\{\sigma_n\}_{n=0}^{\infty} : \lim_{n\to\infty} \sigma_n = 0,\ \sigma_0 = 1 \tag{D.10}$$

Sequences $\Xi$ and $\mathcal{T}$ will specify the desired rates $\xi_i \in \Xi$ of contracting dynamics in (D.4) terms of function $\beta(\cdot,\cdot)$ and time $T_i > \tau_i \in \mathcal{T}$. Let us, therefore, impose the following constraint on the choice of $\Xi$, $\mathcal{T}$

**Condition 2 (Rates of contraction, part 1)** *For the given sequences $\Xi$, $\mathcal{T}$ and function $\beta(\cdot,\cdot) \in \mathcal{KL}$ in (D.4) the following inequality holds:*

$$\beta(\cdot, T_i) \leq \xi_i \beta(\cdot, 0),\ \forall\, T_i \geq \tau_i \tag{D.11}$$

Condition 2 states that for the given, yet arbitrary, factor $\xi_i$ and time instant $t_0$ the amount of time $\tau_i$ is needed for the state $\mathbf{x}$, to reach the following domain:

$$\|\mathbf{x}\|_{\mathcal{A}} \leq \xi_i \beta(\|\mathbf{x}(t_0)\|_{\mathcal{A}}, 0)$$

In order to specify the desired convergence rates $\xi_i$, in addition to (D.11) it will be necessary to define also a measure of propagation of initial conditions $\mathbf{x}_0$ and input $h(\mathbf{z}_0)$ to the state $\mathbf{x}(t)$ of contracting dynamics (D.4) when the system travels in $h(\mathbf{z}(t)) \in [0, h(\mathbf{z}_0)]$. For this reason we introduce two systems of functions, $\Phi$ and $\Upsilon$:

$$\Phi : \begin{array}{ll} \phi_j(s) & = \phi_{j-1} \circ \rho_{\phi,j}(\xi_{i-j} \cdot \beta(s,0)),\ j = 1,\dots,i \\ \phi_0(s) & = \beta(s,0) \end{array} \tag{D.12}$$

$$\Upsilon : \begin{array}{ll} \upsilon_j(s) & = \phi_{j-1} \circ \rho_{\upsilon,j}(s),\ j = 1,\dots,i \\ \upsilon_0(s) & = \beta(s,0) \end{array} \tag{D.13}$$

where functions $\rho_{\phi,j},\ \rho_{\upsilon,j} \in \mathcal{K}$ satisfy the following inequality

$$\phi_{j-1}(a+b) \leq \phi_{j-1} \circ \rho_{\phi,j}(a) + \phi_{j-1} \circ \rho_{\upsilon,j}(b) \tag{D.14}$$

Notice that in case $\beta(\cdot,0) \in \mathcal{K}_\infty$ functions $\rho_{\phi,j}(\cdot)$, $\rho_{\upsilon,j}(\cdot)$ satisfying (D.14) will always exist [12]. The properties of sequence $\Xi$ which ensure the desired rate of propagation of the influence of initial condition $\mathbf{x}_0$ and input $h(\mathbf{z}_0)$ to the state $\mathbf{x}(t)$ are specified in Condition 3

**Condition 3 (Rates of contraction, part 2)** *Sequences*

$$\sigma_n^{-1} \cdot \phi_n(\|\mathbf{x}_0\|_{\mathcal{A}}),\ \ \sigma_n^{-1} \cdot \left( \sum_{i=0}^{n} \upsilon_i(c|h(\mathbf{z}_0)|\sigma_{n-i}) \right),\ n = 0,\dots,\infty$$

*are bounded from above, e.g. there exist functions $B_1(\|\mathbf{x}_0\|)$, $B_2(|h(\mathbf{z}_0)|, c)$ such that*

$$\sigma_n^{-1} \cdot \phi_n(\|\mathbf{x}_0\|_{\mathcal{A}}) \leq B_1(\|\mathbf{x}_0\|_{\mathcal{A}}) \tag{D.15}$$

$$\sigma_n^{-1} \cdot \left( \sum_{i=0}^{n} \upsilon_i(c|h(\mathbf{z}_0)|\sigma_{n-i}) \right) \leq B_2(|h(\mathbf{z}_0)|, c) \tag{D.16}$$

*for all $n = 0, 1, \dots, \infty$*

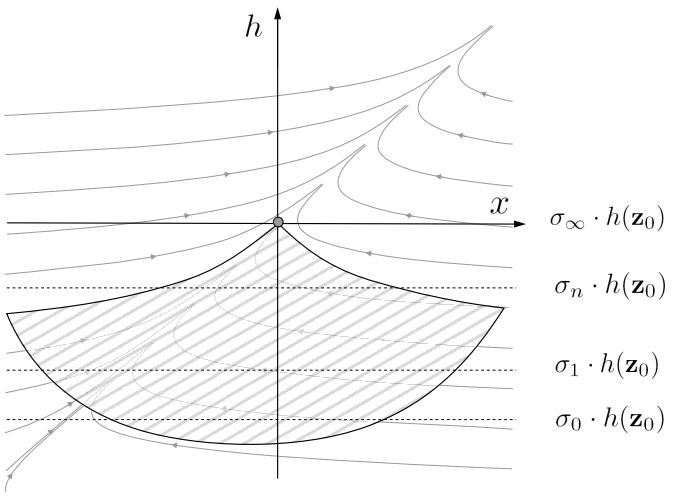


Figure D.2: Non-uniform contraction

It is desirable to stress that for the large class of functions $\beta(s,0)$, for instance Lipschitz in $s$, these conditions reduce to more transparent ones which can always be satisfied by the appropriate choice of sequences $\Xi$ and $\mathcal{S}$. This case is considered in details in section D.4.3 as a corollary of our main results

In order to prove emergence of the trapping region we consider the following collection of volumes induced by sequence $\mathcal{S}_i$ and corresponding partition (D.9) of the interval $[0, h(\mathbf{z}_0)]$:

$$\Omega_i = \{\mathbf{x} \in \mathcal{X}, \mathbf{z} \in \mathcal{Z} |\ h(\mathbf{z}(t)) \in H_i\} \tag{D.17}$$

For the given initial conditions $\mathbf{x}_0 \in \mathcal{X}$, $\mathbf{z}_0 \in \mathcal{Z}$ two alternatives are equally possible. First, the trajectory $\mathbf{x}(t, \mathbf{x}_0) \oplus \mathbf{z}(t, \mathbf{z}_0)$ stays in some $\Omega' \subset \Omega_0$ for all $t > t'$, $t' \geq t_0$. Hence for $t \to \infty$ the state will converge into

$$\Omega_a = \{\mathbf{x} \in \mathcal{X},\ \mathbf{z} \in \mathcal{Z} |\ \|\mathbf{x}\|_{\mathcal{A}} \leq c \cdot h(\mathbf{z}_0),\ \mathbf{z}:\ h(\mathbf{z}) \in [0, h(\mathbf{z}_0)]\} \tag{D.18}$$

Second, trajectory $\mathbf{x}(t, \mathbf{x}_0) \oplus \mathbf{z}(t, \mathbf{z}_0)$ subsequently enters the volumes $\Omega_j$, and $t_j$ are the time instances when it hits the hyper-surfaces $h(\mathbf{z}(t)) = h(\mathbf{z}_0)\sigma_j$. Then the state of the coupled system stays in $\Omega_0$ only if the sequence $\{t_i\}_{i=0}^{\infty}$ disconverges. Conditions specifying such possibility in terms of the characterizing sequences $\mathcal{S}$, $\Xi$, $\mathcal{T}$ and also depending on the properties of function $\gamma_0(\cdot)$ in (D.7) are provided in the Theorem 1. The diagram, schematically illustrating our technique is shown in Fig. 2.

**Theorem 1 (Non-uniform Small-gain Theorem)** *Let systems $\mathcal{S}_a$, $\mathcal{S}_w$ be given and satisfy Assumptions 1, 2. Consider their interconnection (D.7) and suppose there exist sequences $\mathcal{S}$, $\Xi$, and $\mathcal{T}$ satisfying Conditions 1–3. Let us, in addition, suppose that the following conditions hold:*

*1) There exists a positive number $\Delta_0 > 0$ such that*

$$\frac{1}{\tau_i} \frac{(\sigma_i - \sigma_{i+1})}{\gamma_{0,1}(\sigma_i)} \geq \Delta_0 \ \forall\, i = 0, 1, \ldots, \infty \tag{D.19}$$

*2) The set $\Omega_\gamma$ of all points $\mathbf{x}_0$, $\mathbf{z}_0$ satisfying inequality*

$$\gamma_{0,2}(B_1(\|\mathbf{x}_0\|_{\mathcal{A}}) + B_2(|h(\mathbf{z}_0)|, c) + c|h(\mathbf{z}_0)|) \leq h(\mathbf{z}_0)\Delta_0 \tag{D.20}$$

*is not empty.*

*3) Partial sums of elements from $\mathcal{T}$ diverge:*

$$\sum_{i=0}^{\infty} \tau_i = \infty \tag{D.21}$$

*Then for all $\mathbf{x}_0$, $\mathbf{z}_0 \in \Omega_\gamma$ state $\mathbf{x}(t, \mathbf{z}_0) \oplus \mathbf{z}(t, \mathbf{z}_0)$ of system (D.7) converges into the set specified by (D.18)*

$$\Omega_a = \{\mathbf{x} \in \mathcal{X},\ \mathbf{z} \in \mathcal{Z} |\ \|\mathbf{x}\|_{\mathcal{A}} \leq c \cdot h(\mathbf{z}_0),\ \mathbf{z}:\ h(\mathbf{z}) \in [0, h(\mathbf{z}_0)]\}$$

Proof of the theorem is provided in Appendix 1.

The major difference between conditions of Theorem 1 and conventional small-gain theorems [30],[12] is that the latter involve only input-output or input-state mappings (mappings $\gamma_0(\cdot)$ and constant $c$ in our case). This is because interconnected systems are assumed to be input-to-state stable and their internal dynamics, therefore, can be neglected. In our case, however, this is no longer true as dynamics of $\mathcal{S}_w$ is generally unstable in the Lyapunov sense. Hence, in order to ensure boundedness of $\mathbf{x}(t, \mathbf{x}_0)$ and $h(\mathbf{z}(t, \mathbf{z}_0))$, the rate/degree of stability of $\mathcal{S}_a$ should be taken into account. Roughly speaking, system $\mathcal{S}_a$ should ensure a sufficiently high degree of contraction in $\mathbf{x}_0$ while input-output response of $\mathcal{S}_w$ should be sufficiently small. The rate of contraction in $\mathbf{x}_0$ of $\mathcal{S}_a$, according to (D.4), is specified in terms of the function $\beta(\cdot, \cdot)$. Properties of this function that are relevant for convergence are explicitly accounted for in Condition 3 and (D.21). The domain of admissible initial conditions and actually the small-gain condition (input-state-output properties of $\mathcal{S}_w$ and $\mathcal{S}_a$) are defined by (D.19), (D.20) respectively. Notice also that $\Omega_\gamma$ is not necessarily a neighborhood of $\Omega_a$, thus the convergence ensured by Theorem 1 may not be uniform in $\mathbf{x}_0$, $\mathbf{z}_0$.

### D.4.2 Characterization of the attracting set

Small-gain conditions, even in case of interconnection of Lyapunov-stable systems are usually effective for establishing boundedness of state or outputs. Yet, it is still possible to derive the estimates (like, for instance, (D.18)) of the domains to which the state will converge. These estimates, however, are often too conservative. If a more precise characterization of the domains to which the state will converge is required additional information on the dynamics of systems $\mathcal{S}_a$ and $\mathcal{S}_w$ is needed. The question, therefore, is how detailed this information should be? It appears that some additional knowledge of the steady-state characteristics of system $\mathcal{S}_a$ is sufficient to improve the estimates (D.18) substantially.

Let us formally introduce the notion of steady-state characteristic as follows:

**Definition 5** *We say that system (D.4) has steady-state characteristic $\chi : \mathbb{R} \to \mathbb{R}_+$ with respect to the norm $\|\mathbf{x}\|_{\mathcal{A}}$ if and only if for each constant $\bar{u}_a$ the following holds:*

$$\forall\, u_a(t) \in \mathcal{U}_a:\ \lim_{t\to\infty} u_a(t) = \bar{u}_a\ \Rightarrow\ \lim_{t\to\infty} \|\mathbf{x}(t)\|_{\mathcal{A}} \in \chi(\bar{u}_a) \tag{D.22}$$

The key property captured by Definition 5 is that there exists a limit of $\|\mathbf{x}(t)\|_{\mathcal{A}}$ as $t \to \infty$ provided that the limit for $u_a(t)$, $t \to \infty$ is defined and constant. Notice that the graph of mapping $\chi$ should not necessarily be functional. Therefore, our definition shall allow a fairly large amount of uncertainty for $\mathcal{S}_a$. It will be of essential importance, however, that such characterization exists for system $\mathcal{S}_a$.

Not every system, however, obeys the steady-state characteristic $\chi(\cdot)$ of Definition 5. There are relatively simple systems whose state does not converge even in the "norm" sense for constant (converging to) inputs as is required in (D.22). In mechanics, physics and biology such systems present a large class of nonlinear oscillators which can be excited by constant inputs. In order to take such systems into consideration, we introduce a weaker notion, that is steady-state characteristic *on average*:

**Definition 6** *We say that system (D.4) has steady-state characteristic on average $\chi_T : \mathbb{R} \to \mathbb{R}_+$ with respect to the norm $\|\mathbf{x}\|_{\mathcal{A}}$ if and only if for each constant $\bar{u}_a$ and some $T > 0$ the following holds:*

$$\forall\, u_a(t) \in \mathcal{U}_a :\ \lim_{t\to\infty} u_a(t) = \bar{u}_a \ \Rightarrow\ \lim_{t\to\infty} \int_t^{t+T} \|\mathbf{x}(\tau)\|_{\mathcal{A}}\, d\tau \in \chi_T(\bar{u}_a) \tag{D.23}$$

Steady-state characterizations of system $\mathcal{S}_a$ allows us to specify further asymptotic behavior of interconnection (D.7). These results are summarized in Lemmas 1 and 2 below.

**Lemma 1** *Let system (D.7) be given and $h(\mathbf{z}(t, \mathbf{z}_0))$ be bounded for some $\mathbf{x}_0, \mathbf{z}_0$. Let, furthermore, system (D.4) has steady-state characteristic $\chi(\cdot) : \mathbb{R} \to \mathbb{R}_+$ . Then the following limiting relations hold*

$$\lim_{t\to\infty} \|\mathbf{x}(t, \mathbf{x}_0)\|_{\mathcal{A}} = 0,\ \lim_{t\to\infty} h(\mathbf{z}(t, \mathbf{z}_0)) \in \chi^{-1}(0) \tag{D.24}$$

As follows from Lemma 1, in case the steady-state characteristic of $\mathcal{S}_a$ is defined, the asymptotic behavior of interconnection (D.7) is characterized by the zeroes of the steady-state mapping $\chi(\cdot)$. For the steady-state characteristics on average a slightly modified conclusion can be derived

**Lemma 2** *Let system (D.7) be given, $h(\mathbf{z}(t, \mathbf{z}_0))$ be bounded for some $\mathbf{x}_0, \mathbf{z}_0$, $h(\mathbf{z}(t, \mathbf{z}_0)) \in [0, h(\mathbf{z}_0)]$ and system (D.4) admits steady-state characteristic $\chi_T(\cdot) : \mathbb{R} \to \mathbb{R}_+$ on average. Furthermore, let there exist a positive constant $\bar{\gamma}$ such that the function $\gamma_1(\cdot)$ in (D.5) satisfies the following constraint:*

$$\gamma_1(s) \geq \bar{\gamma} \cdot s,\ \forall s \in [0, \bar{s}], \bar{s} \in \mathbb{R}_+ :\ \bar{s} > c \cdot h(\mathbf{z}_0), \tag{D.25}$$

*In addition, suppose that $\chi_T(\cdot)$ has no zeros in the positive domain. Then*

$$\lim_{t\to\infty} \|\mathbf{x}(t, \mathbf{x}_0)\|_{\mathcal{A}} = 0,\ \lim_{t\to\infty} h(\mathbf{z}(t, \mathbf{z}_0)) = 0 \tag{D.26}$$

An immediate outcome of Lemmas 1 and 2 is that in case the conditions of Theorem 1 are satisfied and system (D.4) has steady-state characteristics $\chi(\cdot)$ or $\chi_T(\cdot)$ domain of convergence $\Omega_a$ becomes as follows

$$\Omega_a = \{\mathbf{x} \in \mathcal{X},\ \mathbf{z} \in \mathcal{Z} |\ \|\mathbf{x}\|_{\mathcal{A}} = 0,\ \mathbf{z} :\ h(\mathbf{z}) \in [0, h(\mathbf{z}_0)]\} \tag{D.27}$$

It is possible, however, to improve estimate (D.27) further under additional hypotheses on system $\mathcal{S}_a$ and $\mathcal{S}_w$ dynamics. This result is formulated in the corollary below

**Corollary 1** *Let system (D.7) be given and satisfy assumptions of Theorem 1. Let, in addition,*

*C1) flow $\mathbf{x}(t, \mathbf{x}_0) \oplus \mathbf{z}(t, \mathbf{z}_0)$ is generated by a system of autonomous differential equations with locally Lipschitz right-hand side;*

*C2) subsystem $\mathcal{S}_w$ is practically integral-input-to-state stable:*

$$\|\mathbf{z}(\tau)\|_{\infty,[t_0,t]} \leq C_z + \int_0^t \gamma_1(u_w(\tau))d\tau \tag{D.28}$$

*and function $h(\cdot) \in C^0$ in (D.5)*

*C3) system $\mathcal{S}_a$ has a steady-state characteristic $\chi(\cdot)$.*

*Then for all $\mathbf{x}_0, \mathbf{z}_0 \in \Omega_\gamma$ the state of interconnection converges to the set*

$$\Omega_a = \{\mathbf{x} \in \mathcal{X}, \mathbf{z} \in \mathcal{Z} |\ \|\mathbf{x}\|_{\mathcal{A}} = 0,\ h(\mathbf{z}) \in \chi^{-1}(0)\} \tag{D.29}$$

As follows from Corollary 1 zeros of the steady state characteristic of system $\mathcal{S}_a$ actually "control" domains to which the state of interconnection (D.7) might potentially converge. This is illustrated with Fig. 3. Notice also that in case condition C3 in Corollary 1 is replaced with the alternative:

*C3') system $\mathcal{S}_a$ has a steady-state characteristic on average $\chi_T(\cdot)$,*

it is possible to show that the state converges to

$$\Omega_a = \{\mathbf{x} \in \mathcal{X}, \mathbf{z} \in \mathcal{Z} |\ \|\mathbf{x}\|_{\mathcal{A}} = 0,\ h(\mathbf{z}) = 0\} \tag{D.30}$$

The proof follows straightforwardly from the proof of Corollary 1 and therefore is omitted.

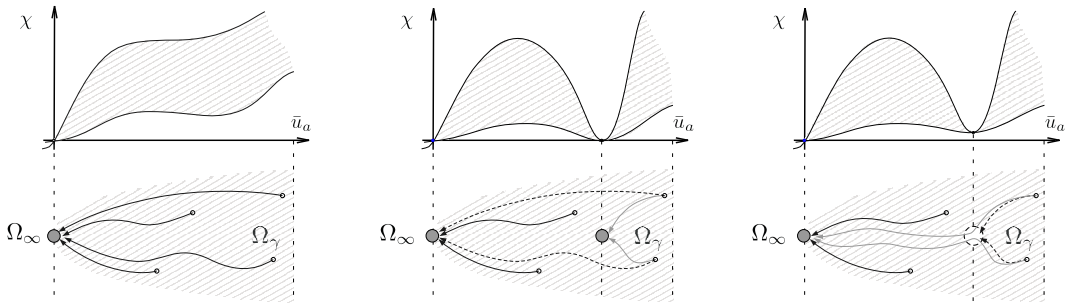


Figure D.3: Control of the attracting set by means of system's steady-state characteristics

### D.4.3 Separable in space-time contracting dynamics

In the previous sections we have presented convergence tests, estimates of the trapping region, and also specified characterization of the attracting sets under mild assumptions of uniform asymptotic stability of $\mathcal{S}_a$ and specific input-output relation in system $\mathcal{S}_w$. The conditions were given for rather general functions $\beta(\cdot,\cdot) \in \mathcal{KL}$ in (D.4) and $\gamma_0(\cdot)$, $\gamma_1(\cdot)$ in (D.5). It appears, however, that these conditions can be substantially simplified if an additional information on properties of functions $\beta(\cdot,\cdot)$ and $\gamma_0(\cdot)$ is available. This information is, in particular, the separability of function $\beta(\cdot,\cdot)$ or, equivalently, the possibility of factorization:

$$\beta(\|\mathbf{x}\|_{\mathcal{A}}, t) \leq \beta_x(\|\mathbf{x}\|_{\mathcal{A}}) \cdot \beta_t(t), \tag{D.31}$$

where $\beta_x(\cdot) \in \mathcal{K}$ and $\beta_t(\cdot) \in \mathcal{C}^0$ is strictly decreasing[9] with

$$\lim_{t\to\infty} \beta_t(t) = 0 \tag{D.32}$$

In principle, as shown in [7], factorization (D.31) is achievable for a large class of uniformly asymptotically stable systems under an appropriate coordinate transformation. An immediate conequence of factorization (D.31) is that the elements of sequence $\Xi$ in Condition 2 are independent on $\|\mathbf{x}(t_i)\|_{\mathcal{A}}$. As a result, verification of Conditions 2, 3 becomes easier. The most interesting case, however, is when function $\beta_x(\cdot)$ in factorization (D.31) is Lipschitz. For this class of functions the conditions of Theorem 1 reduce to a single and easy verifiable inequality. Let us consider this case in detail.

Without loss of generality, we assume that state $\mathbf{x}(t)$ of system $\mathcal{S}_a$ satisfies the following equation

$$\|\mathbf{x}(t)\|_{\mathcal{A}} \leq \|\mathbf{x}(t_0)\|_{\mathcal{A}} \cdot \beta_t(t - t_0) + c \cdot \|h(\mathbf{z}(\tau, \mathbf{z}_0))\|_{\infty,[t_0,t]}, \tag{D.33}$$

where $\beta_t(0)$ is grater or equal to unit. Given that $\beta_t(t)$ is strictly decreasing, mapping $\beta_t : [0,\infty] \mapsto [0,\beta_t(0)]$ is injective. Moreover $\beta_t(t)$ is continuous, then it is surjective and, therefore, bijective. In the other words there is a (continuous) mapping $\beta_t^{-1} : [0,\beta_t(0)] \mapsto \mathbb{R}_+$:

$$\beta_t^{-1} \circ \beta_t(t) = t, \ \forall\, t > 0 \tag{D.34}$$

Conditions for emergence of the trapping region for interconnection (D.7) with dynamics of system $\mathcal{S}_a$ governed by equation (D.33) are summarized below:

[9] If $\beta_t(\cdot)$ is not strictly monotone, it can always be majorated by a strictly decreasing functon

**Corollary 2** *Let interconnection (D.7) be given, system $\mathcal{S}_a$ satisfy (D.33) and function $\gamma_0(\cdot)$ in (D.5) be Lipschitz:*

$$|\gamma_0(s)| \leq D_{\gamma,0} \cdot |s| \tag{D.35}$$

*and domain*

$$\Omega_\gamma : \; D_{\gamma,0} \leq \left(\beta_t^{-1}\left(\frac{d}{\kappa \cdot \beta_t(0)}\right)\right)^{-1} \frac{\kappa-1}{\kappa} \frac{h(\mathbf{z}_0)}{\beta_t(0)\left\|\mathbf{x}_0\right\|_{\mathcal{A}} + \beta_t(0) \cdot c \cdot |h(\mathbf{z}_0)|\left(1+\frac{\kappa}{1-d}\right) + c|h(\mathbf{z}_0)|} \tag{D.36}$$

*is not empty for some $d < 1$, $\kappa > 1$. Then for all initial conditions $\mathbf{x}_0\ \mathbf{z}_0 \in \Omega_\gamma$ state $\mathbf{x}(t, \mathbf{x}_0) \oplus \mathbf{z}(t, \mathbf{z}_0)$ of interconnection (D.7) converges into the set $\Omega_a$ specified by (D.18). If, in addition, conditions C1)–C3) of Corollary 1 hold then the domain of convergence is given by (D.27).*

A practically important consequence of this corollary concerns systems $\mathcal{S}_a$ which are exponentially stable:

$$\left\|\mathbf{x}(t)\right\|_{\mathcal{A}} \leq \left\|\mathbf{x}(t_0)\right\|_{\mathcal{A}} D_\beta \exp(-\lambda t) + c \cdot \left\|h(\mathbf{z}(t, \mathbf{z}_0))\right\|_{\infty,[t_0,t]}, \lambda > 0, \; D_\beta \geq 1 \tag{D.37}$$

For this case domain (D.36) of initial conditions ensuring convergence into $\Omega_a$ is defined as

$$D_{\gamma,0} \leq \max_{\kappa>1,\ d\in(0,1)} -\lambda\left(\ln\frac{d}{\kappa D_\beta}\right)^{-1} \frac{\kappa-1}{\kappa} \frac{h(\mathbf{z}_0)}{D_\beta\left\|\mathbf{x}_0\right\|_{\mathcal{A}} + D_\beta \cdot c \cdot |h(\mathbf{z}_0)|\left(1+\frac{\kappa}{1-d}\right) + c|h(\mathbf{z}_0)|}$$

In the next section we show how this result can be applied to address the problem of output nonlinear identification for systems which cannot be transformed into the canonic observer form or/and with nonlinear parametrization.

## D.5 Discussion

In the literature of adaptive control, observation and identification a few classes of systems are referred as *canonic forms* for their ability to poses solutions to the problem and, at the same time, applicability to large variety of relevant physical phenomena. Among these, perhaps, the most widely known is the *adaptive observer canonical form* [2]. Necessary and sufficient conditions for transformation of the original system into the observer canonical form can be found, for example, in [16]. These conditions, however, include restrictive requirements of linearization of uncertainty-independent dynamics by output injection, and also they require linear parametrization of the uncertainty. Alternative approaches [3] heavily rely on knowledge of the proper Lyapunov function for uncertainty-independent part and still assume linear parametrization.

Let us now demonstrate how these restrictions can be lifted by application our result to the problem of state and parameter observation. Let us consider classes of systems which can be transformed by means of the feedback, static or dynamic[10], into the following form:

$$\dot{\mathbf{x}} = \mathbf{f}_0(\mathbf{x}, t) + \mathbf{f}(\boldsymbol{\xi}(t), \boldsymbol{\theta}) - \mathbf{f}(\boldsymbol{\xi}(t), \hat{\boldsymbol{\theta}}) + \boldsymbol{\varepsilon}(t), \tag{D.38}$$

where

$$\boldsymbol{\varepsilon}(t) \in L_\infty^m[t_0, \infty], \; \left\|\boldsymbol{\varepsilon}(\tau)\right\|_{\infty,[t_0,t]} \leq \Delta_\varepsilon$$

is external perturbation with known $\Delta_\varepsilon$, and $\mathbf{x} \in \mathbb{R}^n$. Function $\boldsymbol{\xi} : \mathbb{R}_+ \to \mathbb{R}^\xi$ is a function of time, which possibly includes available measurements of the state, and $\boldsymbol{\theta}, \hat{\boldsymbol{\theta}} \in \Omega_\theta \subset \mathbb{R}^d$ are the

[10] Notice that conventional observers in control theory could be viewed as dynamic feedbacks of the specific class

unknown and estimated parameters of function $\mathbf{f}(\cdot)$ respectively and set $\Omega_\theta$ is bounded. We assume that function $\mathbf{f}(\boldsymbol{\xi}(t), \boldsymbol{\theta})$ is locally bounded in $\boldsymbol{\theta}$ uniformly in $\boldsymbol{\xi}$:

$$\|\mathbf{f}(\boldsymbol{\xi}(t), \boldsymbol{\theta}) - \mathbf{f}(\boldsymbol{\xi}(t), \hat{\boldsymbol{\theta}})\| \leq D_f \|\boldsymbol{\theta} - \hat{\boldsymbol{\theta}}\| + \Delta_f$$

and the values of $D_f \in \mathbb{R}_+$, $\Delta_f$ are available. Function $\mathbf{f}_0(\cdot)$ in (D.38) is assumed to satisfy the following condition:

**Assumption 3** *System*

$$\dot{\mathbf{x}} = \mathbf{f}_0(\mathbf{x}, t) + \mathbf{u}(t) \tag{D.39}$$

*is forward-complete. Furthermore, for all $\mathbf{u}(t)$ such that*

$$\|\mathbf{u}(t)\|_{\infty,[t_0,t]} \leq \Delta_u + \|\mathbf{u}_0(\tau)\|_{\infty,[t_0,t]},\ \Delta_u \in \mathbb{R}_+$$

*there exist bounded set $\mathcal{A}$, $c > 0$ and function $\Delta : \mathbb{R}_+ \to \mathbb{R}_+$ satisfying the following inequality:*

$$\|\mathbf{x}(t)\|_{\mathcal{A}_{\Delta(\Delta_u)}} \leq \beta(t - t_0)\, \|\mathbf{x}(t_0)\|_{\mathcal{A}_{\Delta(\Delta_u)}} + c\|\mathbf{u}_0(\tau)\|_{\infty,[t_0,t]}$$

*where $\beta(\cdot) : \mathbb{R}_+ \to \mathbb{R}_+$, $\lim_{t\to\infty} \beta(t) = 0$ is strictly decreasing function.*

Let us consider the following auxiliary system

$$\dot{\boldsymbol{\lambda}} = S(\boldsymbol{\lambda}),\ \boldsymbol{\lambda}(t_0) = \boldsymbol{\lambda}_0 \in \Omega_\lambda \subset \mathbb{R}^\lambda \tag{D.40}$$

where $\Omega_\lambda \subset \mathbb{R}^n$ is bounded and $S(\lambda)$ is locally Lipschitz. Further, suppose that the following assumption holds for system (D.40)

**Assumption 4** *System (D.40) is Poisson stable in $\Omega_\lambda$ that is*

$$\forall\, \boldsymbol{\lambda}' \in \Omega_\lambda,\ t' \in \mathbb{R}_+ \ \Rightarrow \exists t'' > t :\ \|\boldsymbol{\lambda}(t'', \boldsymbol{\lambda}') - \boldsymbol{\lambda}'\| \leq \epsilon,$$

*where $\epsilon$ is arbitrary small positive constant. Moreover, trajectory $\lambda(t, \boldsymbol{\lambda}_0)$ is dense in $\Omega_\lambda$:*

$$\forall \boldsymbol{\lambda}' \in \Omega_\lambda,\ \epsilon \in \mathbb{R}_{>0} \Rightarrow \exists\, t \in \mathbb{R}_+ :\ \|\boldsymbol{\lambda}' - \boldsymbol{\lambda}(t, \boldsymbol{\lambda}_0)\| < \epsilon$$

Now we are ready to formulate the following statement:

**Corollary 3** *Let us consider system (D.38) and suppose that the following conditions hold*
*C4) vector-field $\mathbf{f}_0(\mathbf{x}, t)$ in (D.38) satisfies Assumption 3;*
*C5) there exists and known system (D.40) satisfying Assumption 4;*
*C6) there exists locally Lipschitz $\boldsymbol{\eta} : \mathbb{R}^\lambda \to \mathbb{R}^d$:*

$$\|\boldsymbol{\eta}(\boldsymbol{\lambda}') - \boldsymbol{\eta}(\boldsymbol{\lambda}'')\| \leq D_\eta \|\boldsymbol{\lambda}' - \boldsymbol{\lambda}''\|$$

*such that set $\boldsymbol{\eta}(\Omega_\lambda)$ is dense in $\Omega_\theta$;*
*C7) system (D.38) has steady-state characteristic with respect to the norm*

$$\|\cdot\|_{\mathcal{A}_{\Delta(M)}},\ M = 2\Delta_f + \Delta_\varepsilon + \delta$$

*and input $\hat{\boldsymbol{\theta}}$, where $\delta$ is some positive (arbitrary small) constant.*
*Consider the following interconnection of (D.38), (D.40):*

$$\begin{aligned}
\dot{\mathbf{x}} &= \mathbf{f}_0(\mathbf{x}, t) + \mathbf{f}(\boldsymbol{\xi}(t), \boldsymbol{\theta}) - \mathbf{f}(\boldsymbol{\xi}(t), \hat{\boldsymbol{\theta}}) + \boldsymbol{\varepsilon}(t) \\
\hat{\boldsymbol{\theta}} &= \boldsymbol{\eta}(\boldsymbol{\lambda}) \\
\dot{\boldsymbol{\lambda}} &= \gamma\, \|\mathbf{x}(t)\|_{\mathcal{A}_{\Delta(M)}}\, S(\boldsymbol{\lambda}),
\end{aligned} \tag{D.41}$$

*where $\gamma > 0$ satisfies the following inequality*

$$\gamma \leq \left(\beta_t^{-1}\left(\frac{d}{\kappa \cdot \beta_t(0)}\right)\right)^{-1} \frac{\kappa - 1}{\kappa} \frac{1}{D_\lambda\left(\beta_t(0)\left(1 + \frac{\kappa}{1-d}\right) + 1\right)} \tag{D.42}$$
$$D_\lambda = c \cdot D_f \cdot D_\eta \cdot \max_{\boldsymbol{\lambda} \in \Omega\lambda} \|S(\boldsymbol{\lambda})\|$$

*for some $d \in (0,1)$, $\kappa \in (1,\infty)$. Then, for $\boldsymbol{\lambda}(t_0) = \boldsymbol{\lambda}_0$, some $\boldsymbol{\theta}' \in \Omega_\theta$ and all $\mathbf{x}(t_0) = \mathbf{x}_0 \in \mathbb{R}^n$ the following holds:*

$$\lim_{t\to\infty} \|\mathbf{x}(t)\|_{\mathcal{A}_{\Delta(M)}} = 0, \ \lim_{t\to\infty} \hat{\boldsymbol{\theta}}(t) = \boldsymbol{\theta}' \in \Omega_\theta \tag{D.43}$$

Notice that again, as has been pointed out in the previous section, in case the dynamics of (D.39) is exponentially stable with the rate of convergence equal to $\rho$ and $\beta(0) = D_\beta$, condition (D.42) will have the following form:

$$\gamma \leq -\rho\left(\ln \frac{d}{\kappa D_\beta}\right)^{-1} \frac{\kappa - 1}{\kappa} \frac{1}{D_\lambda\left(D_\beta\left(1 + \frac{\kappa}{1-d}\right) + 1\right)}$$

According to Corollary 3, for rather general class of systems (D.38) it is possible to design estimator $\hat{\boldsymbol{\theta}}(t)$ which guarantees that not only "error" vector $\mathbf{x}(t)$ reaches a neighborhood of the origin, but also that the estimates $\hat{\boldsymbol{\theta}}(t)$ converge to some $\boldsymbol{\theta}'$ in $\Omega_\theta$. Both these facts together with additional nonlinear persistent excitation conditions [5],[24]

$$\exists T > 0, \rho \in \mathcal{K} : \ \forall\, \mathcal{T} = [t, t+T], \ t \in \mathbb{R}_+ \Rightarrow \exists \tau \in \mathcal{T} : |\mathbf{f}(\boldsymbol{\xi}(\tau), \boldsymbol{\theta}) - \mathbf{f}(\boldsymbol{\xi}(\tau), \boldsymbol{\theta}')| \geq \rho(\|\boldsymbol{\theta} - \boldsymbol{\theta}'\|)$$

in principle allow to estimate domains of convergence for $\hat{\boldsymbol{\theta}}(t)$.

Concluding this section we would like to mention that statements of Theorem 1 and Corollaries 1–3 constitute additional theoretical tools for analysis of asymptotic behavior of integral input-to-state systems. In particular they are complementary to the results of [1] where *asymptotic stability* of the following type of systems

$$\dot{\mathbf{x}} = \mathbf{f}(\mathbf{x}),$$
$$\dot{\mathbf{z}} = \mathbf{q}(\mathbf{x}, \mathbf{z}), \ \mathbf{f} : \mathbb{R}^n \to \mathbb{R}^n, \ \mathbf{q} : \mathbb{R}^n \times \mathbb{R}^m \to \mathbb{R}^m$$

was considered under assumption that the $\mathbf{x}$-subsystem is globally asymptotically stable and the $\mathbf{z}$-subsystem is integral input-to-state stable. In contrast to this our results apply to establishing *asymptotic convergence* in the systems of the following structure

$$\dot{\mathbf{x}} = \mathbf{f}(\mathbf{x}, \mathbf{z}),$$
$$\dot{\mathbf{z}} = \mathbf{q}(\mathbf{x}, \mathbf{z}), \ \mathbf{f} : \mathbb{R}^n \times \mathbb{R}^m \to \mathbb{R}^n$$

where the $\mathbf{x}$-subsystem is input-to-state stable, and $\mathbf{z}$-subsystem could be practically integral input-to-state stable (see Corollary 1), although in general no stability assumptions are imposed on it.

## D.6 Examples

In this section we provide two examples illustrating proposed techniques in application to the problem of parameter identification of nonlinear parameterized systems and those which cannot be transformed into the canonical adaptive observer form.

The first example is merely academical illustration to Corollary 3, where only one parameter is unknown and the system itself is the first-order differential equation. The second example illustrates possible application of our results to the problems of identification of dynamics in the living cells.

*Example 1.* Let us consider the following system

$$\dot{x} = -kx + \sin(x\theta + \theta) + u,\ k > 0,\ \theta \in [-a, a] \tag{D.44}$$

where $\theta$ is the unknown parameter, and $u$ is the control input. Without loss of the generality we let $a = 1$, $k = 1$. The problem is to estimate parameter $\theta$ from the measurements of $x$ and also to steer the system to the origin. Clearly, choice $u = -\sin(x\hat{\theta} + \hat{\theta})$ transforms (D.44) into the following equation

$$\dot{x} = -kx + \sin(x\theta + \theta) - \sin(x\hat{\theta} + \hat{\theta}) \tag{D.45}$$

which satisfies Assumption 3. Moreover, system

$$\begin{aligned} \dot{\lambda}_1 &= \lambda_1 \\ \dot{\lambda}_2 &= -\lambda_2,\ \lambda_1^2(t_0) + \lambda_2^2(t_0) = 1 \end{aligned}$$

with mapping $\boldsymbol{\eta} = (1,\ 0)^T \boldsymbol{\lambda}$ satisfy Assumption 4 and therefore

$$\begin{aligned} \dot{\lambda}_1 &= \gamma|x|\lambda_1 \\ \dot{\lambda}_2 &= -\gamma|x|\lambda_2,\ \lambda_1^2(t_0) + \lambda_2^2(t_0) = 1 \end{aligned} \tag{D.46}$$

would be a candidate for the control and parameter estimation algorithm. According to Corollary 3, the goal will be reached if parameter $\gamma$ in (D.46) obeys the following constraint

$$\gamma \leq -\rho \left( \ln \frac{d}{\kappa D_\beta} \right)^{-1} \frac{\kappa - 1}{\kappa} \frac{1}{D_\lambda \left( D_\beta \left( 1 + \frac{\kappa}{1-d} \right) + 1 \right)},\ \rho = k = 1,\ D_\beta = 1,\ D_\lambda = 1$$

for some $d \in (0, 1)$, $\kappa \in (1, \infty)$. Hence, choosing, for example, $d = 0.5$, $\kappa = 2$ we obtain that choice

$$0 < \gamma < -\ln \left( \frac{0.5}{2} \right) \frac{1}{2} \cdot \frac{1}{6} = 0.1155$$

suffices to ensure that

$$\lim_{t \to \infty} x(t) = 0,\ \lim_{t \to \infty} \hat{\theta}(t) = \theta$$

We simulated system (D.45), (D.46) with $\theta = 0.3$, $\gamma = 0.1$ and initial conditions $x(t_0)$ randomly distributed in the interval $[-1, 1]$. Results of the simulation are illustrated with Figure 4, where the phase plots of system (D.45), (D.46) as well as the trajectories of $\hat{\theta}(t)$ are provided.

*Example 2.* Let us consider the problem modelling electrical activity in the biological cells from the input-output data in the current clamp experiments. The simplest mathematical model, which captures fairly large variety of phenomena like periodic bursting in response to constant stimulation is the classical Hindmarsh and Rose model without adaptation currents [9]:

$$\begin{aligned} \dot{x}_1 &= -ax_1^3 + bx_1^2 + x_2 + \alpha u \\ \dot{x}_2 &= c - \beta x_2 - dx_1^2 \end{aligned} \tag{D.47}$$

where variable $x_1$ is the membrane potential, $x_2$ stands for the ionic currents in the cell, $u$ is the input current, and $a$, $b$, $c$, $d$, $\alpha$, $\beta \in \mathbb{R}$ are parameters. While parameters of the first equation can, in principle, be identified experimentally by blocking the ionic channels in the cells and measuring the

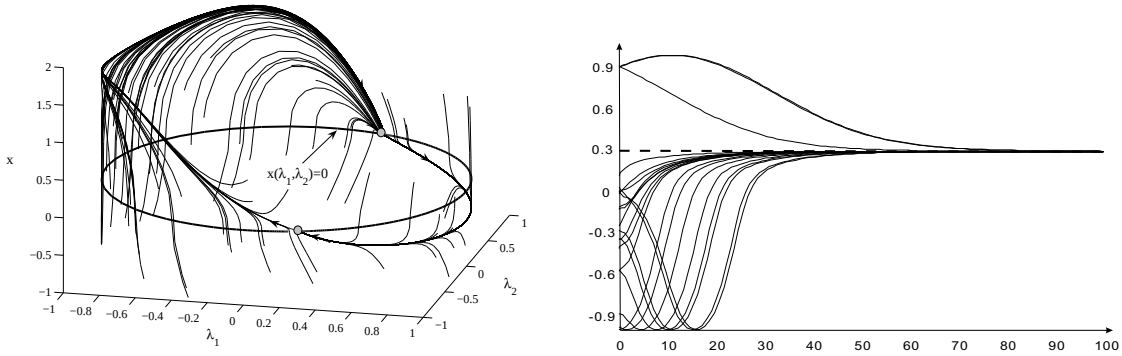


Figure D.4: Trajectories of system (D.45), (D.46) (left panel) and the family of estimates $\hat{\theta}(t)$ of parameter $\theta$ as functions of time $t$ (right panel)

membrane conductance, identification of parameters $\beta$, $d$ is a difficult problem as information about ionic currents $x_2$ is rarely available.

Conventional techniques [2] cannot be applied immediately to this problem as model (D.47) is not in canonical adaptive observer form. Let us illustrate how our results can be used to derive unknown parameters of (D.47) such that reconstructed model fits the observed data. Let us assume, first, that parameters $a$, $b$, $c$, $\alpha$ in the first equation of (D.47) are known, parameters $\beta$, $d$ in the second equation are unknown. This corresponds to the realistic case where the time constant of current $x_2$ and coupling between $x_1$ and $x_2$ are uncertain. In our example we assumed that

$$\beta \in \Omega_\beta = [0.3, 0.7],\ \ d \in \Omega_d = [2, 3],\ a = 1,\ b = 3,\ \alpha = 0.7,\ c = 0.5$$

As a candidate for the observer we select the following system

$$\dot{\hat{x}} = -\rho(x_1 - \hat{x}) - ax_1^3 + bx_1^2 + \alpha u + f(\hat{\beta}, \hat{d}, t),\ \rho \in \mathbb{R}_{>0} \tag{D.48}$$

where $\hat{\beta}$, $\hat{d}$ are parameters to be adjusted and function $f(\hat{\beta}, \hat{d}, t)$ is specified as

$$f(\hat{\beta}, \hat{d}, t) = \int_0^t e^{-\hat{\beta}(t-\tau)}(\hat{d}x_1^2(\tau) + c)d\tau$$

Then dynamics of $\tilde{x}(t) = x(t) - \hat{x}(t)$ satisfies the following differential equation

$$\dot{\tilde{x}} = -\rho\tilde{x} + f(\beta, d, t) - f(\hat{\beta}, \hat{d}, t)$$

Function $f(\beta, d, t)$ satisfies the following inequality

$$\begin{aligned} |f(\beta, d, t) - f(\hat{\beta}, \hat{d}, t)| &\le |f(\beta, d, t) - f(\hat{\beta}, d, t)| + |f(\hat{\beta}, d, t) - f(\hat{\beta}, \hat{d}, t)| \\ &\le D_{f,\beta}|\beta - \hat{\beta}| + D_{f,d}|d - \hat{d}| + \epsilon(t), \end{aligned}$$

where $\epsilon(t)$ is exponentially decaying term, and

$$D_{f,\beta} = \max_{\hat{\beta},\beta\in\Omega_\beta,\ d\in\Omega_d} \left\{ \frac{1}{\beta\hat{\beta}}(d\|x_1(\tau)\|_{\infty,[t_0,\infty]} + c) \right\},\ D_{f,d} = \max_{\hat{\beta}\in\Omega_\beta} \left\{ \frac{1}{\hat{\beta}}\|x_1(\tau)\|_{\infty,[t_0,\infty]} \right\} \tag{D.49}$$

Furthermore, Assumption 3 is satisfied for system

$$\dot{\tilde{x}} = -\rho\tilde{x} + \upsilon(t),\ \|\upsilon(\tau)\|_{\infty,[t_0,t]} \leq \Delta_u + \|\upsilon_0(\tau)\|_{\infty,[t_0,t]}$$

with

$$\Delta(\Delta_u) = \frac{\Delta_u}{\rho},\ c = 1$$

Let us define subsystem (D.40). Consider the following system of differential equations

$$\begin{aligned}
\dot{\lambda}_1 &= \lambda_2 \\
\dot{\lambda}_2 &= -\omega_1^2\lambda_1 \\
\dot{\lambda}_3 &= \lambda_4 \\
\dot{\lambda}_4 &= -\omega_2^2\lambda_3,\ \boldsymbol{\lambda}_0 = (1,0,1,0)^T
\end{aligned} \tag{D.50}$$

where $\Omega_\lambda$ is the $\omega$-limit set of the point $\boldsymbol{\lambda}_0$, and $\omega_1,\ \omega_2 \in \mathbb{R}$. System, therefore, satisfies Assumption 4. Given that domains $\Omega_\beta$, $\Omega_d$ are known, let us select

$$\begin{gathered}
\boldsymbol{\eta} : \mathbb{R}^n \to \mathbb{R}^2,\ \boldsymbol{\eta} = (\eta_1(\boldsymbol{\lambda}), \eta_2(\boldsymbol{\lambda})) \\
\hat{\beta} = \eta_1(\boldsymbol{\lambda}) = \frac{1}{2}\left(\frac{2\arcsin(\lambda_1)}{\pi} + 1\right)\cdot 0.4 + 0.3,\ \hat{d} = \eta_2(\boldsymbol{\lambda}) = \frac{1}{2}\left(\frac{2\arcsin(\lambda_3)}{\pi} + 1\right) + 2
\end{gathered} \tag{D.51}$$

Choosing

$$\frac{\omega_1}{\omega_2} = \pi$$

we ensure that $\boldsymbol{\eta}(\Omega_\lambda)$ id dense in $\Omega_\beta \times \Omega_d$. Given that $\hat{\beta}$, $\hat{d}$ are bounded, $D_{f,\beta}$ and $D_{f,d}$ in (D.49) are also bounded (for the given range of parameters signal $x_1(t)$ is always bounded). Hence, according to Corollary 3, interconnection of (D.48), (D.51) and

$$\begin{aligned}
\dot{\lambda}_1 &= \gamma\|\tilde{x}(t)\|_{\Delta(\delta)}\cdot\lambda_2 \\
\dot{\lambda}_2 &= -\gamma\|\tilde{x}(t)\|_{\Delta(\delta)}\cdot\omega_1^2\lambda_1 \\
\dot{\lambda}_3 &= \gamma\|\tilde{x}(t)\|_{\Delta(\delta)}\cdot\lambda_4 \\
\dot{\lambda}_4 &= -\gamma\|\tilde{x}(t)\|_{\Delta(\delta)}\cdot\omega_2^2\lambda_3,\ \boldsymbol{\lambda}_0 = (1,0,1,0)^T
\end{aligned}$$

with arbitrary small $\delta > 0$ and properly chosen $\gamma > 0$ ensures that

$$\lim_{t\to\infty}\|\tilde{x}(t)\|_{\Delta(\delta)} = 0,\ \lim_{t\to\infty}\hat{\beta}(t) = \beta' \in \Omega_\beta,\ \lim_{t\to\infty}\hat{d}(t) = d' \in \Omega_d$$

This, would in turn imply successful fit of the observations to the model.

We simulated the system with $\rho = 10$ and $\gamma = 3\cdot 10^{-4}$ for $\beta = 0.5$, $d = 2.5$. The results of the simulations are provided in figures 5 (trajectories $x_1(t)$, $\hat{x}(t)$) and 6 (estimates $\hat{\beta}(t)$ and $\hat{d}(t)$). It can be seen from these figures that reconstruction is successful and parameters converge into a small neighborhood of the actual values.

## D.7 Conclusion

We proposed new tools for analysis of asymptotic behavior for a class of dynamical systems. In particular, we considered an interconnection of input-to-state stable system with an unstable or integrally input-to-state dynamics. Our results allow to address a variety of relevant problems when

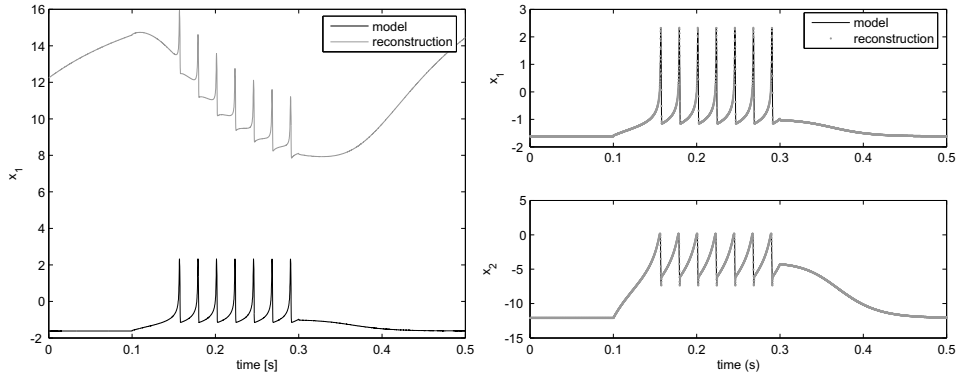


Figure D.5: Trajectories $x_1(t)$ and $\hat{x}(t)$ in the beginning of the simulation (left panel), and at the end of the simulation (right panel)

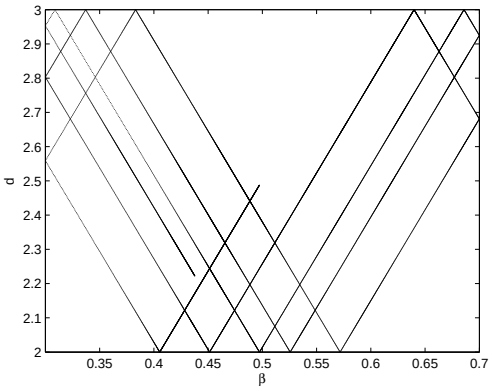


Figure D.6: Searching dynamics in the bounded parameter space

the convergence might not be unform in initial condition. It is necessary to notice that we do not require complete knowledge of the dynamical systems in question. Only qualitative information like, for instance, characterization of input-to-state stability of is necessary for application of our results. We have also demonstrated how our analysis can be used in the problems of synthesis and design. In particular, to the problems of nonlinear regulation and parameter identification of nonlinear parameterized systems. Provided examples show relevance of our approach in those domains where application of the standard techniques is either not possible or complicated.

## D.8 Acknowledgment

The authors are thankful to Peter Jurica and Tatiana Tyukina for their enthusiastic help and comments during preparation of this manuscript.

## D.9 Appendix

*Proof of Theorem 1.* Let conditions of the theorem be satisfied for the given $t_0 \in \mathbb{R}_+$: $\mathbf{x}(t_0) = \mathbf{x}_0$, $\mathbf{z}(t_0) = \mathbf{z}_0$. Notice that in this case $h(\mathbf{z}_0) \geq 0$ overwise requirement (D.20) will be violated. Let us consider the sequence (D.17) volumes $\Omega_i$ induced by $\mathcal{S}$:

$$\Omega_i = \{\mathbf{x} \in \mathcal{X},\ \mathbf{z} \in \mathcal{Z} |\ h(\mathbf{z}(t)) \in H_i\}$$

To prove the theorem we shall show that $0 \leq h(\mathbf{z}(t)) \leq h(\mathbf{z}_0)$ for all $t \geq t_0$. For the given partition (D.17) we consider two alternatives.

First, in the degenerative case, the state $\mathbf{x}(t) \oplus \mathbf{z}(t)$ enters some $\Omega_j$, $j \geq 0$ and stays there for all $t \geq t_0$ which automatically guarantees that $0 \leq |h(\mathbf{z})| \leq h(\mathbf{z}_0)$. Then, according to (D.4) trajectory $\mathbf{x}(t)$ satisfies the following inequality:

$$\|\mathbf{x}(t)\|_{\mathcal{A}} \leq \beta(\|\mathbf{x}_0\|_{\mathcal{A}}, t - t_0) + c\|h(\mathbf{z}(t))\|_{\infty,[t_0,t]} \leq \beta(\|\mathbf{x}_0\|_{\mathcal{A}}, t - t_0) + c|h(\mathbf{z}_0)| \tag{D.52}$$

Taking into account that $\beta(\cdot,\cdot) \in \mathcal{KL}$ we can conclude that (D.52) implies that

$$\limsup_{t\to\infty} \|\mathbf{x}(t)\|_{\mathcal{A}} = c|h(\mathbf{z}_0)| \tag{D.53}$$

Therefore statements of the theorem hold.

Let us consider the second alternative, where the state $\mathbf{x}(t) \oplus \mathbf{z}(t)$ does not belong to $\Omega_j$ for all $t \geq t_0$. Given that $h(\mathbf{z}(t))$ is monotone and non-increasing in $t$, this implies that there exists an ordered sequence of time instants $t_j$:

$$t_0 > t_1 > t_2 \cdots t_j > t_{j+1} \cdots \tag{D.54}$$

such that

$$h(\mathbf{z}(t_i)) = \sigma_i h(\mathbf{z}_0) \tag{D.55}$$

Hence in order to prove the theorem we must show that the sequence $\{t_i\}_{i=0}^{\infty}$ does not converge. In the other words, the boundary $\sigma_\infty h(\mathbf{z}_0) = 0$ will not be reached in finite time.

In order to do this let us estimate the upper bounds for the following differences

$$T_i = t_{i+1} - t_i$$

Taking into account inequality (D.5) and the fact that $\gamma_0(\cdot) \in \mathcal{K}_e$ we can derive that

$$h(\mathbf{z}(t_i)) - h(\mathbf{z}(t_{i+1})) \leq T_i \max_{\tau\in[t_i,t_{i+1}]} \gamma_0(\|\mathbf{x}(\tau)\|_{\mathcal{A}}) \leq T_i \gamma_0(\|\mathbf{x}(\tau)\|_{\mathcal{A}_\infty,[t_i,t_{i+1}]}) \tag{D.56}$$

According to the definition of $t_i$ in (D.55) and noticing that sequence $\mathcal{S}$ is strictly decreasing we have

$$h(\mathbf{z}(t_i)) - h(\mathbf{z}(t_{i+1})) = (\sigma_i - \sigma_{i+1})h(\mathbf{z}_0) > 0$$

Hence $h(\mathbf{z}_0) > 0$ implies that $\gamma_0(\|\mathbf{x}(\tau)\|_{\mathcal{A}_\infty,[t_i,t_{i+1}]}) > 0$ and, therefore, (D.56) results in the following estimate of $T_i$:

$$T_i \geq \frac{h(\mathbf{z}(t_i)) - h(\mathbf{z}(t_{i+1}))}{\gamma_0(\|\mathbf{x}(\tau)\|_{\mathcal{A}_\infty,[t_i,t_{i+1}]})} = \frac{h(\mathbf{z}_0)(\sigma_i - \sigma_{i+1})}{\gamma_0(\|\mathbf{x}(\tau)\|_{\mathcal{A}_\infty,[t_i,t_{i+1}]})} \tag{D.57}$$

Taking into account that $h(\mathbf{z}(t))$ is non-increasing over $[t_i, t_{i+1}]$ and using (D.4) we can bound the norm $\|\mathbf{x}(\tau)\|_{\mathcal{A}_\infty,[t_i,t_{i+1}]}$ as follows

$$\|\mathbf{x}(\tau)\|_{\mathcal{A}_\infty,[t_i,t_{i+1}]} \leq \beta(\|\mathbf{x}(t_i)\|_{\mathcal{A}}, 0) + c\|h(\mathbf{z}(\tau))\|_{\infty,[t_i,t_{i+1}]} \leq \beta(\|\mathbf{x}(t_i)\|_{\mathcal{A}}, 0) + c \cdot \sigma_i h(\mathbf{z}_0) \tag{D.58}$$

Hence, combining (D.57) and (D.58) we obtain that

$$T_i \geq \frac{h(\mathbf{z}_0)(\sigma_i - \sigma_{i+1})}{\gamma_0(\sigma_i(\sigma_i^{-1}\beta(\|\mathbf{x}(t_i)\|_{\mathcal{A}}, 0) + c \cdot h(\mathbf{z}_0)))}$$

Then, using property (D.6) of function $\gamma_0$ we can derive that

$$T_i \geq \frac{h(\mathbf{z}_0)(\sigma_i - \sigma_{i+1})}{\gamma_{0,1}(\sigma_i)} \frac{1}{\gamma_{0,2}(\sigma_i^{-1}\beta(\|\mathbf{x}(t_i)\|_{\mathcal{A}}, 0) + c \cdot h(\mathbf{z}_0)))} \tag{D.59}$$

Taking into account condition (D.21) of the theorem, the theorem will be proven if we assure that

$$T_i \geq \tau_i \tag{D.60}$$

for all $i = 0, 1, 2, \ldots, \infty$. We prove this claim by induction with respect to index $i = 0, 1, \ldots, \infty$. We start with $i = 0$, and then show that for all $i > 0$ the following implication holds

$$T_i \geq \tau_i \Rightarrow T_{i+1} \geq \tau_{i+1} \tag{D.61}$$

Let us prove that (D.60) holds for $i = 0$. For this purpose consider the following term $(\sigma_i - \sigma_{i+1})/\gamma_{0,1}(\sigma_i)$. As follows immediately from conditions of the theorem, equation (D.19), we have that

$$\frac{\sigma_i - \sigma_{i+1}}{\gamma_{0,1}(\sigma_i)} \geq \tau_i \Delta_0 \; \forall \; i \geq 0 \tag{D.62}$$

In particular

$$\frac{\sigma_0 - \sigma_1}{\gamma_{0,1}(\sigma_0)} \geq \tau_0 \Delta_0$$

Therefore, inequality (D.59) reduces to

$$T_0 \geq \tau_0 \Delta_0 \frac{h(\mathbf{z}_0)}{\gamma_{0,2}(\sigma_0^{-1}\beta(\|\mathbf{x}(t_0)\|_{\mathcal{A}}, 0) + c \cdot h(\mathbf{z}_0))} \tag{D.63}$$

Moreover, taking into account Condition 3 and (D.12), (D.13) we can derive the following estimate:

$$\sigma_0^{-1}\beta(\|\mathbf{x}(t_0)\|_{\mathcal{A}}, 0) \leq \sigma_0^{-1}\phi_0(\|\mathbf{x}(t_0)\|_{\mathcal{A}}) + \sigma_0^{-1}\upsilon_0(c \cdot |h(\mathbf{z}_0)|\sigma_0) \leq B_1(\|\mathbf{x}_0\|_{\mathcal{A}}) + B_2(|h(\mathbf{z}_0)|, c)$$

According to the theorem conditions $\mathbf{x}_0$ and $\mathbf{z}_0$ satisfy inequality (D.20). This in turn implies that

$$\gamma_{0,2}(\sigma_0^{-1}\beta(\|\mathbf{x}(t_0)\|_{\mathcal{A}}, 0) + c \cdot h(\mathbf{z}_0)) \leq \gamma_{0,2}(B_1(\|\mathbf{x}_0\|_{\mathcal{A}}) + B_2(|h(\mathbf{z}_0)|, c) + c \cdot h(\mathbf{z}_0)) \leq \Delta_0 \cdot h(\mathbf{z}_0) \tag{D.64}$$

Combining (D.63) and (D.64) we obtain the desired inequality

$$T_0 \geq \tau_0 \Delta_0 \frac{h(\mathbf{z}_0)}{\gamma_{0,2}(\sigma_0^{-1}\beta(\|\mathbf{x}(t_0)\|_{\mathcal{A}}, 0) + c \cdot h(\mathbf{z}_0))} \geq \tau_0 \frac{\Delta_0 h(\mathbf{z}_0)}{\Delta_0 h(\mathbf{z}_0)} = \tau_0$$

Thus the basis of induction is proven.

Let us assume that (D.60) holds for all $i = 0, \ldots, n$, $n \geq 0$. We shall prove now that implication (D.61) holds for $i = n$. Consider the term $\beta(\|\mathbf{x}(t_{n+1})\|_{\mathcal{A}}, 0)$:

$$\begin{aligned}\beta(\|\mathbf{x}(t_{n+1})\|_{\mathcal{A}}, 0) &\leq \beta(\beta(\|\mathbf{x}(t_n)\|_{\mathcal{A}}, T_n) + c\|h(\mathbf{z}(\tau))\|_{\infty,[t_n,t_{n+1}]}, 0) \\ &\leq \beta(\beta(\|\mathbf{x}(t_n)\|_{\mathcal{A}}, T_n) + c \cdot \sigma_n \cdot h(\mathbf{z}_0), 0)\end{aligned}$$

Taking into account Condition 2 (specifically, inequality (D.11)) and (D.12)– (D.14) we can derive that

$$\beta(\|\mathbf{x}(t_{n+1})\|_{\mathcal{A}}, 0) \leq \beta(\xi_n \cdot \beta(\|\mathbf{x}(t_n)\|_{\mathcal{A}}), 0) + c \cdot \sigma_n \cdot h(\mathbf{z}_0), 0) \leq \phi_1(\|\mathbf{x}(t_n)\|_{\mathcal{A}}) + \upsilon_1(c \cdot |h(\mathbf{z})_0| \cdot \sigma_n) \tag{D.65}$$

Notice that, according to the inductive hypothesis ($T_i \geq \tau_i$) the following holds

$$\|\mathbf{x}(t_{i+1})\|_{\mathcal{A}} \leq \beta(\|\mathbf{x}(t_i)\|_{\mathcal{A}}, T_i) + c \cdot \sigma_i \cdot h(\mathbf{z}_0) \leq \xi_i \beta(\|\mathbf{x}(t_i)\|_{\mathcal{A}}, 0) + c \cdot \sigma_i \cdot h(\mathbf{z}_0) \tag{D.66}$$

for all $i = 0, \ldots, n$. Then (D.65), (D.66), (D.12)– (D.14) imply that

$$\begin{aligned}&\beta(\|\mathbf{x}(t_{n+1})\|_{\mathcal{A}}, 0) \leq \phi_1(\xi_i \beta(\|\mathbf{x}(t_{n-1})\|_{\mathcal{A}}, 0) + c \cdot \sigma_{n-1} \cdot h(\mathbf{z}_0)) + \upsilon_1(c \cdot |h(\mathbf{z})_0| \cdot \sigma_n) \\ &\leq \phi_2(\|\mathbf{x}(t_{n-1})\|_{\mathcal{A}}) + \upsilon_2(c \cdot |h(\mathbf{z}_0)| \cdot \sigma_{n-1}) + \upsilon_1(c \cdot |h(\mathbf{z}_0)| \cdot \sigma_n) \\ &\leq \phi_{n+1}(\|\mathbf{x}_0\|_{\mathcal{A}}) + \sum_{i=1}^{n+1} \upsilon_i(c \cdot |h(\mathbf{z}_0)|\sigma_{n+1-i}) \leq \phi_{n+1}(\|\mathbf{x}_0\|_{\mathcal{A}}) + \sum_{i=0}^{n+1} \upsilon_i(c \cdot |h(\mathbf{z}_0)|\sigma_{n+1-i})\end{aligned} \tag{D.67}$$

According to Condition 3, term

$$\sigma_{n+1}^{-1}\left(\phi_{n+1}(\|\mathbf{x}_0\|_{\mathcal{A}}) + \sum_{i=0}^{n+1} \upsilon_i(c \cdot |h(\mathbf{z}_0)|\sigma_{n+1-i})\right)$$

is bounded from above by the sum

$$B_1(\|\mathbf{x}_0\|_{\mathcal{A}}) + B_2(|h(\mathbf{z}_0)|, c)$$

Therefore, monotonicity of $\gamma_{0,2}$, estimate (D.67) and inequality (D.20) lead to the following inequality

$$\gamma_{0,2}(\sigma_{n+1}^{-1}\beta(\|\mathbf{x}(t_{n+1}\|_{\mathcal{A}}), 0) + c \cdot h(\mathbf{z}_0)) \leq \gamma_{0,2}(B_1(\|\mathbf{x}_0\|_{\mathcal{A}}) + B_2(|h(\mathbf{z}_0)|, c) + c \cdot h(\mathbf{z}_0)) \leq \Delta_0$$

Hence, according to (D.59), (D.62) we have:

$$T_{n+1} \geq \frac{(\sigma_{n+1} - \sigma_n)}{\gamma_{0,1}(\sigma_{n+1})} \frac{h(\mathbf{z}_0)}{\gamma_{0,2}(\sigma_{n+1}^{-1}\beta(\|\mathbf{x}(t_{n+1})\|_{\mathcal{A}}, 0) + c \cdot h(\mathbf{z}_0))} \geq \tau_{n+1} \frac{\Delta_0 h(\mathbf{z}_0)}{\Delta_0 h(\mathbf{z}_0)} = \tau_{n+1}$$

Thus implication (D.61) is proven. This implies that $h(\mathbf{z}(t)) \in [0, h(\mathbf{z}_0)]$ for all $t \geq t_0$ and, consequently, that (D.53) holds. *The theorem is proven.*

*Proof of Lemma 1.* As follows from the lemma assumptions, $h(\mathbf{z}(t, \mathbf{z}_0))$ is bounded. Let us, for certainty, it and belongs to the following interval $[a, h(\mathbf{z}_0)]$, $a \leq h(\mathbf{z}_0)$. Therefore, as follows from (D.5) we can conclude that

$$0 \leq \int_{t_0}^{\infty} \gamma_1(\|\mathbf{x}(\tau, \mathbf{x}_0)\|_{\mathcal{A}}) d\tau \leq h(\mathbf{z}_0) - h(\mathbf{z}(t, \mathbf{z}_0)) \leq \infty \tag{D.68}$$

On the other hand, taking into account that $h(\mathbf{z}(t,\mathbf{z}_0))$ is bounded and monotone in $t$ (every subsequence of which is again monotone) and applying Bolzano-Weierstrass theorem we can conclude that $h(\mathbf{z}(t,\mathbf{z}_0))$ converges in $[a, h(\mathbf{z}_0)]$. In particular, there exists $\bar{h} \in [a, h(\mathbf{z}_0)]$ such that

$$\lim_{t\to\infty} h(\mathbf{z}(t,\mathbf{z}_0)) = \bar{h} \tag{D.69}$$

According to the lemma assumptions, system $\mathcal{S}_a$ has the steady-state characteristics. This means that there exists constant $\bar{x} \in \mathbb{R}_+$ such that

$$\lim_{t\to\infty} \|\mathbf{x}(t,\mathbf{x}_0)\|_{\mathcal{A}} = \bar{x} \tag{D.70}$$

Suppose that $\bar{x} > 0$. Then it follows from (D.70) that there exists time instant $t_1 < \infty$ and some constant $0 < \delta < \bar{x}$ such that

$$\|\mathbf{x}(t)\|_{\mathcal{A}} \geq \delta \; \forall t \geq t_1$$

Hence using (D.68) and noticing that $\gamma_1 \in \mathcal{K}_e$ we obtain

$$\infty > h(\mathbf{z}_0) - h(\mathbf{z}_0) \geq \lim_{T\to\infty} \int_{t_1}^{T} \gamma_1(\delta) d\tau = \infty$$

Thus we obtained the contradiction. Hence, $\bar{x} = 0$ and, consequently,

$$\lim_{t\to\infty} \|\mathbf{x}(t)\|_{\mathcal{A}} = 0$$

Then, according to the notion of steady-state characteristic in Definition 5 this is only possible if $\bar{h} \in \chi^{-1}(0)$. *The lemma is proven.*

*Proof of Lemma 2.* Analogously to the proof of Lemma 1 we notice that (D.68) holds. This, however, implies that for any constant and positive $T$ the following limit

$$\lim_{t\to\infty} \int_{t}^{t+T} \gamma_1(\|\mathbf{x}(\tau)\|_{\mathcal{A}}) d\tau$$

exists and equals to zero. Furthermore, $h(\mathbf{z}(t,\mathbf{z}_0)) \in [0, h(\mathbf{z}_0)]$ for all $t \geq t_0$. Hence, there exists time instant $t'$ such that

$$\|\mathbf{x}(t)\|_{\mathcal{A}} \leq c \cdot h(\mathbf{z}_0) + \varepsilon, \; \forall\, t \geq t',$$

where $\varepsilon > 0$ is arbitrary small. Then taking into account (D.25) we can conclude that

$$\lim_{t\to\infty} \int_{t}^{t+T} \gamma_1(\|\mathbf{x}(\tau)\|_{\mathcal{A}}) d\tau \geq \bar{\gamma} \int_{t}^{t+T} \|\mathbf{x}(\tau)\|_{\mathcal{A}} \, d\tau = 0 \tag{D.71}$$

Given that (D.69) holds, system (D.4) has steady-state characteristic on average and that $\chi_T(\cdot)$ has no zeros in the positive domain, limiting relation (D.71) is possible only if $\bar{h} = 0$. Then, according to (D.4), $\lim_{t\to\infty} \|\mathbf{x}(t)\|_{\mathcal{A}} = 0$. *The lemma is proven.*

*Proof of Corollary 1.* As follows from Theorem 1, state $\mathbf{x}(t,\mathbf{x}_0) \oplus \mathbf{z}(t,\mathbf{z}_0)$ converges to the set $\Omega_a$ specified by (D.18). Hence $h(\mathbf{z}(t,\mathbf{z}_0))$ is bounded. Then, according to (D.5), estimate (D.68) holds. This in combination with condition (D.28) implies that $\mathbf{z}(t,\mathbf{z}_0)$ is bounded. In the over words

$$\mathbf{x}(t,\mathbf{x}_0) \oplus \mathbf{z}(t,\mathbf{z}_0) \in \Omega' \; \forall\, t \geq t_0$$

where $\Omega'$ is a bounded subset in $\mathbb{R}^n \times \mathbb{R}^m$. Applying Bolzano-Weierstrass theorem we can conclude that for every point $\mathbf{x}_0 \oplus \mathbf{z}_0 \in \Omega_\gamma$ there is an $\omega$-limit set $\omega(\mathbf{x}_0 \oplus \mathbf{z}_0) \subseteq \Omega'$ (non-empty).

As follows from C3) and Lemma 1 the following holds:

$$\lim_{t\to\infty} h(\mathbf{z}(t,\mathbf{z}_0)) \in \chi^{-1}(0)$$

Therefore, given that $h(\cdot) \in \mathcal{C}^0$ we can obtain that

$$\lim_{t_i\to\infty} h(\mathbf{z}(t_i,\mathbf{z}_0)) = h(\lim_{t_i\to\infty} \mathbf{z}(t_i,\mathbf{z}_0)) = h(\omega_z(\mathbf{x}_0 \oplus \mathbf{z}_0)) \in \chi^{-1}(0)$$

In the other words:

$$\omega_z(\mathbf{x}_0 \oplus \mathbf{z}_0) \subseteq \Omega_h = \{\mathbf{x} \in \mathbb{R}^n,\ \mathbf{z} \in \mathbb{R}^m |\ h(\mathbf{z}) \in \chi^{-1}(0)\}$$

Moreover

$$\omega_x(\mathbf{x}_0 \oplus \mathbf{z}_0) \subseteq \Omega_a = \{\mathbf{x} \in \mathbb{R}^n,\ \mathbf{z} \in \mathbb{R}^m |\ \|\mathbf{x}\|_{\mathcal{A}} = 0\}$$

According to assumption C1, flow $\mathbf{x}(t,\mathbf{x}_0) \oplus \mathbf{z}(t,\mathbf{z}_0)$ is generated by a system of autonomous differential equations with locally Lipschitz right-hand side. Then, as follows from [13] (Lemma 4.1, page 127)

$$\lim_{t\to\infty} \operatorname{dist}(\mathbf{x}(t,\mathbf{x}_0) \oplus \mathbf{z}(t,\mathbf{z}_0), \omega(\mathbf{x}_0 \oplus \mathbf{z}_0)) = 0$$

Noticing that

$$\operatorname{dist}(\mathbf{x}(t,\mathbf{x}_0) \oplus \mathbf{z}(t,\mathbf{z}_0), \omega(\mathbf{x}_0 \oplus \mathbf{z}_0)) \geq \operatorname{dist}(\mathbf{x}(t,\mathbf{x}_0), \Omega_a) + \operatorname{dist}(\mathbf{z}(t,\mathbf{z}_0), \Omega_h)$$

we can finally obtain that

$$\lim_{t\to\infty} \operatorname{dist}(\mathbf{x}(t,\mathbf{x}_0), \Omega_a) = 0,\ \lim_{t\to\infty} \operatorname{dist}(\mathbf{z}(t,\mathbf{z}_0), \Omega_h) = 0$$

*The corollary is proven.*

*Proof of Corollary 2.* As follows from Theorem 1, the corollary will be proven if Conditions 1 – 3 are satisfied and also (D.19), (D.20), (D.21) hold. In order to satisfy Condition 1 we select the following sequence $\mathcal{S}$:

$$\mathcal{S} = \{\sigma_i\}_{i=0}^{\infty},\ \sigma_i = \frac{1}{\kappa^i},\ \kappa \in \mathbb{R}_+,\ \kappa > 1 \tag{D.72}$$

Let us chose sequences $\mathcal{T}$ and $\Xi$ as follows:

$$\mathcal{T} = \{\tau_i\}_{i=0}^{\infty},\ \tau_i = \tau^*, \tag{D.73}$$

$$\Xi = \{\xi_i\}_{i=0}^{\infty},\ \xi_i = \xi^*, \tag{D.74}$$

where $\tau^*$, $\xi^*$ are positive, yet to be defined, constants. Notice that choosing $\mathcal{T}$ as in (D.73) automatically fulfills condition (D.21) of Theorem 1. On the other hand, taking into account (D.33) and that $\beta_t(t)$ is monotonically decreasing in $t$, this choice defines constant $\xi^*$ as follows:

$$\beta_t(\tau^*) \leq \xi^* < \beta_t(0) \tag{D.75}$$

Given that inverse $\beta_t^{-1}$ exists (see, (D.34)), this choice is always possible. In particular, (D.75) will be satisfied for the following values of $\tau^*$:

$$\tau^* \geq \beta_t^{-1}(\xi^*) \tag{D.76}$$

Let us now find the values for $\tau^*$ and $\xi^*$ such that Condition 3 is also satisfied. For this reason consider systems of functions $\Phi$, $\Upsilon$ specified by equations (D.12), (D.13). Notice that function $\beta(s,0)$ in (D.12), (D.13) is linear for system (D.33)

$$\beta(s,0) = s \cdot \beta_t(0),$$

and therefore functions $\rho_{\phi,j}(\cdot)$, $\rho_{\upsilon,j}$ are the identity maps. Hence, $\Phi$, $\Upsilon$ reduce to the following

$$\Phi: \begin{array}{ll} \phi_j(s) & = \phi_{j-1} \cdot \xi^* \cdot \beta(s,0) = \xi^* \cdot \beta_t(0) \cdot \phi_{j-1}(s),\ j = 1, \dots, i \\ \phi_0(s) & = \beta_t(0) \cdot s \end{array} \tag{D.77}$$

$$\Upsilon: \begin{array}{ll} \upsilon_j(s) & = \phi_{j-1}(s),\ j = 1, \dots, i \\ \upsilon_0(s) & = \beta_t(0) \cdot s \end{array} \tag{D.78}$$

Taking into account (D.72), (D.77), (D.78) let us explicitly formulate requirements (D.15), (D.16) in Condition 3. These conditions are equivalent to boundedness of the following functions

$$\|\mathbf{x}(t_0)\|_{\mathcal{A}} \cdot \beta_t(0) \cdot \kappa^n (\xi^* \cdot \beta_t(0))^n \tag{D.79}$$

$$\begin{aligned} &\kappa^n \left( \beta_t(0) \frac{c|h(\mathbf{z}_0)|}{\kappa^n} + \frac{\beta_t(0) c|h(\mathbf{z}_0)|}{\kappa^{n-1}} + \beta_t(0) \sum_{i=2}^{n} c|h(\mathbf{z}_0)| \frac{1}{k^{n-i}} (\xi^* \cdot \beta_t(0))^{i-1} \right) \\ &= \beta_t(0) c|h(\mathbf{z}_0)| + \beta_t(0) c|h(\mathbf{z}_0)| \kappa \left( 1 + \sum_{i=2}^{n} \kappa^{i-1} (\xi^* \cdot \beta_t(0))^{i-1} \right) \end{aligned} \tag{D.80}$$

Boundedness functions $B_1(\|\mathbf{x}_0\|_{\mathcal{A}})$ and $B_2(|h(\mathbf{z}_0)|, c)$ is ensured if $\xi^*$ satisfy the following inequality

$$\xi^* \leq \frac{d}{\kappa \cdot \beta_t(0)} \tag{D.81}$$

for some $0 \leq d < 1$. Notice that $\kappa > 1$, $\beta_t(0) \geq 1$ imply that $\xi^* \leq 1$ and therefore constant $\tau^*$ satisfying (D.76) will always be defied. Hence, according to (D.79), (D.80), functions $B_1(\|\mathbf{x}_0\|_{\mathcal{A}})$ and $B_2(|h(\mathbf{z}_0)|, c)$ satisfying Condition 3 can be chosen as

$$B_1(\|\mathbf{x}_0\|_{\mathcal{A}}) = \beta_t(0) \|\mathbf{x}_0\|_{\mathcal{A}};\ B_2(|h(\mathbf{z}_0)|, c) = \beta_t(0) \cdot c \cdot |h(\mathbf{z}_0)| \left( 1 + \frac{\kappa}{1-d} \right) \tag{D.82}$$

In order to apply Theorem 1 we have to check the remaining conditions (D.19) and (D.20). This will involve availability of factorization (D.6) for the function $\gamma_0(\cdot)$. According to assumption (D.35) of the corollary function $\gamma_0(\cdot)$ is Lipschitz:

$$|\gamma_0(s)| \leq D_{\gamma,0} \cdot |s|$$

This allows us to choose function $\gamma_{0,1}(\cdot)$ and $\gamma_{0,2}(\cdot)$ as follows:

$$\gamma_{0,1}(s) = s,\ \gamma_{0,2}(s) = D_{\gamma,0} \cdot s \tag{D.83}$$

Condition (D.19), therefore, is equivalent to solvability of the following inequality:

$$\left( \frac{1}{\kappa^i} - \frac{1}{\kappa^{i+1}} \right) \frac{\kappa^i}{\tau^*} \geq \Delta_0 \tag{D.84}$$

Taking into account inequalities (D.76), (D.81) we can derive that solvability of

$$\Delta_0 = \left( \beta_t^{-1} \left( \frac{d}{\kappa \cdot \beta_t(0)} \right) \right)^{-1} \frac{\kappa - 1}{\kappa} \tag{D.85}$$

implies existence of $\Delta_0 > 0$ satisfying (D.84) and, consequently, condition (D.19) of Theorem 1. Given that $d < 1$, $\kappa > 1$ and $\beta_t(0) \geq 1$ positive solution to (D.85) is always defined. Hence, the proof will be complete and the claim is non-vacuous if domain

$$D_{\gamma,0} \leq \left( \beta_t^{-1} \left( \frac{d}{\kappa \cdot \beta_t(0)} \right) \right)^{-1} \frac{\kappa - 1}{\kappa} \frac{h(\mathbf{z}_0)}{\beta_t(0) \|\mathbf{x}_0\|_{\mathcal{A}} + \beta_t(0) \cdot c \cdot |h(\mathbf{z}_0)| \left( 1 + \frac{\kappa}{1-d} \right) + c|h(\mathbf{z}_0)|}$$

is not empty. *The corollary is proven.*

*Proof of Corollary 3.* Let $\boldsymbol{\lambda}(\tau, \lambda_0)$ be a solution of system (D.40). Consider it as a function of variable $\tau$. Let us pick some monotone, strictly increasing function $\sigma$ such that the following holds

$$\tau = \sigma(t),\ \sigma : \mathbb{R}_+ \to \mathbb{R}_+$$

Given that $\boldsymbol{\eta}(\Omega_\lambda)$ is dense in $\Omega_\theta$, for any $\boldsymbol{\theta} \in \Omega_\theta$ there always exists vector $\boldsymbol{\lambda}_\theta \in \Omega_\lambda$ such that $\boldsymbol{\eta}(\boldsymbol{\lambda}_\theta) = \boldsymbol{\theta} + \epsilon_\theta$, where $\|\epsilon_\theta\|$ is arbitrary small. Furthermore, $\boldsymbol{\lambda}(\tau)$ is dense in $\Omega_\lambda$, hence there is a point $\boldsymbol{\lambda}^* = \boldsymbol{\lambda}(\tau^*, \boldsymbol{\lambda}_0)$, which is arbitrary close to $\boldsymbol{\lambda}_\theta$. Consider the following difference

$$\mathbf{f}(\boldsymbol{\xi}(t), \boldsymbol{\theta}) - \mathbf{f}(\boldsymbol{\xi}(t), \hat{\boldsymbol{\theta}}) = \mathbf{f}(\boldsymbol{\xi}(t), \boldsymbol{\theta}) - f(\boldsymbol{\xi}(t), \boldsymbol{\eta}(\boldsymbol{\lambda}^*)) + \mathbf{f}(\boldsymbol{\xi}, \boldsymbol{\eta}(\boldsymbol{\lambda}^*)) - \mathbf{f}(\boldsymbol{\xi}, \boldsymbol{\eta}(\boldsymbol{\lambda}(\sigma(t))))$$

Function $\mathbf{f}(\cdot)$ is locally bounded and $\boldsymbol{\eta}(\cdot)$ is Lipschitz, then

$$\|\mathbf{f}(\boldsymbol{\xi}, \boldsymbol{\theta}) - \mathbf{f}(\boldsymbol{\xi}, \boldsymbol{\eta}(\boldsymbol{\lambda}^*))\| \leq D_f \|\epsilon_\theta\| + \Delta_f = \Delta_\theta + \Delta_f$$

where $\Delta_\theta$ is arbitrary small. Hence

$$\begin{aligned} &\|\mathbf{f}(\boldsymbol{\xi}, \boldsymbol{\eta}(\boldsymbol{\lambda}^*)) - \mathbf{f}(\boldsymbol{\xi}, \boldsymbol{\eta}(\boldsymbol{\lambda}(\sigma(t))))\| \leq D_f \|\boldsymbol{\eta}(\boldsymbol{\lambda}^*) - \boldsymbol{\eta}(\boldsymbol{\lambda}(\sigma(t)))\| + \Delta_f + \Delta_\theta \\ &\leq D_f \cdot D_\eta \|\boldsymbol{\lambda}^* - \boldsymbol{\lambda}(\sigma(t))\| + \Delta_f + \Delta_\theta \end{aligned} \tag{D.86}$$

Noticing that $\boldsymbol{\lambda}^* = \boldsymbol{\lambda}(\tau^*, \boldsymbol{\lambda}_0) = \boldsymbol{\lambda}(\sigma(t^*), \boldsymbol{\lambda}_0)$ and taking into account Poisson stability of (D.40), we can always choose $\boldsymbol{\lambda}^*(\sigma^*, \boldsymbol{\lambda}_0)$ such that $\sigma^* > \sigma(t_0) = \tau_0$ for any $\tau_0 \in \mathbb{R}_+$. Hence, according to (D.86) the following estimate holds:

$$\begin{aligned} &\|\mathbf{f}(\boldsymbol{\xi}, \boldsymbol{\eta}(\boldsymbol{\lambda}^*)) - \mathbf{f}(\boldsymbol{\xi}, \boldsymbol{\eta}(\boldsymbol{\lambda}(\sigma(t))))\| \leq D_f \cdot D_\eta \| \int_{\sigma(t)}^{\sigma^*} S(\boldsymbol{\lambda}(\sigma(\tau))) d\tau\| + \Delta_f + \Delta_\theta \\ &\leq D_f \cdot D_\eta \cdot \max_{\boldsymbol{\lambda} \in \Omega_\lambda} \|S(\boldsymbol{\lambda})\| |\sigma^* - \sigma(t)| = \mathcal{D} \cdot |\sigma^* - \sigma(t)| + \Delta_f + \Delta_\theta,\ \mathcal{D} = D_f \cdot D_\eta \cdot \max_{\boldsymbol{\lambda} \in \Omega_\lambda} \|S(\boldsymbol{\lambda})\| \end{aligned} \tag{D.87}$$

Denoting $\mathbf{u}(t) = \mathbf{f}(\boldsymbol{\xi}(t), \boldsymbol{\theta}) - \mathbf{f}(\boldsymbol{\xi}(t), \hat{\boldsymbol{\theta}}) + \varepsilon(t)$ we can conclude now that

$$\begin{aligned} \|\mathbf{u}(t)\| &\leq \Delta_\epsilon + \Delta_f + \|\mathbf{f}(\boldsymbol{\xi}(t), \boldsymbol{\theta}) - f(\boldsymbol{\xi}(t), \boldsymbol{\eta}(\boldsymbol{\lambda}^*))\| + \mathcal{D} \cdot |\sigma^* - \sigma(t)| \\ &\leq \Delta_\epsilon + 2\Delta_f + \Delta_\theta + D_f \|\boldsymbol{\theta} - \boldsymbol{\eta}(\boldsymbol{\lambda}^*)\| + \mathcal{D} \cdot |\sigma^* - \sigma(t)| \end{aligned} \tag{D.88}$$

Notice that due to the denseness of $\boldsymbol{\lambda}(t, \boldsymbol{\lambda}_0)$ in $\Omega_\lambda$ it is always possible to choose $\boldsymbol{\lambda}^*$ such that

$$D_f \|\boldsymbol{\theta} - \boldsymbol{\eta}(\boldsymbol{\lambda}^*)\| = D_f \|\boldsymbol{\eta}(\boldsymbol{\lambda}_\theta) - \boldsymbol{\eta}(\boldsymbol{\lambda}^*)\| \leq D_f D_\eta \|\boldsymbol{\lambda}_\theta - \boldsymbol{\eta}(\boldsymbol{\lambda}^*)\| \leq \Delta_\lambda$$

Hence, according to (D.88), we have

$$\|\mathbf{u}(t)\|_{\infty,[t_0,t]} \leq 2\Delta_f + \Delta_\varepsilon + \delta + \mathcal{D} \cdot \|\sigma^* - \sigma(t)\|_{\infty,[t_0,t]}$$

where the term $\delta > \Delta_\theta + \Delta_\lambda$ can be made arbitrary small.

Therefore Assumption 3 implies that the following inequality holds:

$$\|\mathbf{x}(t)\|_{\mathcal{A}_{\Delta(M)}} \leq \beta(t - t_0) \|\mathbf{x}(t_0)\|_{\mathcal{A}_{\Delta(M)}} + c \cdot \mathcal{D} \cdot \|\sigma^* - \sigma(t)\|_{\infty,[t_0,t]} \tag{D.89}$$

Let us now define $\sigma(t)$ as follows

$$\sigma(t) = \int_{t_0}^{t} \gamma \|\psi(\mathbf{x}(\tau))\|_{\mathcal{A}_{\Delta(M)}} d\tau \tag{D.90}$$

Moreover, let us introduce the following notation

$$h(t) = \sigma^* - \sigma(t) = \sigma^* - \int_{t_0}^{t} \gamma \left\| \psi(\mathbf{x}(\tau)) \right\|_{\mathcal{A}_{\Delta(M)}} d\tau$$

then for all $t',\ t \geq t_0, t \geq t'$ we have that

$$h(t') - h(t) = \int_{t'}^{t} \gamma \left\| \psi(\mathbf{x}(\tau)) \right\|_{\mathcal{A}_{\Delta(M)}} d\tau$$

Taking into account equation (D.86), (D.87), equality

$$\frac{\partial \boldsymbol{\lambda}(\sigma(t), \boldsymbol{\lambda}_0)}{dt} = \frac{\partial \sigma(t)}{dt} S(\boldsymbol{\lambda}(\sigma(t), \boldsymbol{\lambda}_0)) = \gamma \left\| \psi(\mathbf{x}(\tau)) \right\|_{\mathcal{A}_{\Delta(M)}} S(\boldsymbol{\lambda}(\sigma(t), \boldsymbol{\lambda}_0)),$$

equation (D.89), and denoting $D_\lambda = c\mathcal{D}$, we can conclude that the following holds along the trajectories of (D.41):

$$\begin{aligned} \left\| \mathbf{x}(t) \right\|_{\mathcal{A}_{\Delta(M)}} &\leq \beta(t - t_0) \left\| \mathbf{x}(t_0) \right\|_{\mathcal{A}_{\Delta(M)}} + D_\lambda \| h(\tau) \|_{\infty, [t_0, t]} \\ h(t_0) - h(t) &= \int_{t_0}^{t} \gamma \left\| \psi(\mathbf{x}(\tau)) \right\|_{\mathcal{A}_{\Delta(M)}} d\tau \end{aligned} \tag{D.91}$$

Hence, according to Corollary 1, limiting relation (D.43) holds for all $|h(t_0)|$, $\left\| \mathbf{x}(t_0) \right\|_{\mathcal{A}_{\Delta(M)}}$ which belong to the domain

$$\Omega_\gamma : \gamma \leq \left( \beta_t^{-1} \left( \frac{d}{\kappa \cdot \beta_t(0)} \right) \right)^{-1} \frac{\kappa - 1}{\kappa} \frac{h(t_0)}{\beta_t(0) \left\| \mathbf{x}(t_0) \right\|_{\mathcal{A}_{\Delta+\delta}} + \beta_t(0) \cdot D_\lambda \cdot |h(t_0)| \left( 1 + \frac{\kappa}{1-d} \right) + D_\lambda |h(t_0)|}$$

for some $d < 1$, $\kappa > 1$. Notice, however, that $\left\| \mathbf{x}(t) \right\|_{\mathcal{A}_{\Delta+\delta}}$ is always bounded as $\mathbf{f}(\cdot)$ is Lipschitz in $\theta$ and both $\boldsymbol{\theta}$ and $\hat{\boldsymbol{\theta}}$ are bounded ($\boldsymbol{\eta}(\cdot)$ is Lipschitz and $\boldsymbol{\lambda}(t, \boldsymbol{\lambda}_0)$ is bounded according to assumptions of the corollary). Moreover, due to the Poisson stability of (D.40) it is always possible to choose point $\boldsymbol{\lambda}^*$ such that $h(t_0) = \sigma^*$ is arbitrary large. Hence choice of $\gamma$ in (D.91) as (D.42) suffices to ensure that $h(t)$ is bounded. Moreover, that $h(t)$ converges to a limit as $t \to \infty$. This implies that $\gamma \int_{t_0}^{t} \left\| \mathbf{x}(\tau) \right\|_{\mathcal{A}_{\Delta(M)}}$ also converges as $t \to \infty$, and, consequently, $\boldsymbol{\lambda}(t, \boldsymbol{\lambda}_0)$ converges to some $\boldsymbol{\lambda}' \in \Omega_\lambda$. Hence the following holds

$$\lim_{t \to \infty} \hat{\boldsymbol{\theta}}(t) = \boldsymbol{\theta}'$$

for some $\boldsymbol{\theta}' \in \Omega_\theta$. According to the corollary conditions, system (D.39) has steady state characteristics with respect to $\hat{\boldsymbol{\theta}}$. Then, in the same way as in the proof of Lemma 1 we can show that (D.43) holds. The corollary is proven.

# Bibliography


[1] M. Arcak, D. Angeli, and E. Sontag. A unifying intergal ISS framework for stability of nonlinear cascades. *SIAM J. Control and Optimization*, 40:1888–1904, 2002.

[2] G. Bastin and M. Gevers. Stable adaptive observers for nonlinear time-varying systems. *IEEE Trans. on Automatic Control*, 33(7):650–658, 1988.

[3] G. Besancon. Remarks on nonlinear adaptive observer design. *Systems and Control Letters*, 41(4):271–280, 2000.

[4] G.-I. Bischi, L. Stefanini, and L. Gardini. Synchronization, intermittency and critical curves in a duopoly game. *Mathematics and Computers in Simulation*, 44:559–585, 1998.

[5] C. Cao, A.M. Annaswamy, and A. Kojic. Parameter convergence in nonlinearly parametrized systems. *IEEE Trans. on Automatic Control*, 48(3):397–411, 2003.

[6] J. Carr. *Applications of the Center Manifold Theory*. Springer-Verlag, 1981.

[7] L. Grune, E. Sontag, and F. R. Wirth. Asymptotic stability equals exponential stability, and ISS equals finite energy gain - if you twist your eyes. *Systems & Control Letters*, 38:127–134, 1999.

[8] J. Guckenheimer and P. Holmes. *Nonlinear Oscillations, Dynamical Systems and Bifurcations of Vector Fields*. Springer, 2002.

[9] J. L. Hindmarsh and R. M. Rose. A model of the nerve impulse using two first-order differential equations. *Nature*, 269:162–164, 1982.

[10] R. Horst and P.M. Pardalos, editors. *Handbook of Global Optimization*. Kluwer, Dordrecht, 1995.

[11] A. Ilchman. Universal adaptive stabilization of nonlinear systems. *Dynamics and Control*, (7):199–213, 1997.

[12] Z.-P. Jiang, A. R. Teel, and L. Praly. Small-gain theorem for ISS systems and applications. *Mathematics of Control, Signals and Systems*, (7):95–120, 1994.

[13] H. Khalil. *Nonlinear Systems (3d edition)*. Prentice Hall, 2002.

[14] J. P. La Salle. Stability theory and invariance principles. In J.K. Hale L. Cesari and J.P. La Salle, editors, *Dynamical Systems, An International Symposium*, volume 1, pages 211–222, 1976.

[15] A. M. Lyapunov. The general problem of the stability of motion. *Int. J. Control, Lyapunov Centenary Issue*, 55(3):531–773, 1992.

[16] R. Marino. Adaptive observers for single output nonlinear systems. *IEEE Trans. Automatic Control*, 35(9):1054–1058, 1990.

[17] J. Milnor. On the concept of attractor. *Commun. Math. Phys.*, 99:177–195, 1985.

[18] I. Miroshnik, V. Nikiforov, and A. Fradkov. *Nonlinear and Adaptive Control of Complex Systems*. Kluwer, 1999.

[19] E. Ott and J.C. Sommerer. Blowout bifurcations: the occurence of riddled basins. *Phys. Lett. A.*, 188(1), 1994.

[20] A. Y. Pogromsky, G. Santoboni, and H. Nijmeijer. An ultimate bound on the trajectories of the Lorenz system and its applications. *Nonlinearity*, 16(5):1597–1605, 2003.

[21] J.-B. Pomet. Remarks on sufficient informtation for adaptive nonlinear regulation. In *31-st IEEE Conferense on Decision and Control*, pages 1737–1741. 1992.

[22] E. Sontag and Y. Wang. New characterizations of input-to-state stability. *IEEE Transactions on Automatic Control*, 41(9):1283–1294, 1995.

[23] Y. Suemitsu and S. Nara. A solution for two-dimensional mazes with use of chaotic dynamics in a recurrent neural network model. *Neural Computation*, 16:1943–1957, 2004.

[24] I. Y. Tyukin, D. V. Prokhorov, and C. van Leeuwen. Adaptation and parameter estimation in systems with unstable target dynamics and nonlinear parametrization. *http://arxiv.org/abs/math.OC/0506419*, 2005.

[25] I.Yu. Tyukin and C. van Leeuwen. Adaptation and nonlinear parameterization: Nonlinear dynamics prospective. In *Proceedings of the 16-th IFAC World Congress*. Prague, Czech Republic, 4 – 8 July 2005.

[26] C. van Leeuwen and A. Raffone. Coupled nonlinear maps as models of perceptual pattern and memory trace dynamics. *Cognitive Processing*, 2:67–111, 2001.

[27] C. van Leeuwen, S. Verver, and M. Brinkers. Visual illusions, solid/outline-invariance, and non-stationary activity patterns. *Connection Science*, 12:279–297, 2000.

[28] V.I. Vorotnikov. *Partial Stability and Control*. Birkhauser, 1998.

[29] T. Yoshizawa. Stability and boundedness of systems. *Arch. Rational Mech. Anal.*, 6:409–421, 1960.

[30] G. Zames. On the input-output stability of time-varying nonlinear feedback systems. part i: Conditions derived using concepts of loop gain, conicity, and passivity. *IEEE Trans. on Automatic Control*, AC-11(2):228–238, 1966.